N87-19332

CHAPTER 2:
PARTICLE ACCELERATION

L. Vlahos[1], *M. E. Machado*[2], *R. Ramaty*[3], *R. J. Murphy*[1,3], C. Alissandrakis[4], T. Bai[5], D. Batchelor[3], A. O. Benz[6], E. Chupp[7], D. Ellison[1], P. Evenson[8], D. J. Forrest[7], G. Holman[3], S. R. Kane[9], P. Kaufmann[10], M. R. Kundu[1], R. P. Lin[9], A. Mackinnon[11], H. Nakajima[3], M. Pesses[3], M. Pick[12], J. Ryan[7], R. A. Schwartz[9], D. F. Smith[13], G. Trottet[12], S. Tsuneta[14], and G. Van Hoven[15].

[1]University of Maryland, College Park, Maryland
[2]Observatorio de Fisica Cosmica — CNIE, Argentina
[3]NASA Goddard Space Flight Center, Greenbelt, Maryland
[4]University of Athens, Athens, Greece
[5]Stanford University, Stanford, California
[6]Institute of Astronomy, Zurich, Switzerland
[7]University of New Hampshire, Durham, New Hampshire
[8]University of Delaware, Newark, Delaware
[9]University of California, Berkeley, California
[10]Instituto de Pesquisas Espaciasi, Brazil
[11]University of Glasgow, United Kingdom
[12]Meudon Observatory, France
[13]Berkeley Research Associates, Berkeley, California
[14]University of Tokyo, Tokyo, Japan
[15]University of California, Irvine, California

Rest is a special form of motion
G. Kirchhoff

2.1. INTRODUCTION

Electrons and ions are accelerated to high energies before, during and after the impulsive phase of flares. The presence of high energy particles at the sun during a solar flare is inferred from the observed electromagnetic radiation resulting from the interaction of the energized particles with the ambient plasma and/or the magnetic field as well as from direct particle observations in the interplanetary space. In this chapter we compile data from the SMM and HINOTORI satellites, particle detectors in several satellites and from ground based instruments and balloon flights and attempt to answer a number of fundamental questions that are stated below. We have also reviewed the progress made on the theory of mechanisms for particle acceleration in flares.

We define the term acceleration here as the preferential gain of energy by a small population of electrons and ions. Heating, on the other hand, is defined as the bulk energization of the ambient plasma. In other words, the development of a long nonthermal tail in the ambient distribution will be the result of "acceleration" but the increase of the random mean-square velocity of the ambient particles the result of "heating". The critical velocity, above which, "acceleration" dominates heating varies from flare to flare. The variability of the critical velocity has created in the past many discussions and divisions of flares into "thermal" or "nonthermal" classes. Another important "distinction" between "heating" and "acceleration" is the time that is required for the accelerated particles to reach the chromosphere and thermalize vs the time resolution of our instruments. For example, if the acceleration of the tail lasts only a few seconds, the propagation and thermalization of high energy particles can be faster than 10 secs, which is below the resolution of several current instruments. In this case, the division between thermal and nonthermal flares will be a time dependent phenomenon. Thus, one may argue (paraphrasing Kirchhoff's words), that "heating" is a special kind of acceleration. In the rest of this chapter we will show that heating and acceleration are always present in flares and we will discuss mechanisms that will achieve bulk heating *and* tail acceleration of the ambient plasma. We will adopt the more general term "energization" for the bulk heating *and* acceleration.

As a primary goal for our study, we attempted to answer the following questions:

(1) What are the requirements for the coronal magnetic field structure in the vicinity of the energization source?
(2) What is the height (above the photosphere) of the energization source?
(3) Does the energization start before and continue after the impulsive phase?
(4) Is there a transition between coronal heating and flares? What are the microflares?
(5) Is there evidence for purely thermal, purely nonthermal or a hybrid type flare?
(6) What are the time characteristics of the energization source?
(7) Does every flare accelerate protons?
(8) What is the location of the interaction site of the ions and relativistic electrons?
(9) What are the energy spectra for ions and relativistic electrons? Does the spectrum vary from flare to flare?
(10) What is the relationship between particles at the Sun and interplanetary space?
(11) Is there any evidence for more than one acceleration mechanisms?
(12) Is there a single mechanism that will accelerate particles to all energies and also heat the plasma?
(13) How fast will the existing mechanisms accelerate electrons up to several MeV and ions to 1 GeV?

(14) If shocks are formed in a few seconds, can they be responsible for the prompt acceleration of ions and electrons? How are these shocks related to large-scale shocks which are responsible for the Type II bursts?

(15) Can the electron-cyclotron maser spread the acceleration region?

(16) Which of the acceleration mechanisms discussed above can explain the observed energy spectra?

We concentrate on these questions in Sections 2.2, 2.3 and 2.4. In Section 2.4 we also review the progress made during the last few years on mechanisms for particle acceleration in flares and in the last Section we summarize the still open observational and theoretical questions. We will attempt to answer the questions (1)-(16) in Sections 2.2.7, 2.3.6 and 2.4.8. Hence, for a quick review of the status of our understanding of the problem of particle acceleration in flares the reader may go directly to these Sections and Section 2.5.

Section 2.2 was prepared by M. Machado and L. Vlahos from inputs from C. Alissandrakis, T. Bai, D. Batchelor, A. O. Benz, G. Holman, S. R. Kane, P. Kaufmann, M. R. Kundu, R. P. Lin, A. Mackinnon, H. Nakajima, M. Pick, J. Ryan, D. F. Smith, G. Trottet, S. Tsuneta. Section 2.3 was prepared by R. Ramaty and R. J. Murphy from contributions from T. Bai, E. Chupp, D. Ellison, P. Evenson, D. J. Forrest and M. Pesses and Section 2.4 was prepared by L. Vlahos from inputs from G. Holman, R. P. Lin, D. F. Smith and G. Van Hoven.

Finally, it is important to stress that this is a report of the discussions carried out during the Workshops and reflects strongly the opinions (and in many Sections even the biases) of the authors.

2.2 PHENOMENA ASSOCIATED WITH MILDLY-RELATIVISTIC ELECTRONS

In this Section we focus our discussion on phenomena associated with mildly relativistic electrons (10-400 keV) while in the next we concentrate on phenomena related to energetic ions and relativistic electrons ($E \geq 500$ keV). This division is in many ways artificial, since particles of all energies are produced during a flare. Thus, our discussion in this Section overlaps with Section 2.3 and vice-versa. In fact, our effort in this chapter will be to unify aspects related to subjects of Sections 2.2 and 2.3.

Hard X-ray imaging from SMM and HINOTORI satellites and the stereoscopic hard X-ray observations made with the International Sun Earth Explorer 3 (ISEE-3) and Pioneer Venus Orbiter (PVO) spacecraft are reviewed in this Section. Imaging of microwave bursts is also one of our main new sources of information about particle acceleration. The results from the Very Large Array (VLA) telescope have made a large impact on our understanding of flare models. The spatial maps from the Nancay (France) Radioheliograph obtained with a high time resolution (0.04 secs) provide several new features of the topology of field lines near the acceleration site. The high time and spectral resolution of the Zürich radio spectrometer and 45 ft. radome-enclosed antenna at Itapentinga (Brazil), have opened a new window on the microinstabilities in flares. Balloon measurements with sensitive hard X-ray detectors have also been carried out with remarkable success.

2.2.1 Soft and Hard X-ray Source Structure, Location and Development

2.2.1.1 X-ray Imaging

Before the launch of the SMM and HINOTORI spacecraft, only isolated observations were available on the spatial structure of hard X-ray emission from flares. These were mainly provided by stereoscopic observations from two spacecrafts (PVOs and ISEE-3, see Kane, 1983 and 2.2.1.2 below). Real imaging was first provided by the Hard X-ray Imaging Spectrometer (HXIS) aboard the SMM, and subsequently by the Hinotori hard X-ray telescopes, (SXT).

The HXIS imaged simultaneously in six energy bands within 3.5-30.0 keV, with temporal resolution between 1.5 and 7 seconds and a spatial resolution of $8'' \times 8''$ (van Beek *et al.*, 1980). The SXT's spatial resolution was $15'' \times 15''$ and the temporal resolution 7 seconds (Oda, 1983; Makishima, 1982; Tsuneta, 1984).

A heated controversy on the interpretation of impulsive phase hard X-ray emission motivated the early studies of hard X-ray images. Two competing models were, and still are, considered. The nonthermal model (Brown, 1971; Lin and Hudson, 1976; Hoyng *et al.*, 1976) postulates that most of the flare energy is carried by a beam of fast electrons which are created within an active region loop and precipitates at its chromospheric footpoints, where it produces hard X-rays by thick target emission. On the other hand a qualitative model was developed, postulating that a large fraction of the hard X-ray emission at low energies (tens of keV) could be due to thermal bremsstrahlung (Brown *et al.*, 1979; Smith and Lilliequist, 1979; Vlahos and Papadopoulos, 1979; Emslie and Vlahos, 1980). This model relies on the possibility of creating a hot source ($T \approx 5 \times 10^8$K), confined by plasma instabilities which lead to ion acoustic turbulence at the expanding conduction fronts which move at the ion sound speed (see discussion on 2.2.6.2).

In the imaging data, for the range of energies covered by the HXIS and SXT, the distinction between the two models is, *ideally*, quite clear (see e.g., Emslie 1981b, and 2.2.1.3 below for the complications). The beam model predicts strong emission at the footpoints of loops, while the dissipative thermal alternate should show a bright, expand-

ing source within the coronal loop, and minor contribution from the footpoints, due to the escaping tail of electrons which traverse the turbulent fronts.

Figure 2.2.1 (from Duijveman *et al.*, 1982) shows that, at least in some cases, the HXIS observations seem to favor the nonthermal model. Widely separated footpoints are seen in three flares shown in the Figure, even as far as 70,000 km away from each other (November 5, 1980 footpoint C in Figure 2.2.1c). These footpoints overlay regions of enhanced chromospheric and transition zone emission, which brighten in temporal coincidence, in ultraviolet radiation, with the hard X-ray peaks (see Canfield *et al.* in this volume and references therein). Duijveman *et al.* (1982) analysed the events and concluded that the observations were consistent only with thick target emission in which the beam power implied a 20% acceleration efficiency during the early impulsive phase.

This result is not general however, and the HINOTORI investigators (Tanaka, 1983; Ohki *et al.*, 1983 and Tsuneta, 1983b) have been able to identify at least three types of hard X-ray flares from the characteristics of the hard X-ray image, spectrum and impulsiveness of the time profile. The general characteristics of the three types (A, B and C) are listed in Table 2.2.1.

The three flares shown in Figure 2.2.1 correspond to the type B, which are typical impulsive burst events. Their duration ranges from tens of seconds to minutes, and the time profile consists of an impulsive phase with spiky structure and effective power law index ranging from 3 to 5, and a gradual phase, generally softer, with smoother structure. During the gradual phase the hard X-ray morphology changes drastically, the footpoints disappear and a single elongated source is seen at high altitude. This behavior of type B flares is shown in Figure 2.2.2 (from Machado, 1983a; see

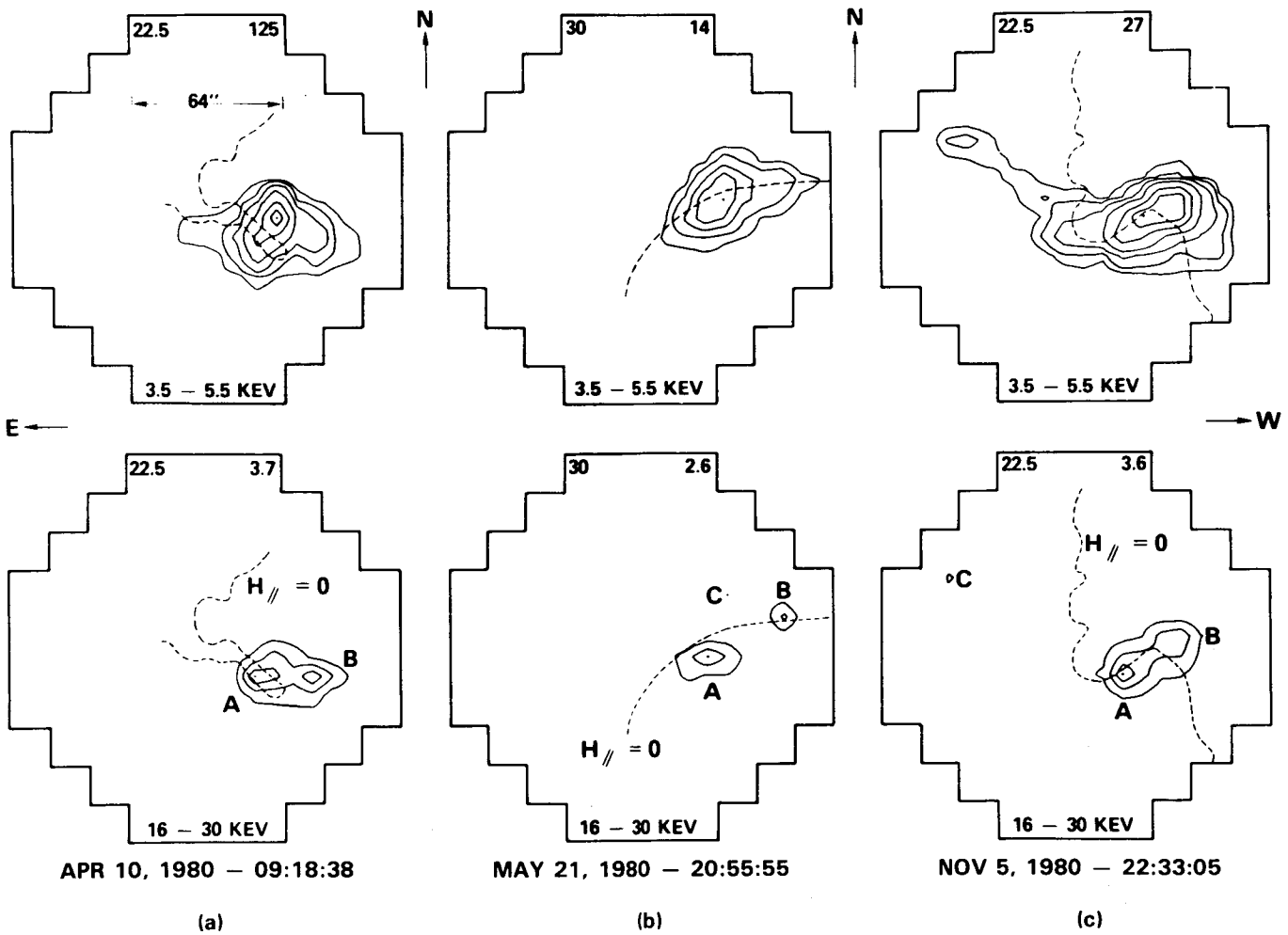

Figure 2.2.1 HXIS contour plots in soft (top) and hard (bottom) X-rays, for three flares discussed by Duijveman *et al.* (1982). The integration is over the impulsive spikes and the dashed lines show the magnetic neutral lines. The hard X-ray footpoints (16 - 30 keV) are labelled as A, B and C.

Table 2.2.1 Main Characteristics of Solar Hard X-Ray Flares

Type	Time Profile ($E \gtrsim 20$ keV)	Hard X-ray spectrum ($E > 15$ keV)	Hard X-ray image ($E \sim 20$ keV)	Electron density (cm^{-3})	Magnetic field strength (Gauss)
A	$E \lesssim 40$ keV intense smooth time profile $E > 50$ keV no substantial emission with small spikes	very soft $\gamma \sim 7$–9 hot plasma ($T = 3\times10^7$ K) ($EM = 10^{49}$ cm^{-3}) dominantly contributed $E \lesssim 40$ keV. FeXXVI emission	small point-like hard X-ray source ($\sim$ 15 arcsec) low altitude ($\sim$ 5000 km)	$\sim 10^{11}$	$\geq$ 330
B	*Impulsive phase* spiky with time scale of sec. *Gradual phase* smooth with time scale of min.	power-law (10 - 70 keV) thermal sp. ($T = 3\times10^7$ K below 40 keV + power-law	footpoint double source coronal loop-like hard X-ray source	$\leq 10^{10}$ $\geq 10^{11}$	550
C	smooth time profile with time scale of min. even above 100 keV	power-law $\gamma \sim 3$ - 5 (30 - 150 keV) systematic hardening even in the decay phase	high altitude ($\sim$ 40000 km) coronal hard X-ray and microwave sources	3×10^{10}	50

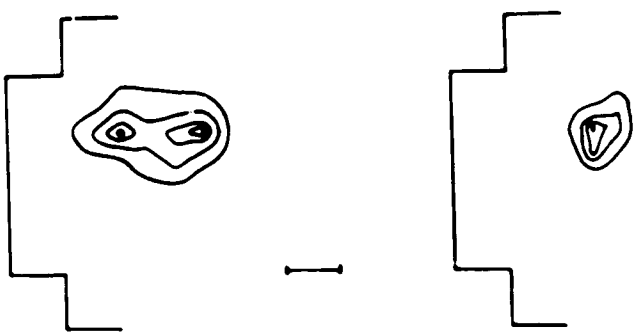

Figure 2.2.2 Hard X-ray (16 to 30 keV) observations of the April 10, 1980 flare. The doubled shaped structure (left) corresponds to the time of the impulsive burst (see Duijveman *et al.* (1982)), and the single structure to the gradual burst (see Machado *et al.* (1982)). The edge of the HXIS field of view is shown as reference. The soft X-ray emission (not shown) encompass the entire region with its maximum located at the position of the gradual component in the second image. The scale corresponds to 16 arc secs.

Machado *et al.*, 1982 for a complete discussion) for the April 10, 1980 event shown in Figure 2.2.1. We see a transition from footpoint to single source morphology of the 16-30 keV sources; similar behavior has been observed in the other two HXIS flares of Figure 2.2.1 (Hoyng *et al.*, 1981; Duijveman *et al.*, 1982 Machado *et al.*, 1984b).

The transition from footpoint to single hard X-ray structure may reflect, as proposed by Machado *et al.* (1982) and Tsuneta (1983b), a change in the mode of the energy release from strong particle acceleration to plasma heating. A possible scenario on the way this may happen is described by Smith (1985, see Section 2.2.6.2) and Tsuneta (1985), but we should also be aware of the limitations of available imaging observations, discussed below. However, before reaching a definite conclusion on this subject, we must keep in mind that *most* of the SMM and HINOTORI type B flares (and all of type A) show single source structure (Duijveman and Hoyng, 1983; Takakura *et al.*, 1985a).

There is, however, good evidence of high temperature plasma components in the gradual phase of *some* flares. These are given by the recent high resolution spectral ob-

servations of an impulsive flare, obtained with a solid state detector (Lin *et al.*, 1981). In the impulsive phase the spectrum is a power law, while in the gradual phase a hot thermal component with $T \approx 3 \times 10^7$K appears as the power law gradually fades. Also, observations of a coronal source seen by the HXIS after the two ribbon flare of May 21, 1980 (cf. later phase of the flare shown in Figure 2.2.1.b), have been interpreted as evidence of a long lasting high temperature ($\geq 4 \times 10^7$K) source (Hoyng *et al.*, 1981; Duijveman, 1983). Duijveman (1983) discussed the heat balance of this source and found that its cooling rate by classical heat conduction would have been much larger than the saturated limit. He finds that the energy needed to maintain the hot source throughout its life time of several minutes is of the same order of magnitude as that needed to maintain the cooler (10^7K) soft X-ray emitting component. These imaging and spectral observations show that high temperature plasma of about 3×10^7K or more is generated during the development of at least some flares.

Further evidence of high temperature components in the hard X-ray emission is given from the analysis of the type A flares. Their integrated hard X-ray emission shows smooth time profiles, a steep power law index (7-9) and a duration $\geq$ 10 minutes. An example of type A flare is the July 17, 1981 flare observed by the HINOTORI (Tsuneta *et al.*, 1984b). Line ratio analysis of the FeXXVI lines, detected throughout the flare development (Tanaka *et al.*, 1982; Moriyama *et al.*, 1983) indicate the presence of 3 to 3.5×10^7K plasma, with emission measure of the order of 10^{49} cm^{-3}. A possible interpretation of this type of flare is that intense heating occurs from the start of the flare, with lesser amount of power being spent in particle acceleration (Tsuneta *et al.*, 1984b). An example of this type of event as observed by the HXIS is the July 14, 1980 event described by Duijveman and Hoyng (1983).

Finally, the type C flares show long lasting time profiles with power law indices of 2 to 5 between 30 and 200 keV, which tend to decrease with time. An example of this type is the May 13, 1981 event (Tsuneta *et al.*, 1984a), when a stationary hard X-ray source was observed at an altitude of $\approx 4 \times 10^4$ km, coincident with a gyrosynchrotron source at 35 GHz (Kawabata *et al.*, 1983). These flares seem to belong to the microwave rich type (Kai and Kosugi, 1985) which are discussed in Section 2.2.4, and show relatively large energy dependent delays in X-rays which we treat in Section 2.2.3.3 and 2.2.6.

A possible interpretation for the type C flares (Tsuneta *et al.*, 1984a) invokes a coronal thick target trap model. As shown in Table 2.2.1 the target density of several type C flares was obtained by assuming that the delay is caused by complete trapping of nonthermal electrons (Bai and Ramaty, 1979; see 2.2.6 below). Also, Yoshimori *et al.* (1983) have found typical time delays of tens of seconds between MeV and lower energy hard X-ray emission while type B flares typically show delays of a few seconds. This may indicate differences in the particle acceleration timescales between type B and C flares. More details on the characteristics of these events can be found in the references we have listed.

It is worth pointing out that only a few events (less than ten total) from each spacecraft can be placed in one of the types mentioned above. The majority of the events observed does not fall in any of the above classes of flares. Thus, we believe that more complex magnetic structures and energization processes are at work during a flare (see discussion in Section 2.2.7).

From the data discussed above, it is clear that hard X-ray imaging has been achieved with SMM and HINOTORI. The imaging, however, is restricted to energies below 25-30 keV, with a spatial resolution of 8'' (5800 km) at most. Let us now discuss some of the implications of these results, looking more closely at the data.

MacKinnon *et al.* (1985) emphasized that analyses of HXIS data to date have not adequately considered instrumental effects and data noise. The claim that three flares (April 10, May 21 and November 5, 1980) display ''footpoint'' emission, and therefore constitute evidence for the thick target beam interpretation of hard X-ray emission, has rested on morphological conclusions drawn from non-deconvolved images. Further, the count levels in these images are sometimes so low that consideration of photon shot noise must lead one to question the reality of morphological features. MacKinnon *et al.* (1984) developed a deconvolution routine, which takes into account all the instrumental effects, by use of the Maximum Entropy (ME) method. The advantages of this method, particularly the way it assesses reality of features are discussed in MacKinnon *et al.* (1984). MacKinnon *et al.* applied the above operation to images produced in the energy range 16-30 keV for the three HXIS flares which showed distinct bright points (Duijveman *et al.*, 1982 and earlier references therein) and concluded that, in the *16-30 keV* range, the presence of distinct bright points is stable to these procedures, and to the addition of noise (although other morphological features may be changed, as may such quantities as ''contrast ratio''); it should also be stated that this is not always true in the *20-30 keV* range due to poor counts statistics.

Further, evidence for distinct bright points has taken the form of comparison of individual pixel time profiles, either to establish simultaneity of footpoint brightening or to distinguish the footpoint pixels from their neighbors (see Duijveman *et al.*, 1982). MacKinnon *et al.* have investigated these conclusions quantitatively using cross-correlation coefficients. These findings, detailed in MacKinnon *et al.* (1984), vary slightly over the three flares, but in general they find that such comparisons do not serve to distinguish the ''footpoints'' either because the count statistics are not good enough, or because other, non-footpoint pixels also brighten simultaneously. Finally, they emphasize that all the above

conclusions are based on band 5 data (16-30 keV), since the lower bands are not really "hard" X-rays. However, it has been pointed out that the correlation of points A and C in the November 5, 1980 (see Figure 2.2.1) flare is well borne out in the lower energy channels where the number of counts is much higher. MacKinnon *et al.* feel that this must be a question which requires careful consideration, in view of the undoubted role of hot (a few $\times$ 10^7K) thermal plasmas in these energy bands.

2.2.1.2 Stereoscopic Observation

Simultaneous observations of solar hard X-ray bursts from two widely separated spacecrafts has recently offered new possibilities for testing source models, in terms of both directivity and spatial distribution of the emission (Kane *et al.*, 1979, 1982; Kane, 1981b). Such stereoscopic observations of the sun, using the ISEE-3 and PVO spacecraft, have shown that most of the impulsive hard X-ray emission originates at altitudes $\lesssim$ 2500 km above the photosphere (see Figure 2.2.3). The five events analyzed so far fall into two groups according to the occultation altitude involved. First, there is the series of three successive events occuring in a single active region on November 5, 1979, which were occulted from PVO at low chromospheric altitudes, increasing from about zero for the first event to about 2500 km for the third, due to the rotation of the Sun (Kane *et al.*, 1982). For each of these events the ratio of occulted to unocculted flux was evaluated at photon energies of 150 and 350 keV, and for the third event the time evolution of this ratio was determined. Second, there are two events (October 5, 1978 and September 14, 1979) for which the occultation altitudes are coronal (25,000 km and 30,000 km respectively). Flux ratios are again available at two energies and their time evolution is known for the September 14 event. The main conclusions are: (a) about 90% of the impulsive X-ray emission and about 70% of gradual (extended) X-ray emission originate at altitudes $\lesssim$ 2500 km above the photosphere. In the 100-500 keV range, this altitude dependence is essentially independent of photon energy. (b) The brightness of the impulsive X-ray source decreases rapidly with increase in altitude, in a manner similar to that shown in Figure 2.2.3.

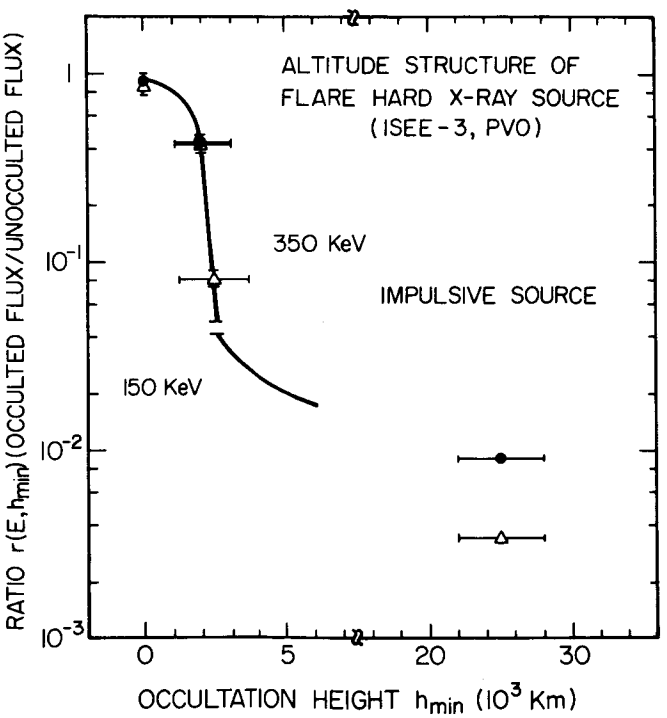

Figure 2.2.3 The ratio r(E, h_{min}) of occulted to unocculted X-ray flux plotted against the minimum altitude h_{min} observable from the occulted spacecraft (from Kane, 1983).

2.2.1.3 Implications of Hard X-ray Imaging and Stereoscopic Observations

Following the work of Brown and McClymont (1976) and Emslie (1981b), Machado *et al.* (1985) have computed the spatial distribution of hard X-rays in flare loops and the chromosphere by applying Brown and McClymont's method to the analysis of some well-observed SMM flares. Their results show that, due to the combination of spatial resolution and rather low energy imaging, only under particular circumstances could chromospheric footpoints be seen in the images. This is readily seen from the fact that, under the best conditions,the flare loops have to cover three HXIS pixels (i.e. $\geq$ 15000 km) to be able to show separated footpoints. This implies that in order to have a strong chromosphere brightening at 20 keV, electrons with similar or higher energy must have a collisional mean free path equal to or larger than the above distance, or in other words the loop densities should be $\leq 4 \times 10^{10}$ cm^{-3}.

A transition from footpoints to single source hard X-ray structures was observed (cf. 2.2.1.1) in the November 5, 1980 flare studied by Duijveman *et al.* (1982). This transition occurred within the main flare region, where footpoints A and B were observed in the early flare phase. Figure 2.2.4 shows a light curve of the hard X-ray emission of the event, in which two hard X-ray peaks, P1 and P2, have been defined. P1 corresponds to the time when the footpoints were observed, while P2 (more gradual and softer) shows a single source in the hard X-ray (16-30 kev) images which is located between the two footpoints, coinciding with the locus of maximum emission in the soft X-ray images. An approximate estimate of the flare volume V $\approx 2.3 \times 10^{26}$ cm^3 can be obtained, leading to densities n(P1) $\approx 5 \times 10^{10}$ cm^{-3} and n(P2) $\approx 10^{11}$ cm^{-3} of the loop plasma during each peak (the density increase is presumably due to chromospheric evaporation). These densities are a lower limit, since a filling factor $\simeq$ 1 is assumed (see Wolfson *et al.* (1983) for a critical discussion). The expected spatial distribution of hard

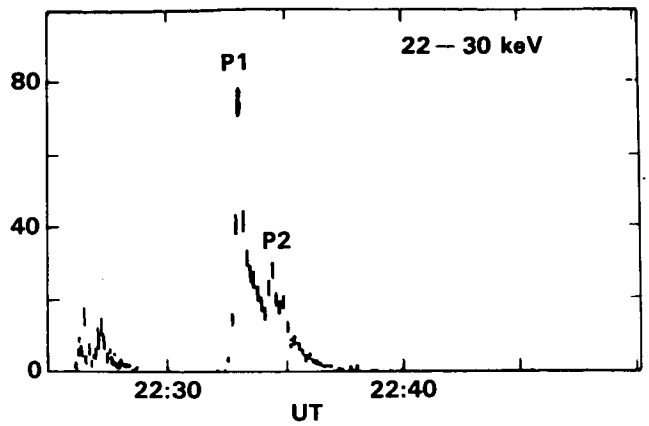

Figure 2.2.4 Hard X-ray emission light curves of the November 5, 1980 event. In the 22-30 keV lightcurve the two peaks are marked with P1 and P2 and correspond to the the points that the spatial distribution of hard X-rays has been computed.

X-rays can be calculated under simplified assumptions (cf. Brown and McClymont, 1976; Machado *et al.*, 1985) of the predominance of Coulomb losses and parallel injection of electrons along field lines. We should note that this is the most favorable case for footpoint prediction, since it neglects any effect (like e.g., pitch angle distribution, Leach and Petrosian, 1981) that could increase beam stopping.

Machado *et al.* (1985) calculated the intensity distribution of hard X-rays using idealized loop models. They analyzed three different models for the energy release (see Figure 2.2.5a). Case A represents a situation in which the acceleration site is located at the boundary between two pixels, presumably at the loop's apex, and the beam strength is symmetrical towards both sides. In case B it has been assumed that the acceleration region is at the middle of a pixel, and the beam is predominantly towards one side of the loop. Finally, in case C, the acceleration site is also located at the middle of a pixel, but beam strengths towards both sides are equal. The boxes shown in Figure 2.2.5a represent the pix-

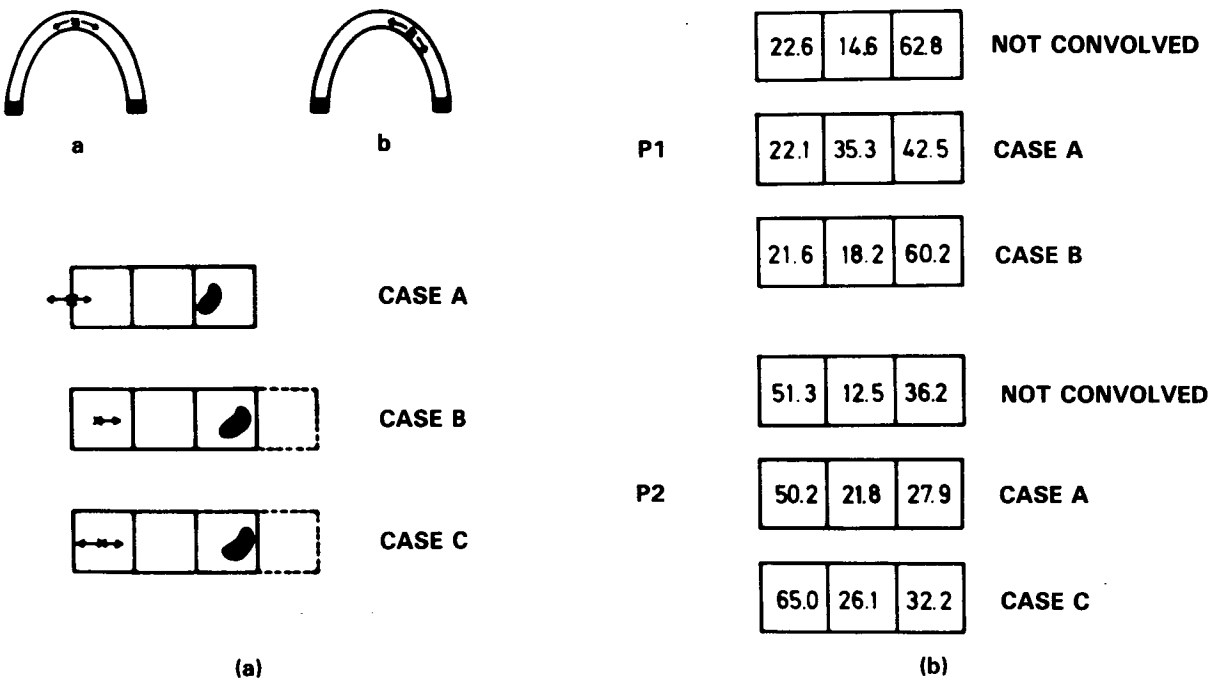

Figure 2.2.5 (a) The three cases of convolution discussed in the text. The cross marks the place where particle acceleration is presumed to occur and the arrows the predominant direction of beam injection. The shaded area in the third pixel is the chromospheric footpoint, which is assumed to be smaller than a HXIS 8″ × 8″ pixel and is shifted in location across the "footpoint pixel". Note that in cases B and C, due to its spatial overlap with its neighbor to the right, a fourth pixel should contain part of the footpoint emission. (b) Result of the intensity distribution of hard X-rays in percentage of the total emission. Cases A, B and C correspond to those shown in Figure 2.2.1. The "footpoint pixel" contains the total of the emission which should be spread in two (see cases B and C of Figure 2.2.1). Note the strong changes that can be expected by changing the location of the acceleration source and/or the footpoint location. In particular case A of P1 shows a large change in the brightness of the pixel located to the left of the footpoint, and case C of P2 the increase in brightness of the loop source.

els from the HXIS instrument, the total emission over half of a loop length assumed to cover two HXIS 8″ pixels and the third pixel from the left is the "footpoint pixel". The "footpoint pixel" shows the emission of the chromospheric part of the hard X-ray distribution. In Figure 2.2.5b Machado *et al.* displayed the percentage of the total emission for all three cases using a photon energy $\epsilon = 19$ keV. These idealized calculations clearly show a transition from footpoint to predominantly single structure in the hard X-ray distribution of P1 and P2. We also present in Figure 2.2.5b the results obtained from the convolution of the unconvolved distribution (c.f. earlier comments and Svestka *et al.*, 1983). The general result here is that the convolution tends to *decrease* the footpoint/loop brightness ratio, a result consistent with the observations reported by Duijveman *et al.* (1982), Hoyng *et al.* (1981) and Machado *et al.* (1982). The Machado *et al.* results tend to reinforce the conclusions about the reality of hard X-ray footpoints, and provide a warning against the direct interpretation of single hard X-ray sources as indicative of regions heated by a mechanism different from the one leading to acceleration (cf. implications of footpoint to single source transition in type B flares).

Another important aspect to take into account is the heating effect of beam particles along the loop, due to Coulomb collisions with the ambient plasma. Calculations of energy deposition rate as a function of column density, $N(cm^{-2})$, have been performed by many authors (Brown, 1972, 1973; Lin and Hudson, 1976; Emslie, 1978, 1980, 1983), generally in connection with chromospheric heating calculations. Machado *et al.* (1985) have been able to show that in the cases of high-density flare loops (like e.g., the July 14, 1980 event described by Duijveman and Hoyng, 1983) single sources are not only likely to appear because of particle stopping within the loop and high efficiency in the nonthermal bremsstrahlung production, but also because their localized heating causes an increase in the thermal contribution to the hard X-ray output below 25 keV (note also that if the heating is very large it invalidates the condition $E >> E_{th}$ of the thick target approximation, where E is the particle's energy and E_{th} the mean thermal energy of the particles in the target). It is also worth noting that these single source (type A or C) flares often show less "spiky" time profiles, which can result as a natural consequence of the fact that the temporal behavior is no longer exclusively related to time variations in the beam intensity but also to the conductive cooling timescale of the heated regions. A detailed analysis of this latter possibility has not yet been carried out. An alternative for the beam induced heating may also be related to the opposite case, i.e. low loop densities, which can lead to beam - plasma - return current instabilities and increase the beam losses due to non-collisional effects, (Vlahos and Rowland (1984), Rowland and Vlahos (1984)). This is another field in which more work is needed before reaching definite conclusions.

Machado *et al.* concluded that, in spite of the instrumental limitations, the presence of footpoints in the hard X-ray images, seems to give support to the thick target interpretation of the bursts. MacKinnon *et al.* (1985) on the other hand, feel that no aspect of the images demands such an interpretation uniquely, and find that some aspects of the data are difficult to accommodate in any conventional (thick target or dissipative thermal) model.

There are several pieces of evidence that indicate that a substantial fraction of the low energy ($E < 30$ keV) impulsive emission in flares is not purely due to thick target bremsstrahlung. Machado (1983b) reached this conclusion by the analysis of the energy and particle content of a compact flare loop, where a pure thick target analysis was shown to be incompatible with the parameters derived from the soft X-ray plasma.

Brown *et al.* (1983b), from the analysis of stereoscopic observations, find that the detailed quantitative dependence of occultation ratio on height, energy and time are not compatible with the basic thick target model as the sole source of the hard X-rays. Either emission from thermal sources or from magnetically trapped electrons have to be invoked to explain the observations.

Finally, Machado and Lerner (1984) re-analyzed the observations of a limb flare of April 13, 1980, which showed a bright X-ray (16-30 keV) source at the boundary between two distinct magnetic structures (see Machado *et al.*, 1983). They find that the spatial distribution in intensity and spectral behavior of the hard X-rays is incompatible with a pure nonthermal interpretation. They conclude that a large fraction ($> 50\%$) of the emission in the 20 keV range is due to thermal bremsstrahlung of plasma with temperatures $> 5 \times 10^7$K. The spatial distribution of the emission leads them to propose that the site of the maximum hard X-ray brightness is located where energy is released (at the region of interconnection between two field structures) both in the form of heating and particle acceleration.

2.2.2 Microwave Source Structure, Location and Development

Accelerated electrons produce microwave radiation through their interaction with the magnetic field. High resolution observations at cm-wavelengths have given important information about the magnetic structure of the flaring region. Observations at several frequencies can, in principle, provide valuable diagnostics of both the magnetic field and the distribution function of the energetic electrons as a function of time. However, so far there have been very few multifrequency observations at high spatial resolution and consequently the discussion has been focused on the diagnosis of the magnetic field configuration.

Two dimensional images with the Very Large Array (VLA) radio telescope suggest that interacting magnetic loops

and magnetic field reconnection have important roles to play in solar flares. This can occur as a result of emergence of new flux interacting with pre-existing flux, or as a consequence of rearrangement and/or reactivation (e.g., twisting) of two or more systems of loops. Kundu (1981) illustrated this phenomenon with a set of 6 cm observations made with the VLA (spatial resolution $\sim 2''$) that pertains to changes in the coronal magnetic field configurations that took place before the onset of an impulsive burst observed on 14 May 1980 (Kundu, 1981; Kundu *et al.*, 1982; Velusamy and Kundu, 1982). The burst appeared as a gradual component on which was superimposed a strong impulsive phase (duration $\sim$ 2 minutes) in coincidence with a hard X-ray burst. Soft X-ray emission (1.6-25 keV) was associated with the gradual 6 cm burst (before the impulsive burst), as is to be expected. There was a delay of hard X-ray emission ($>$ 28 keV) relative to 6 cm emission. The most remarkable feature of the 6 cm burst source evolution was that an intense emission extending along the north-south neutral line, possible due to reconnections, appeared, just before the impulsive burst occurred, as opposed to the preflare and initial gradual emission being extended along an east-west neutral line. This north-south neutral line must be indicative of the appearance of a new system of loops. Ultimately the loop systems changed and developed into a quadrupole structure near the impulsive peak. This field configuration is reminiscent of flare models in which current sheet develops at the interface between two closed loops. The impulsive energy release must have occurred due to magnetic reconnection of the field lines connecting the two oppositely polarised bipolar regions (Kundu *et al.*, 1982).

A second burst observed by Kundu *et al.* 1984 on 24 June 1980, 19:57 UT provides a good example of interacting loops being involved in triggering the onset of a 6 cm impulsive flare associated with a hard X-ray burst. It also provides evidence of preflare polarization changes on time scales of a minute or so, which may be related to coronal magnetic field configurations responsible for triggering the burst. The 6 cm burst source is complex, consisting initially of two oppositely polarized bipolar sources separated E-W by $\sim 1.5'$ arc. The first brightening occurs in one component at 19:57:10 UT, the western component being much weaker at this time. It then brightens up at 19:58:05 UT, just at the onset of the impulsive rise of the burst and is accompanied by changes in its polarization structure. It then decays and splits into two weak sources separated E-W by $\sim 12''$ arc. The eastern component brightens up at 19:58:41 UT, accompanied by significant polarization changes, including reversal of polarization. A third component appears approximately midway between the eastern and western component at 19:58:45 UT during the peak of the associated hard X-ray burst. The appearance of this source is again associated with polarization changes, in particular the clear appearance of several bipolar loops; its location overlaps two opposite polarities implying that it might be situated near the top of a loop. During the peak of the associated hard X-ray burst (1980 June 24, 19:57:00 event), a third (perhaps another bipolar) loop appears in between the previous two sources. Kundu believes that we are dealing with interaction between multiple loop structures, resultant formation of current sheets and magnetic field reconnection, which is responsible for the acceleration of electrons.

Lantos, Pick and Kundu (1984) combined observations of three solar radiobursts obtained with the VLA at 6 cm wavelength and with Nancay Radioheliograph at 1.77m. A small change in the centimetric burst location by about 10″ arc corresponds to a large change by about 0.5 R_O in the related metric location. The metric bursts occur successively at two different locations separated by about 3.10^5 km. During the same period, an important change in the microwave burst source is observed. This may indicate the existence of discrete injection/acceleration regions and the presence of very divergent magnetic fields in agreement with the suggestions made by Kane *et al.* (1980).

The Westerbork Synthesis Radio Telescope (WSRT) was used by Alissandrakis and Kundu (1985) for solar observations at 6.16 cm with a spatial resolution as good as 3″ and a time resolution of 10 sec. In spite of the limitations of one-dimensional fan-beam scans in total intensity (I) and circular polarization (V) of burst sources, several interesting features could be discovered in their structure.

Out of the 76 bursts observed, 57% consisted of two or more components in total intensity. An example of a burst with two components is shown in Figure 2.2.6a,b, where contours of 1-D brightness temperature as a function of position and time are plotted. In total intensity (I), the burst consists of two impulsive components, A and B, with their peaks separated by 26″ and a total duration of about 4 minutes. The peaks are almost simultaneous with a possible delay of component B by no more than 5 sec with respect to component A. Component A is fairly symmetric with a width of 7″ and a maximum 1-D brightness temperature of 6.5×10^7K arc sec above the background; assuming a circular shape this value corresponds to a brightness temperature of about 10^7K. The other component is asymmetric with a width of 11″ and an estimated brightness temperature of about 4×10^6K. Alissandrakis and Kundu pointed out that near the maximum the two components appear to be connected by a bridge of low intensity emission. Such interconnections between burst components are the rule rather than the exception in their sample of bursts. In the example shown there is a definite extension of component B is the direction of component A. The circular polarization map shows that both components, as well as the bridge between them are polarized. Component A shows two peaks of opposite sense with the total intensity peak coinciding with the region of zero polarization; the degree of polarization at the V peaks is about 50%. The polarization of the other component is

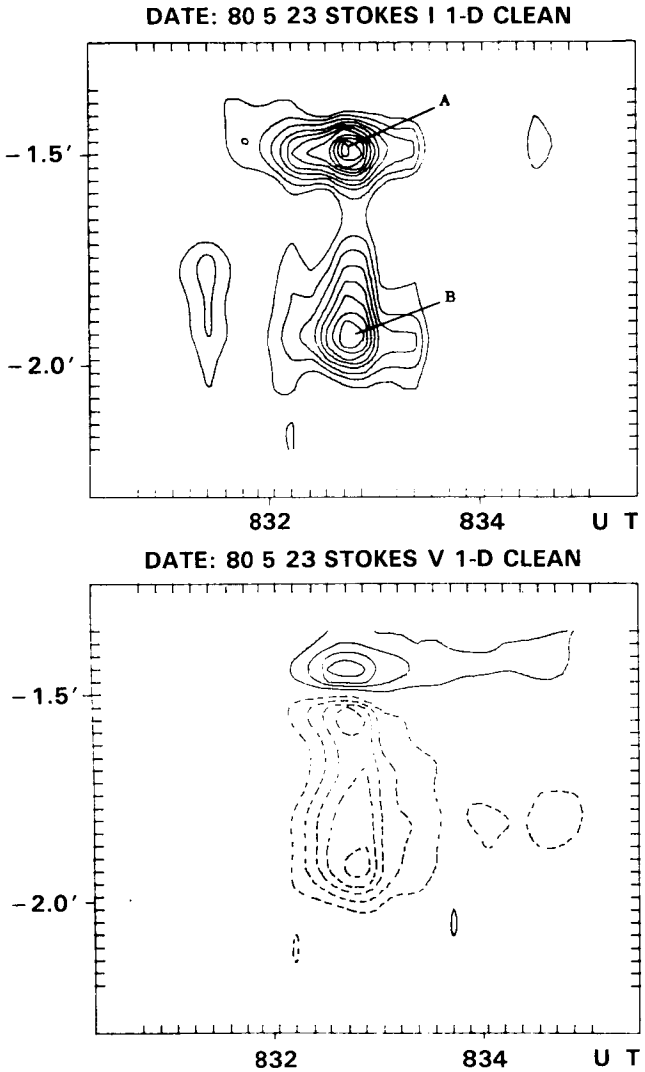

Figure 2.2.6 A two component burst observed with the WSRT at 6.16 cm. (a) The contours of equal brightness temperature (integrated in the direction perpendicular to the resolution) as a function of one-dimensional position and time in Stokes parameters I and V. (b) The I map is 10^7K arcsec with a contour interval of 0.5 × 10^7K arcsec, while the V map the lowest contour and the counter interval are 0.3 × 10^7K arcsec. Dashed lines show negative (left handed) circular polarization (from Alissandrakis and Kundu, 1985).

uniform with a 40% maximum near the I maximum. The sense of polarization of component B is the same as that of the nearest V peak of component A, as well as that of the bridge; the latter is almost 100% polarized. Such a polarization structure of 6 cm burst sources is quite common.

If we assume that the sense of circular polarization corresponds to the polarity of the magnetic field, we can interpret the observations in terms of a small flaring loop, corresponding to component A and a larger loop connecting component A with component B. The large loop emits mainly at the footpoints with some emission from the rest of the loop which corresponds to the bridge; the emission from the top of the large loop is weak because it is located higher in the corona where the magnetic field is weak. This scenario is similar to the schematic model presented by Kundu and Shevgaonkar (1985) for the impulsive onset of the microwave burst radiation as a result of two interesting loops. However, as pointed out by Alissandrakis and Preka-Papadema (1984) that the observed sense of circular polarization can be influenced by propagation effects in the corona outside of the flaring region, so that the polarization-inversion line does not necessarily coincide with the neutral line of the magnetic field. If polarization inversion does indeed take place, the observations can also be interpreted in terms of a single large loop connecting the two components and radiating predominantly at the footpoints.

Using the Nobeyama 17-GHz interferometer Nakajima *et al.*, (1984a) observed on November 8, 1980 a microwave burst occurring at a site (Hale region 17255) 8 × 10^5 km remote from the primary flare site (Hale region 17244). The time profiles of the secondary microwave bursts are similar in form to the primary bursts even in details. The overall time profiles of the secondary microwave bursts are delayed relative to those of the primary bursts by 11 or 25 secs. The velocity of a triggering agent inferred from this delay and the spatial separation is about 4 × 10^4 or 8 × 10^4 km s^{-1} and therefore is probably due to fast electrons which were transferred from the primary site to the secondary site along a huge coronal loop. The SMM-HXIS data showed that a new X-ray loop was excited in the region adjacent to the secondary microwave source. The X-ray loop was associated with a faint, compact Hα brightening at its footpoints. The event occurred twice with a similar behavior within a time interval of ~ 40 min and therefore the occurrence of the correlated events is not random. The observations suggest that a new flare (a sympathetic flare) was triggered at the secondary site by an energetic electron stream from the primary site. Similar observations were first reported by Kundu, Rust and Bobrowsky (1982) for a flare observed on May 14, 1980, with practically the same conclusions.

Heights and sizes of microwave burst sources at 17 GHz were obtained as shown in Figure 2.2.7. The events were selected from those which were observed with the 17 GHz one-dimensional interferometer between October 1978 and February 1981. An additional selection condition is that the longitude of the associated Hα flare is $\geq 70°$ and the peak flux density at 17 GHz is ≥ 50 sfu. The heights were estimated on the assumption that the microwave sources were above the corresponding Hα flares. Both the heights and sizes of the impulsive bursts (12 events) are roughly correlated and range from about 10 to 20 arc sec above the photosphere with an average value of 13 arc sec (10^4 km). The long-

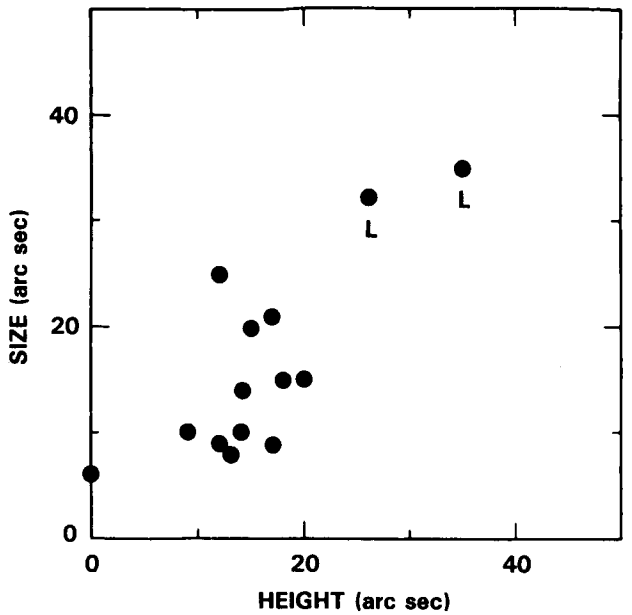

Figure 2.2.7 Heights and sizes of microwave burst sources at 17 GHz. L indicates long-enduring burst. The remaining events are impulsive (from Nakajima *et al.* (1984a)).

enduring bursts (2 events) are located higher (30 arc sec) and larger (35 arc sec) in size as compared to those of the impulsive bursts. Although SMM-HXIS and HINOTORI-SXT hard X-ray imaging observations show in several cases that the hard X-ray component of the impulsive burst is located in the chromosphere (e.g., Duijveman, Hoyng, and Machado, 1982; Tsuneta *et al.*, 1983), the observations reported by Nakajima *et al.*, 1984a show that the microwave emission from the impulsive burst comes from the corona. The VLA observations have often shown a compact (very small compared to the distance between Hα kernels) source of the impulsive bursts located spatially between Hα kernels (Marsh and Hurford, 1980; Velusamy and Kundu, 1982; Hoyng *et al.*, 1983). On the other hand, the observation reported above shows that the source size and height are roughly the same. The height observations of the long-enduring bursts confirm the results reported by Kosugi *et al.* (1983) and Kawabata *et al.* (1983).

2.2.3 Time Structures and Time Delays in Radio and Hard X-rays

2.2.3.1 Centimeter-Decimeter Millisecond Pulses and Electron Cyclotron Masering

Spikes of durations less than 100 ms are well known in the 200 - 3000 MHz radio band. At meter wavelengths some have been reported near the starting frequency of type III bursts (Benz *et al.*, 1982), at decimeter wavelengths as a part of type IV events (Dröge, 1977) and at centimeter wavelengths superposed on a gradual event (Slottje, 1978). In an analysis of 600 short decimetric events (excluding type IV's), Benz, Aschwanden and Wiehl (1984) have found 36 events consisting only of spikes. An example of the data is presented in the Figure 2.2.8 together with a hard X-ray time profile and a blow-up of some single spikes. A detailed analysis (Benz, 1984) shows that the groups of spikes are always associated with groups of metric type III bursts. The spikes tend to occur in the early phase of the type III groups and predominantly in the rising phase of hard X-rays. The half-power duration of the spikes is less than 100 ms, the time resolution of the instrument used. The spectrum of the spikes has been recorded and the typical half-power widths are 3-10 MHz at 500 MHz, i.e. about 1% of the center frequency. This puts a severe constraint on the spectral width of the radio emission and therefore on the generating mechanism. The most plausible interpretation is emission at the electron cyclotron frequency or harmonic (e.g., upper hybrid wave emission or cyclotron maser). Even then, the requirement on the homogeneity of the source is formidable: assuming a locally homogeneous corona with a magnetic field scale length of 10,000 km, the source size in the direction of the field gradient must be equal to or less than 100 km. This is less than the upper limit of the size imposed by time variation. Assuming this dimension for the lateral extent of the source, the lower limit of brightness temperature is up to 10^{15}K. Provided that the emission is radiated close to the plasma frequency, the source density amounts to about 3×10^9 cm^{-3}. The spikes have peak fluxes of up to 800 sfu and are circularly polarized. The polarization ranges from 25-100%. The sense of polarization is righthanded, opposite to most type III bursts occurring at lower frequencies at the same time.

The high brightness temperature of short duration (1-100 msec) spikes observed during the impulsive phase of some flares at microwave frequencies ($\sim$ 3 GHz) indicates that a coherent radiation mechanism is responsible. Coherent plasma radiation at the electron plasma frequency was originally suggested as the radiation mechanism (Slottje, 1978; Kuijpers, van der Post, and Slottje, 1981). Holman, Eichler and Kundu (1980) argued that electron cyclotron masering at frequencies just above the electron gyrofrequency or its second or third harmonic was a likely mechanism for the spike emission. As a third possibility, coherent emission at twice the upper hybrid frequency, has been suggested by Vlahos, Sharma and Papadopoulos (1983). Electron cyclotron masering has been the most highly studied of the three mechanisms. The mirroring of suprathermal electrons in a flaring loop naturally leads to a loss-cone particle distribution, which is unstable to electron cyclotron maser emission (Wu and Lee, 1979). The attractive features of this mechanism are that it is a linear process, not requiring wave-wave interactions, and the conditions for it to operate are essen-

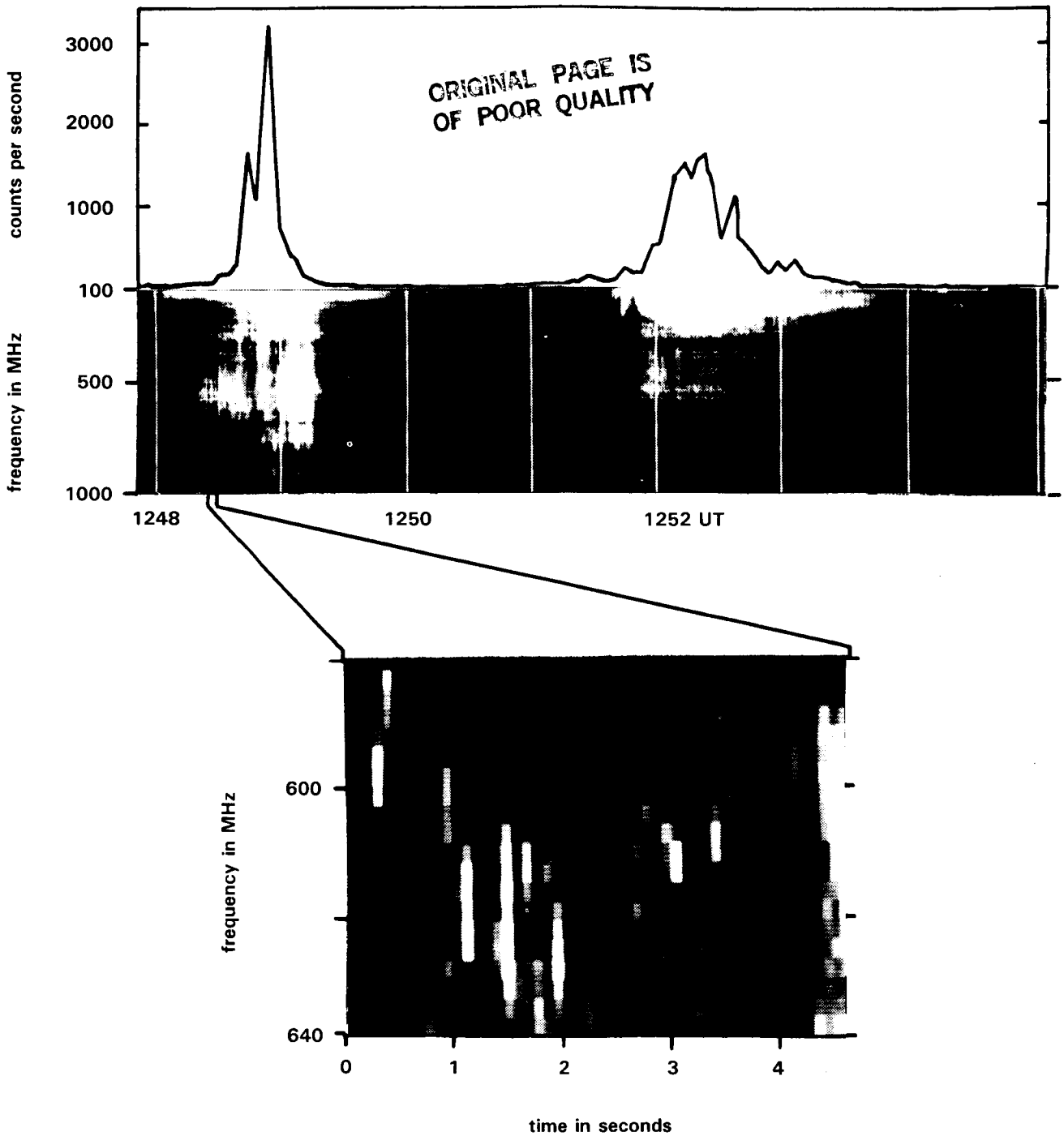

Figure 2.2.8 Top: Composed figure showing hard X-ray counts (> 30 keV, observed by HXRBS on board the Solar Maximum Mission) vs. time, of the double flare of August 31, 1980 and radio spectrogram registered by the analog spectrograph at Bleien (Zürich). The spectrogram shows type III bursts at low frequency having starting frequencies in correlation with the X-ray flux and spike activity above 300 MHz. Bottom: Blow-up of a small fraction of spectrogram produced from data of the digital spectrometer at Bleien (Zürich). The blow-up shows single spikes which are resolved in frequency (from Benz, 1984).

tially the same as those required for an incoherent microwave source: trapped, mildly relativistic electrons (roughly the same number as required for the incoherent emission) with moderately high pitch angles. The masering occurs as long as the loss-cone distribution of the mirrored electrons is maintained. As shown by Melrose and Dulk (1982) and Sharma, Vlahos, and Papadopoulos (1982), the saturated level of the emission is sufficient to provide the observed high brightness temperatures. The emission must escape thermal cyclotron absorption at the next higher harmonic, however, and this requirement favors second harmonic emission, since emission at the fundamental will generally not be able to escape the second harmonic absorption layer. Growth of the first harmonic poses a problem for second harmonic emission however, since the first harmonic growth can saturate the maser before the second harmonic is able to grow significantly. Sharma *et al.* (1982) and Sharma and Vlahos (1984) have shown that the first harmonic, extraordinary mode growth will be suppressed by the ambient thermal plasma if $\omega_e \gtrsim 0.4\,\Omega_c$, ($\omega_e$ is the plasma frequency; Ω_c is the gyrofrequency). The growth of the first harmonic ordinary mode is still large, however, so the conditions under which the second harmonic emission can grow and escape are still not entirely clear. Vlahos and Sharma (1984) analyzed the role of the filling of the loss-cone distribution and suggested that loss-cone driven electron cyclotron emission will be localized at the bottom of the corona and the emitted radiation will have a narrow bandwidth. This is in agreement with the observations reported above.

Finally, in a recent study Zaitsev, Stepanov and Sterlin (1985) suggested that the millisecond pulsations are due to a non-linear induced scattering of plasma waves by background plasma ions. They reduced the coupled non-linear system of equations, that describe the wave-particle interactions, to the well known Voltera equations which describe the "predator-prey" problem. The duration of the pulses (a few milliseconds) is used to determine the density of the energetic electrons that cause the radio emission.

2.2.3.2 Ultrafast Time Structure in Microwaves and Hard X-rays and their Time Delays

The use of antennas with large collecting areas has considerably improved the observation of solar bursts at centimeter and millimeter wavelengths with high sensitivity and time resolution (Kaufmann *et al.*, 1975, 1982a; Butz *et al.*, 1976; Tapping, 1983). The 45 ft. diameter radome-enclosed radio telescope, at Itapetinga, Brazil, operating at 22 GHz and 44 GHz, was extensively used during the period of SMM operation, providing high sensitivity (0.03 s.f.u. in single linear polarization) and high time resolution (1 ms) data; these data revealed new aspects of low level solar activity as well as fine time structures in larger bursts. In practically all the bursts studied with high sensitivity at mm-cm wavelengths, fine time structures (< 1 sec) were identified superimposed on the slower time structures (seconds). The repetition rate of the ultrafast structures appear to be higher, for higher mean fluxes of 22 GHz bursts (see Figure 2.2.9). Kaufmann *et al.* (1980a, 1980b) suggested a possible interpretation of this behavior in terms of a quasi-quantization in energy of the burst response to the energetic injections. A similar suggestion was made earlier from the statistical properties of a collection of X-ray bursts ($\sim$ 10 keV) (Kaufmann *et al.*, 1978). A trend similar to that shown in Figure 2.2.9 was found independently at 10.6 GHz (Wiehl and Matzler, 1980) but for bursts with larger flux and timescales. Kaufmann *et al.* (1980a) showed that for a given burst flux level S at 22 GHz there is a minimum repetition rate of ultrafast structures R, such as $S \leq k.R$, where k is a constant. One of the faster repetition rates was found at the peak of an intense spike-like burst (Figure 2.2.10) which was also observed in hard X-rays by SMM-HXRBS (Kaufmann *et al.*, 1984). A striking example obtained simultaneously in microwaves and hard X-rays is the burst of November 4, 1981 at 1928 UT (Takakura *et al.*, 1983b).

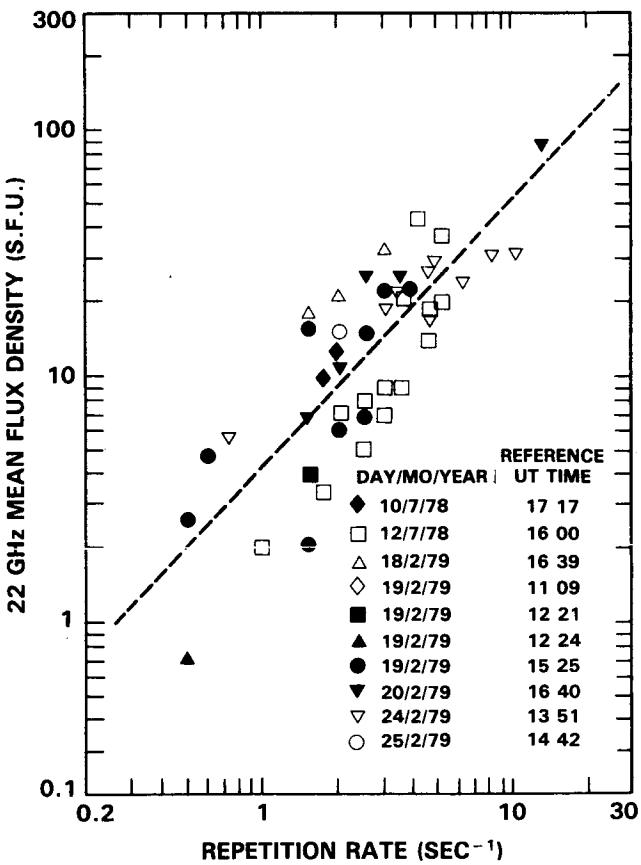

Figure 2.2.9 Scatter diagram of repetition rates $R(s^{-1})$ of fast time structures superimposed on solar bursts at 22 GHz against the mean flux value S (s.f.u.) for various bursts observed in 1978-1979 with the 13.7-m Itapetinga antenna (from Kaufmann *et al.*, 1980a).

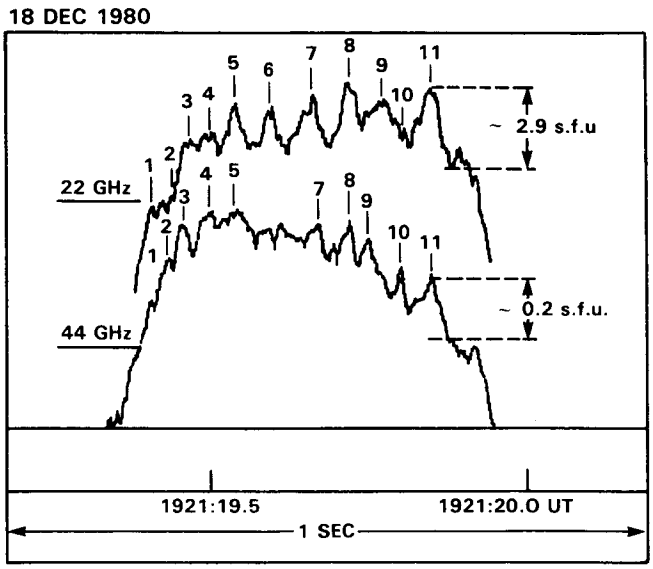

Figure 2.2.10 One-second section at the peak of an intense spike-like burst, displaying ultrafast time structures repeating every 30-60 ms at 22 GHz and 44 GHz (from Kaufmann *et al.*, 1984).

High sensitivity 10.6 GHz data for the same burst was obtained with the 45-m antenna at Algonquin Radio Observatory, (Tapping, private communication). The presence of a "ripple" is evident at all microwave frequencies and is very significant at 30-40 keV range (HINOTORI-HXM). The ripple relative amplitude ($\Delta S/S$) is about 30% at 30-40 keV, 1% at 22 and 44 GHz and 0.4% at 10.6 GHz. The aparent lack of phase agreement for certain peaks might or might not be real. Confirmation of a nearly one-to-one correspondence of mm-cm vs hard X-ray association of superimposed ripples was obtained for the November 13, 1981, 1102 UT burst. The most important findings of such studies are: (a) the slow time structure (seconds) are often poorly correlated, or not correlated, between the four microwaves frequencies (7, 10.6, 22 and 44 GHz) and 30-40 keV X-rays; (b) the superimposed "ripple" components are present and correlated (although phase differences might be present) in data obtained simultaneously by two radio observatories widely separated from each other (Brazil and Canada) and by the HINOTORI-HXM X-ray experiment.

The time structures in complex microwave bursts are frequently not correlated in time at various frequencies. Delays of peak emission at different microwave frequencies range from near coincidence to 3 sec, both toward higher and lower frequencies (Kaufmann *et al.*, 1980a; 1982b). Delays toward lower frequencies only have been reported by Uralov and Nefed'ev (1976) and Wiehl *et al.* (1980). One long-lasting pulsating burst (quasi-period 0.15 sec) has shown a systematic delay of 300 ms for 44 GHz pulses relative to 22 GHz pulses (Zodi *et al.*, 1984). It might be meaningful, however, to stress that the faster time structures found seem to be well correlated (as the case of the "ripple" structures discussed above). In relation to hard X-rays, the microwave burst emission time structures often appear delayed in time. For relatively slower (and smoothed) time structures, the hard X-rays appear to occur 1-2 sec prior to microwave emission (Crannell *et al.*, 1978).

There are several ways to intepret the time delays reported above, for example, convolution effects of multiple emitting kernels (Brown *et al.*, 1980, 1983a; MacKinnon and Brown, 1984, see also discussion on Section 2.2.6.2) or the fact that microwave emitting source may move in a varying magnetic field (Costa and Kaufmann, 1983) are among the suggested candidates. For the large delays between the microwave and hard X-ray peaks (several seconds), it has been suggested that microwave emission originates from another population than the one that produces the X-rays (Tandberg-Hanssen *et al.*, 1984). Finally, the long-enduring persistent quasi-periodic pulsations in bursts, presenting pseudo-delays at different microwave frequencies, might be a phenomenon of a different nature, and might be conceived as due to simple modulation of synchrotron emission by a varying magnetic field (Gaizauskas and Tapping, 1980; Zodi *et al.*, 1984). Some bursts appear to be strictly coincident in time, at various microwave frequencies and X-ray energy ranges (to less than $<$ 100 ms) (Kaufmann *et al.*, 1984).

The impulsive phase X-ray and microwave emission, examined with high sensitivity and high time resolution put several constraints on the models of the bursting region. Among the new observations that require theoretical interpretations are the "ripple" structures, the trend of flux vs. repetition rates, and the possible quasi-quantized energetic injections. Sturrock *et al.* (1985) suggest that "elementary flare bursts" may arise from the energy release of an array of "elementary flux tubes", which are nearly "quantized" in flux. As a stochastic process of reconnection sets in, by mode interaction, explosive reconnection of magnetic islands may develop in each tube, accounting for the ultrafast time structures (or "ripple") with subsecond timescales.

2.2.3.3 Time Delays in Hard X-ray Bursts

Before the launch of SMM, energy-dependent delay of hard X-rays had been observed only from a small number of flares (Bai and Ramaty, 1979; Vilmer, Kane and Trottet, 1982; Hudson *et al.*, 1980). Hard X-ray delay was first observed from the two intense flares observed on August 4 and 7, 1972 (Hoyng, Brown and van Beek, 1976; Bai and Ramaty, 1979), which happen to be the first gamma-ray line flares (Chupp *et al.*, 1973). Hudson *et al.* (1980) analyzed a very intense gamma-ray line flare observed with the first High Energy Astronomical Observatory (HEAO-1), and reported a delay of the continuum above 1 MeV with respect to the X-ray continuum about 40 keV. Vilmer, Kane and Trottet (1982) studied the hard X-ray delays exhibited in a

flare observed with ISEE-3. The HXRBS experiment aboard SMM, which has a large area and good time resolution (71 cm^2 and 0.128 s in normal mode, respectively; cf. Orwig *et al.*, 1980), is most suitable for studying energy-dependent delays of hard X-rays. In collaboration with the HXRBS group, Bai studied the delay of hard X-rays for many flares (Bai *et al.*, 1983a; Bai and Dennis, 1985; Bai, Kiplinger and Dennis, 1985). A balloon-borne detector and the hard X-ray detector aboard HINOTORI also detected hard X-ray delays (Bai *et al.*, 1983b; Ohki *et al.*, 1983). The energy dependence of hard X-ray delays is not simple. In some flares the delay seems to increase smoothly with hard X-ray energy, but in others, it seems to show a sudden increase. For example, in the impulsive flares of June 27, 1980 (Bai *et al.*, 1983b; Schwartz, 1984) and of February 26, 1981 (Bai and Dennis, 1985), the delay is negligibly small below a certain energy, and it suddenly increases above that energy. The energy at which a sudden increase occurs varies from burst to burst (Schwartz, 1984). In the August 4 and 7, 1972 flares, the delay increased gradually with increasing energy to about 5 s, and then for energies above ~ 150 keV it increased to ~ 15 s (Bai and Ramaty, 1979). In the flare of August 14, 1979 flare, the delay was about 10 ± 5 s for the energy channel 154-389 keV, but it increased to 32 ± 10 s for the next energy channel 389-874 keV (cf. Vilmer *et al.*, 1982). (It is important to keep in mind that fast increases may also be the result of the fact that the energy channels are wider in higher energies). However, in other flares the delay seems to increase smoothly with hard X-ray energy (cf. Bai and Dennis, 1985). The energy-dependent delay of hard X-rays is equivalent to flattening of the hard X-ray spectrum. In flares with the delay increasing like a step function at a certain energy (such as the ones on June 27, 1980 and February 26, 1981), the spectral shape at low energies remains unchanged while the spectrum at high energies flattens as time progresses during the burst. If the delay is a smooth function of energy, the hard X-ray spectrum flattens with time both at low energies and high energies (Bai, Kiplinger and Dennis, 1985). Often single power law spectra give good fits to the data. The flares exhibiting hard X-ray delays form a *small* but significant fraction of the total number observed. Another important observational fact is that energy dependent hard X-ray delays have been mostly observed in flares which produced observable nuclear gamma-rays and/or energetic interplanetary protons (Bai and Ramaty, 1979; Hudson *et al.*, 1980; Bai *et al.*, 1983a, 1983b; Bai and Dennis, 1985; Ohki *et al.*, 1983).

Figure 2.2.11a shows a smoothed plot of the 60-120 keV and 120-235 keV rates observed by the UC Berkeley balloon experiment during the impulsive phase of the 27 June 1980 flare (Schwartz, 1984). The smoothed rate during each 0.128 sec interval is computed by averaging the rates over the surrounding bins using a Gaussian weighting function with a 0.5 sec FWHM for the 60-120 keV rate and with a

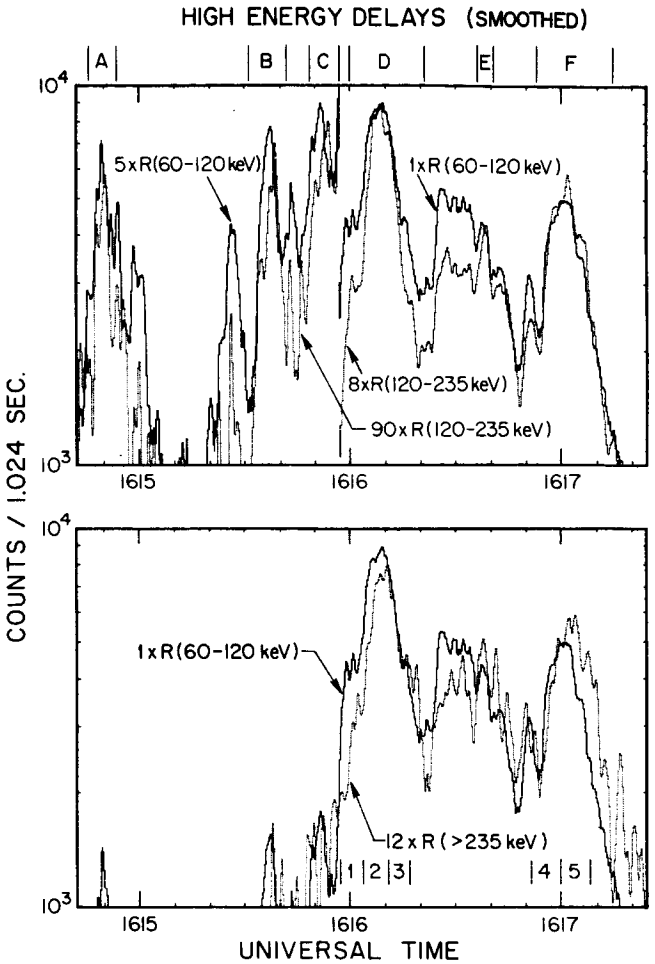

Figure 2.2.11 Delayed bursts of photon energies > 120 keV. (a) Delay of 120–135 keV profile with respect to 60–120 keV rate. (b) Delay of > 235 keV rate with respect to 60–120 keV rate (from Schwartz, 1984).

1 sec FWHM for the two rates above 120 keV. This filters out the high frequency fluctuations, both real and statistical, but does not move the bursts centroids. The cross-correlation function has been computed between the rate pairs (22-33 keV, 60-120 keV), (60-120 keV, 120-235 keV), and (60-120 keV, > 235 keV) for the six bursts, A through F. The smoothed rates were used only for the rates above 120 keV. The delay times found by cross-correlating various energy channels are given in Table 2.2.2. For the burst at 1616:38 UT, the > 235 keV rate is too low to accurately determine a centroid. The delay listed between the 22-33 keV and 60-120 keV rates is an upper limit based on the count rate statistics. Only burst C, at 1615:52 UT, has a real delay for the 60-120 keV rate of 0.128 seconds. Above 120 keV, all of these bursts show real delays. There is a delay of ~ 1-2 seconds in the 120-235 keV rate for the medium sized and shorter duration bursts A, B, C, and E. For the two most

Table 2.2.2 Cross Correlation Delays

Cross-Correlation Delays

Burst	A	B	C	D	E	F
Time after 1600 UT	14:48	15:37	15:52	16:08	16:38	17:02
(22–33, 60–120 keV)	$<.05$	$<.05$	$<.20$	$<.05$	$<.05$	$<.05$
(60–120, 120, 235 keV)	$.8\pm.5$	$1.1\pm.5$	1.9 ± 5	$.4\pm.25$	$.9-.5$	$.2\pm.25$
(60–20 > 235 keV)	—	—	—	$1.5\pm.5$	—	$1.88\pm.5$

Delay Expected for Collisional Loss Process

(22–33, 60–120 keV)	.13	.13	.60	.12	.26	.15

intense and longest duration bursts, D and F, the longest delay is for the > 235 keV rate with only a smaller delay for the 120-235 keV rate (Bai *et al.*, 1983b). The lack of significant delays between the 22-33 keV and 60-120 keV channels make it unlikely that the large delays at higher energies can be explained purely by simultaneous injection at all energies followed by energy-dependent decay due to collisional energy loss (see bottom of Table 2.2.2). Figure 2.2.12, shows five spectra which were accumulated over the intervals marked in Figure 2.2.11. The evolution is similar over both bursts. The double power law becomes a single a power law although the counting rate sensitivity is not enough to observe the hardening in detail. There are two important aspects of the spectral evolution which may provide important clues to the acceleration process. First, the power law exponent at low energies ($\lesssim$ 70 keV) does not change throughout the acceleration. Secondly, the spectrum at high energies hardens up to the point where the power law exponent is the same as at low energies, but not harder. It is not clear whether the spectral hardening occurs because the break in the spectrum has moved to very high ($\gtrsim$ 200 keV) energies or whether the entire high energy portion has hardened to form a single power law at all energies.

2.2.3.4 Hard X-ray Microflares

The U.C. Berkeley balloon flight of June 27, 1980 was the first to observe the Sun with high energy resolution ($\lesssim$ 1 keV) and sensitivity (50 cm² germanium plus 300 cm² scintillation detectors, both well collimated and actively shielded for low background) in the energy range $\gtrsim$ 20 keV (Lin *et al.*, 1984). They discovered the phenomenon of solar hard X-ray microflares which have peak fluxes ~ 10-100 times less than in normal flares. These bursts occurred about once every five minutes through the 141 minutes of solar observations. Although they are associated with small increases in soft X-rays, their spectra are best fit by power laws which can extend up to $\gtrsim$ 70 keV. These microflares are thus probably nonthermal in origin. The integral number of events varies roughly inversely with the X-ray intensity (Figure 2.2.13), so that many more bursts may be occurring with peak fluxes below their sensitivity. The rate of energy released in these microflares may be significant compared

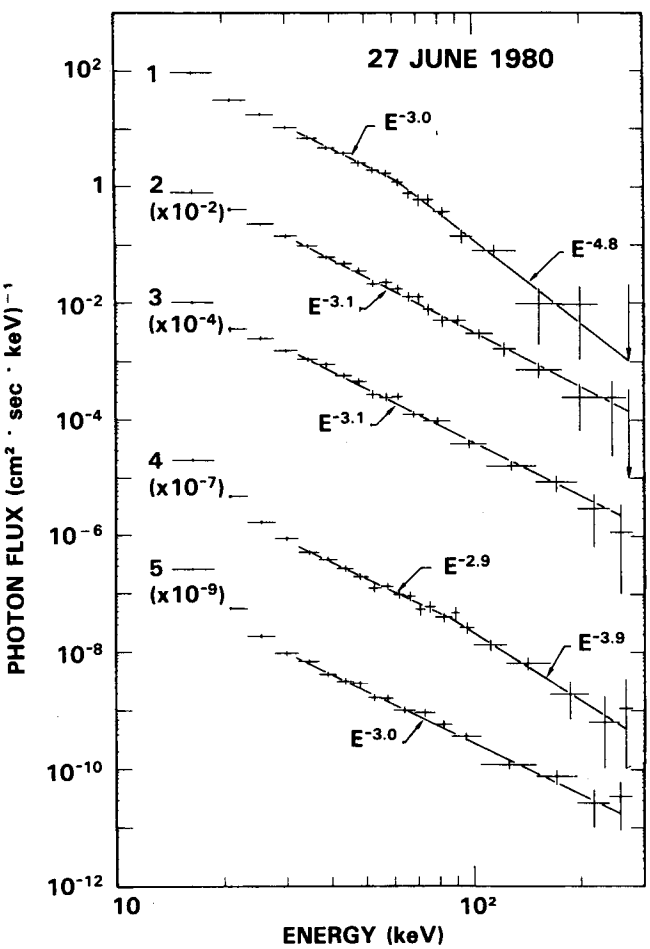

Figure 2.2.12 Five spectra accumulated over the intervals marked in Figure 2.2.11 (from Schwartz, 1984).

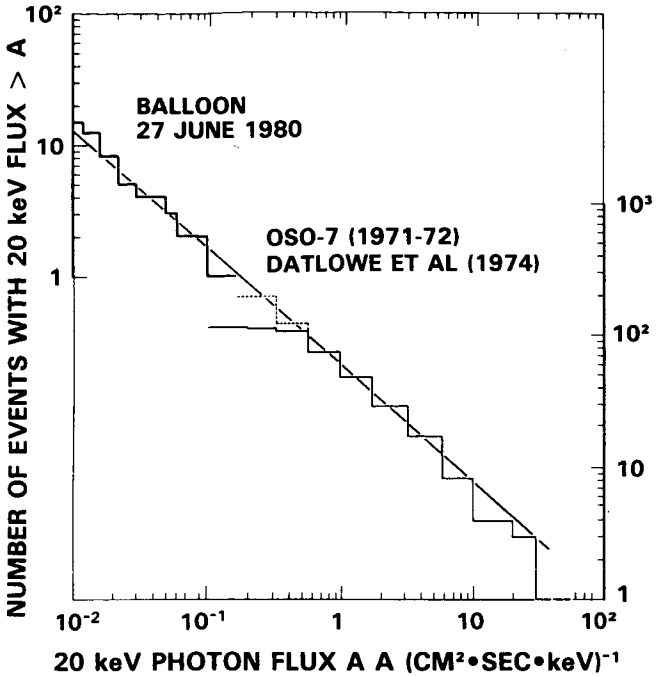

Figure 2.2.13 The distribution of the integral number of events versus peak 20 keV photon flux for the solar hard X-ray microflares observed in this balloon flight. Also shown for comparison is the distribution of solar flares hard X-ray bursts reported by Datlowe *et al.* (1974). The distributions have been arbitrarily moved vertically to show that their slopes are approximately the same (from Lin *et al.*, 1983).

to the rate of heating of the active corona (see also Athay, 1984 for similar conclusions and theoretical discussions by Parker, 1983a,b, and Heyvaerts and Priest, 1984). There is also some indication that these bursts may be made up of spikes of ~ 1 sec duration (Figure 2.2.14). Perhaps these are the real "elementary" bursts, a factor of 10^2-10^3 smaller than the elementary flare bursts reported by de Jager and de Jonge (1978). Kaufmann *et al.* (1985) reached a similar conclusion regarding such microbursts in the microwave domain (see Section 2.2.3.2). These hard X-ray microflares indicate that impulsive electron acceleration to above 20 keV energy is a very common phenomenon and may be the primary transient energy release mode in the solar corona.

2.2.3.5 Pre- and Post-Impulsive Phase Hard X-ray Pulses

Elliot (1969) proposed that flares could be the result of sudden precipitation of energetic ions stored high in the corona where their lifetime is long. Electrons, too, might be stored in a low density region where their collision loss rate would be low and then precipitate during the flare. This scenario allows the acceleration of electrons over a much longer timescale at much lower rate. The stored electrons, however, would radiate via bremsstrahlung. The high sensitivity of the UC Berkeley balloon hard X-ray measurements made on June 27, 1980 permit the study of the pre- and post-impulsive phase nonthermal emissions of a large flare (Figure 2.2.15) in great detail (Schwartz, 1984). Using the high sensitivity of the X-ray detectors upper limits have been set to the preflare flux during 1600 - 1610 UT. The three sigma upper limit to the flux at 20 keV is 8.3×10^{-4} $(cm^{-2}$ sec $keV)^{-1}$. This gives an upper limit to the power law emission measure (Hudson, Canfield and Kane, 1978), $N_{20}n_i < 2.4 \times 10^{39}$ cm^{-3}, where N_{20} is the average number of electrons above 20 keV at any instant of time in a region with an ion density n_i. Conceivably, the electrons could be stored very high in the corona where the density could be as low as 1×10^5 cm^{-3}. This would give a 50 hour collisional lifetime for a 20 keV electron. Thus, up to 2×10^{35} electrons could have remained undetected. This is about the number of fast electrons in the small early burst at 1616:00 UT and it represents less than 1% of the total accelerated electron population (see Figure 2.2.15). Schwartz (1984) concluded that while it is possible that a stored electron population could have triggered one of the early small bursts, the vast majority of the flare electrons could not have been stored in the corona but must be energized during the impulsive phase. The question is if there is any acceleration in the post-impulsive phase. In Figure 2.2.15 one can see that at ~ 1617:30 UT the > 60 keV X-ray flux falls to < 1% of peak intensity. Also, the 22-33 keV rate, mostly from the superhot component, is falling more slowly. Of great interest for this discussion on electron acceleration is the series of impulsive bursts occurring during 1617:30 - 1630 UT and most clearly seen in the 30-60 keV rate. These post-impulsive phase bursts are similar to the impulsive phase bursts but have a peak intensity of about 0.5% of the largest impulsive phase peak. All the bursts contain fast spikes which rise and fall in 4-10 seconds. The spectral index γ, uncertain due to the large low energy continuum rates, is obtained by comparison with the count rates during the impulsive phase. These values are consistent with a nonthermal spectrum, similar to the bursts in the impulsive phase. Certainly, this continual bursting is evidence of electron acceleration throughout the post-impulsive phase, as proposed by Klein *et al.* (1983).

2.2.4 Microwave-Rich Flares

Figure 2.2.16 is a correlation diagram between HXRBS peak count rates and peak microwave fluxes; each point in this figure represents the peak HXRBS count rate and the peak flux density of 9 GHz microwaves for a particular flare. The frequency 9 GHz is chosen because for the majority of flares the microwave emission peaks near 9 GHz and because it is in a frequency range well observed world wide. As can be seen, there is a positive correlation between peak

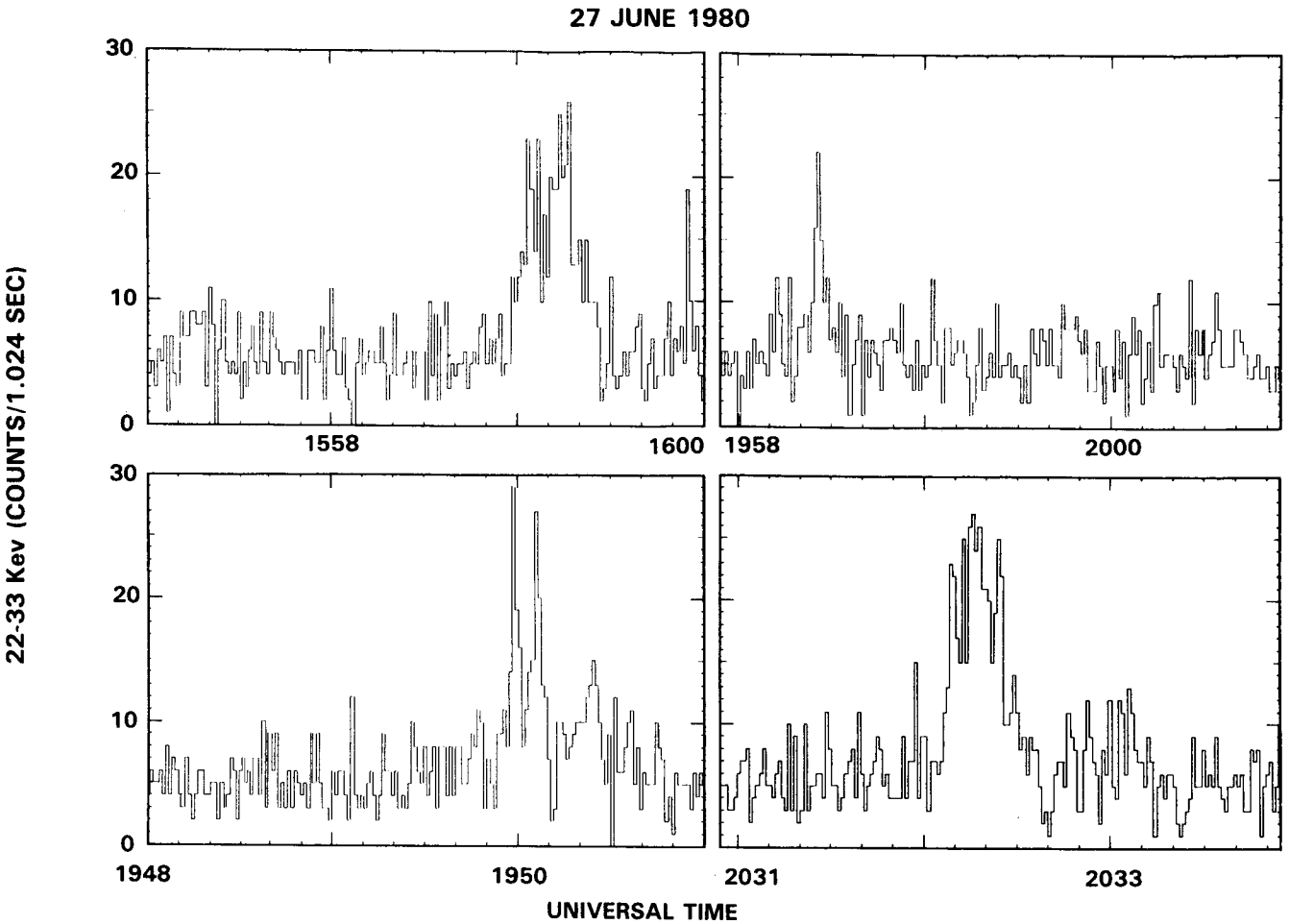

Figure 2.2.14 The four largest hard X-ray microflares are shown here at 1.024 sec resolution (from Lin *et al.*, 1983).

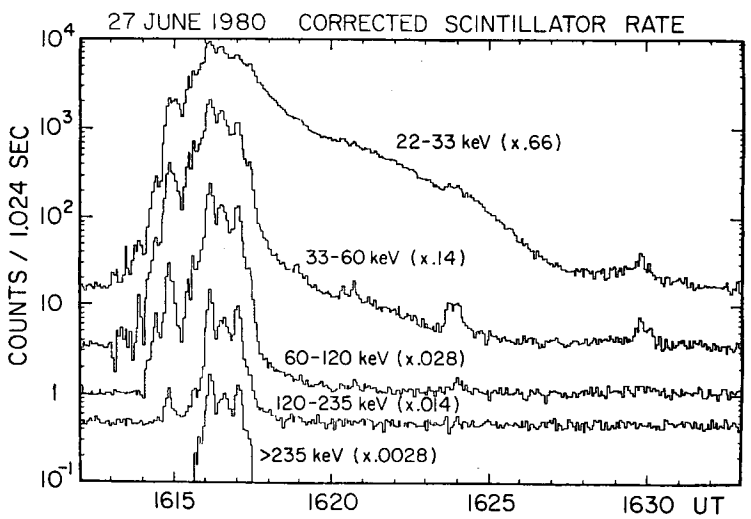

Figure 2.2.15 The hard X-ray burst observed by the scintillation detector. The low decay in the 22-23 keV channel lasts till $\gtrsim$ 16:31 UT. This is due to the super-hot component. The small bursts of non-thermal emission occur till 16:31 UT (from Schwartz, 1984).

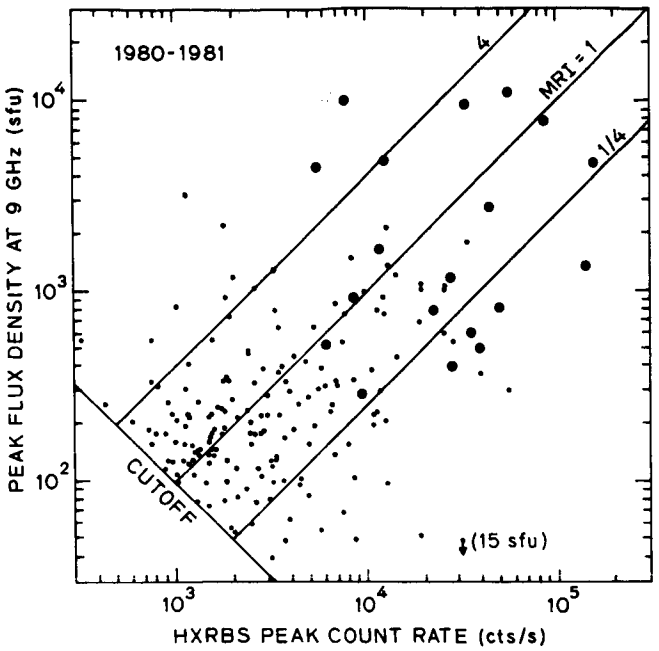

Figure 2.2.16 Correlation diagram between peak count rates measured by HXRBS and peak flux densities of 9 GHz microwaves for 1980 through 1981. Although there is quite a lot of scatter, there seems to be a positive correlation between these quantities. The median value of MRIs is about 1 (0.85 to be precise). The three straight diagonal lines indicate constant values of MRI, 1/4, 1 and 4. The large dots indicate GRL flares. Note that the HXRBS peak rates of the GRL flares are > 5000 cts/s (from Bai, Kiplinger, and Dennis, 1985).

hard X-ray counts rates and peak microwave flux densities (cf. Kane, 1973), consistent with our understanding that both hard X-rays and microwaves are produced by energetic electrons of the same origin. Bai, Kiplinger, and Dennis (1985) defined the "microwave-richness index" (MRI) for each flare as follows:

$$\text{MRI} = \frac{\text{peak flux density of 9 GHz microwaves (sfu)}}{\text{HXRBS peak count rate (counts/s)}} \times 10$$

Here the multiplication by 10 is to make the median value of MRI about 1. The diagonal straight lines in Figure 2.2.16 represent constant values of MRI. The line for MRI=1 divides the population into roughly equal numbers. As can be seen from this figure, there is large scatter: MRI varies more than an order of magnitude (from less than 1/4 to more than 4). Bai, Kiplinger, Dennis (1985) studied the characteristics of the "microwave-rich flares" (with MRI > 4). They noticed that among the gamma-ray line flares studied by Bai and Dennis (1985) gradual gamma-ray line flares exhibit large delays of hard X-rays and large values of MRI. They studied 17 microwave-rich flares (12 flares in Figure 2.2.16 plus 5 microwave-rich flares observed in 1982), and found that these flares share many common characteristics. (1) Large values of MRI (> 4). This was the selection criterion. (2) Long durations of hard X-ray bursts. Microwave rich flares last several minutes, as opposed to the ordinary flares that usually last less than 1 minute. (3) Large H-alpha area. Except for one microwave-rich flare observed at the limb, all belong to H-alpha importance class 1 or higher, and 13 out of 17 belong to H-alpha class 2 or 3. (4) Long delay times (> 10s) of high-energy hard X-rays with respect to low-energy hard X-rays. In a given burst the delay time increases with hard X-ray energy. Such delays are equivalent to hardening of the X-ray spectrum with time during the burst (see Figure 2.2.17). (5) Long delay times (10 ~ 300s) of microwave time profiles with respect to low-energy hard X-ray time profiles. (6) Flat hard X-ray spectra. The average of the power-law spectral indices is 3.5. (Compare with 3.36, which is the value for the gamma-ray line flares studied by Bai and Dennis (1985)). (7) Association with type II and IV radio bursts. All of them produced type II or type IV bursts or both. Seven of the 13 microwave-rich flares have HXRBS peak count rates between 1000 and 5000 cts/s. Considering that the largest HXRBS count rates are of the order of 10^5 cts/s (Dennis *et al.*, 1983), the above count rates are moderate. (8) Emission of nuclear gamma-rays. Only six of the 17 microwave-rich flares produced observable nuclear gamma-rays, but it is interesting to note that all the microwave-rich flares which did not produce observable nuclear gamma-rays have HXRBS peak rates < 4000 cts/s. None of the gamma-ray line flares observed during 1980 through 1981 have HXRBS peak rates < 4000 cts/s (Bai and Dennis, 1985). Therefore, the failure to observe nuclear gamma-rays from the microwave-rich flares with low HXRBS count rates are most likely to be due to the threshold effect of GRS. Another interesting point is that the microwave-rich flares share all the characteristics of gamma-ray line flares. Detailed discussions on the correlation of microwave rich flares and gamma-ray line flares, as well as a possible scenario for their interpretation can be found in Bai and Dennis (1985).

2.2.5 Decimetric-Metric Observations and Comparison with X-ray Observations

Previous studies have already shown that type III bursts and soft X-ray increases are often observed several minutes prior to the occurrence of the flare itself (Kane *et al.*, 1974). Evidence for hard X-rays observed before the flash phase was also reported by Kane and Pick (1976). A systematic study, using more sensitive spectrometers, was carried out by Benz *et al.* (1983b); they listed 45 major events observed by the HXRBS experiment aboard SMM. For most of these events, metric type III bursts and decimetric pulsation were

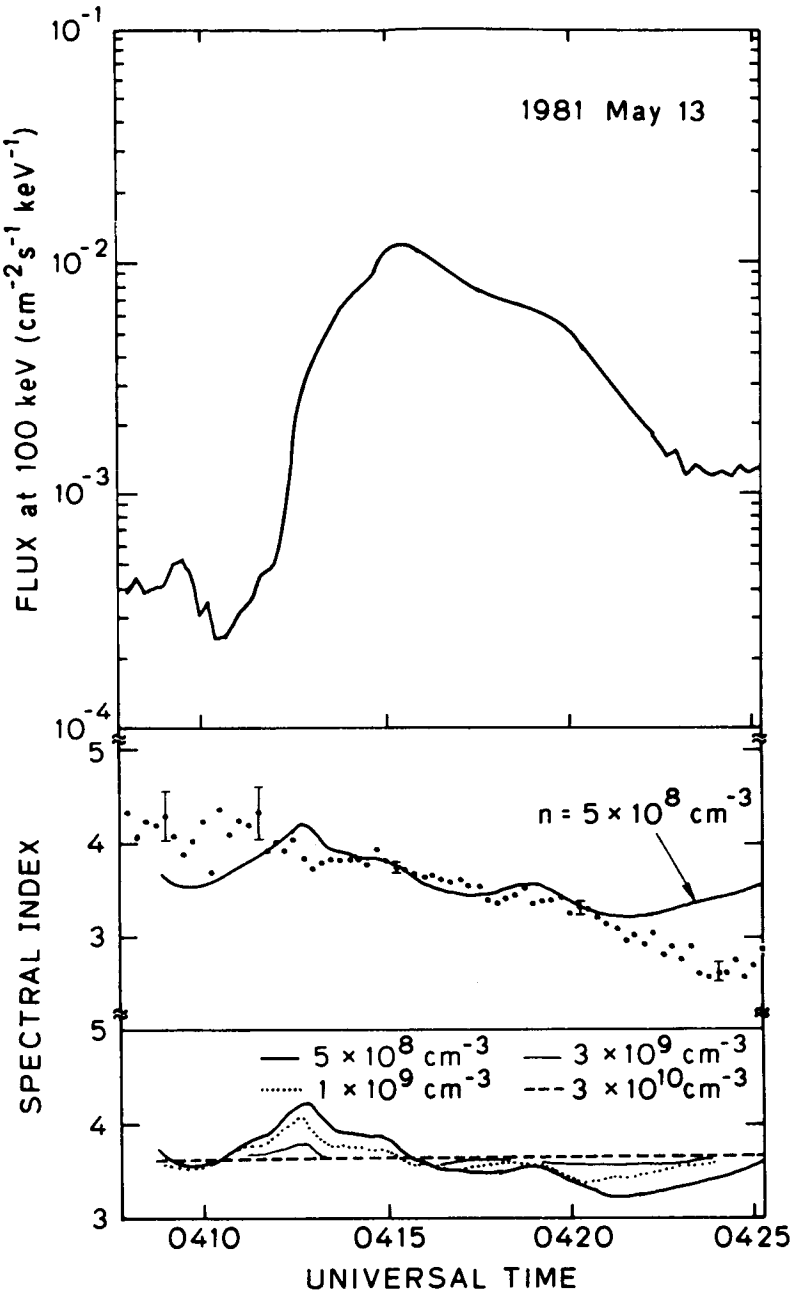

Figure 2.2.17 Spectral evolution of hard X-ray emission from the 1981 May 13 flare. The top panel shows the hard X-ray flux at 100 keV, and the middle panel shows the observed spectral evolution (with dots) together with a spectral evolution calculated using a perfect-trap model. In the last panel the spectral evolutions were obtained by using various values for the ambient density. In order to get a reasonable fit to the data, the ambient density should be as low as 5×10^{8} cm^{-3}. However, this density is incompatible with other observations as mentioned in the text, Tsuneta *et al.* (1984) found that the images of the hard X-ray source and the soft X-ray source are almost the same. These authors also deduced from the emission measure and the size of the soft X-ray source that the density of the flare loop is 3×10^{10} cm^{-3}. As the density increases, the spectral index change will be less and less, approaching the steady state case. For $n = 3 \times 10^{10}$ cm^{-3}, the resultant spectral index evolution is hardly different from a straight line, which is for the steady state case. Before the hard X-ray peak the spectral index is larger than the steady state case and after the peak it is smaller, but near the peak the spectral index is similar to that of the steady state case independent of the density (from Bai and Dennis, 1985).

observed *preceding* the hard X-ray emission. In 7 of the 45 flares, significant hard X-ray fluxes were observed before the rapid general exponential increase. This phase in the flare development was called "preflash phase". It usually lasts for about one minute. These observations give evidence for electron acceleration before the impulsive phase (see also Section 2.2.3.5).

It is commonly believed that electrons responsible for type III bursts and hard X-ray emission have a common origin (Kane, 1972, 1981a) since their temporal evolution is well correlated. Simultaneous observations of X-ray and radio emission with a time resolution of less than 1 sec have shed new light on our understanding of the electron acceleration process. The main conclusions can be summarized as follows: (a) Some hard X-rays peaks are well correlated with type III bursts and show delays of the order of or shorter than one second (Kane, Pick and Raoult, 1980; Benz *et al.*, 1983b). The type III source may consist of several elementary components widely separated (by more than 100,000 kms) which radiates quasi-simultaneously or successively. This implies that the acceleration/injection region covers a wide range of magnetic fields (Mercier, 1975; Raoult and Pick, 1980). (b) Kane and Raoult (1981) reported an increase in the starting frequency of type III bursts during the development of the impulsive phase. This variation is correlated with an increase in the hard X-ray flux. As the type III bursts radiation is emitted at the local plasma frequency, the starting frequency corresponds to the density at the point where the electron beams become unstable. Thus this fast variation of the starting frequency may be explained either by a real variation of the electron density in the source (downward shift or compression of the injection/acceleration site) or to a variation in the distance from the acceleration site, travelled by the electron beam before it becomes unstable (Kane *et al.*, 1982). A systematic study was carried out by Raoult *et al.* (1985) to determine if the presence of an increase in the starting frequency of type III bursts influences the probability of their correlation with hard X-ray bursts. A total of 55 type III groups were selected which had been observed with the Nancay Radiospectrograph (Dumas *et al.*, 1982) in the frequency range 450 - 150 MHz, and with the ISEE-3 X-ray spectrometer. Of the 55 events, 32 cases, (58%) were associated with X-ray emission. In this sample, 28 events (52%) showed an increase in the starting frequency. 75% of these events were associated with X-ray emission, resulting in significant improvement of the correlation. Conversely, 75% of the X-ray associated events show an increase in the starting frequency. Thus, an increase in starting frequency seems to be a significant factor that improves the association between type III burst groups and X-ray bursts. (c) However, Raoult *et al.* (1985) pointed out that among these 55 events, 15 events were associated with type V continuum visible in the frequency range 450 - 150 MHz with a typical duration of about one minute or less. All these events have an X-ray response. Thus, the presence of a type V continuum at frequencies > 150 MHz appears to be a decisive factor in increasing the correlation between X-rays and type III bursts.

Raoult *et al.* (1985) also suggested that type III/V events have a consistently large X-ray response. Stewart (1978) first reported that among a list of X-ray associated radio bursts, 80% contained a type V burst. They performed a detailed data analysis for meter events which have an X-ray response. Their main findings are: (a) *Pure* type III bursts groups are not associated with intense X-ray emission. The hard X-ray bursts associated with these events have fluxes < 1 photon cm^{-2} sec^{-1} keV^{-1} at about 30 keV and are not detectable above 100 keV. The corresponding radio burst source is often multiple. The X-ray response around 30 keV closely follows the starting frequency evolution. (b) When a radio event is associated with strong X-ray emission (> 1 photon cm^{-2} sec^{-1} keV^{-1} at 30 keV and detectable above 100 keV), a continuum emission (type V) in the range 450 - 150 MHz appears along with the type III groups. The typical evolution of these events is illustrated in Figures 2.2.18 and 2.2.19, and may be described as follows: The first part of the event, "preflash phase", contains only type III (or U) bursts coming from locations (A). Then a new source "B" (see Figure 2.2.19) appears at the time of the fast increase in the X-ray emission. This is also coincident with an increase in the radio starting frequency. At that time, one of the pre-existing type III burst sources (A') becomes predominant. Sources B and A' have similar sizes (2' - 3' arc at 169 MHz), and they fluctuate simultaneously within short time delays of less than one second. Thus both sources contribute to the spiky and smoothed parts of the radio emission identified as type III and type V bursts, respectively. There is an overall correlation between the radio flux and X-ray fluctuations, although there is no correlation on short timescales. When the rapid radio fluctuations are no longer present, both X-ray and radio fluxes decrease sharply and the X-ray emission appears at energies below 30 keV. The total X-ray flux and radio flux decrease rather smoothly, the source B being usually the predominant one. The duration of the type V burst increases with increasing wavelength. Similarly the duration of the X-ray emission increases with decreasing energy.

The results described above have implications on the geometry of the magnetic field structure at the site of injection of electrons. The presence of sources A' and B, which fluctuate quasi-simultaneously, implies that the electrons are quasi-simultaneously injected into two structures (or two unresolved groups of structures). According to Raoult *et al.* (1985) most flares that are associated with a small hard X-ray emission correspond to an electron injection/acceleration site that covers several diverging magnetic flux tubes. The fact that during the impulsive increase of the hard X-ray flux, the radio emission is reinforced in one pre-existing location and appears quasi-simultaneously in a new location, suggests

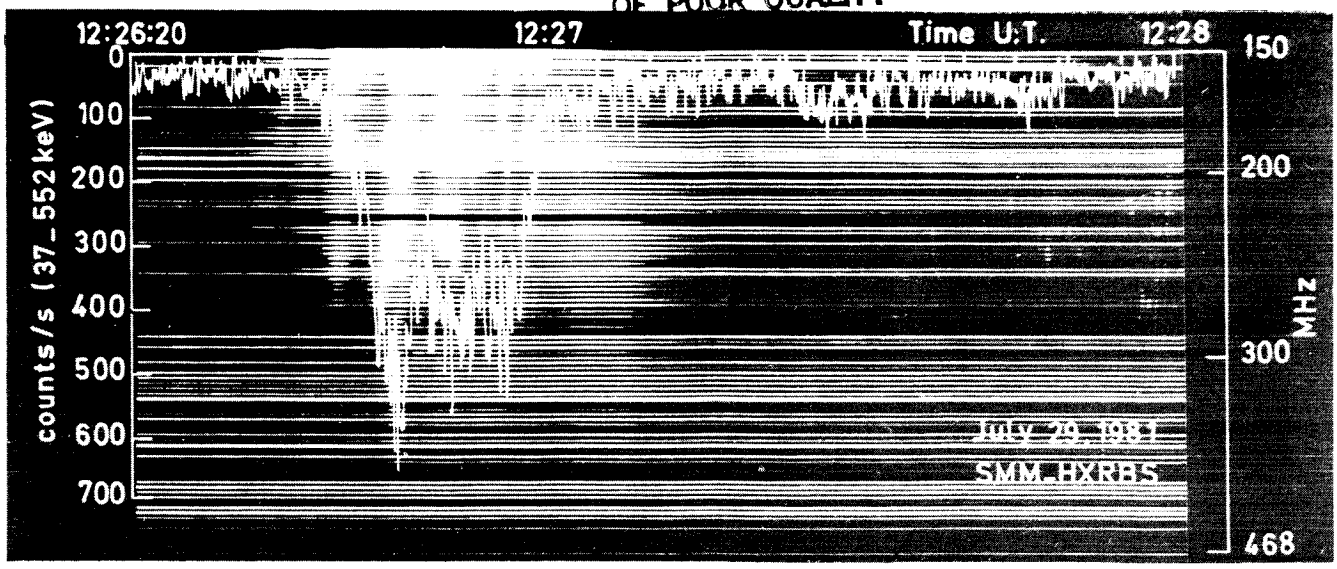

Figure 2.2.18 Type III/V bursts on 1981 July 29, observed with the Nancay Radiospectrograph (Dumas *et al.*, 1982) and the associated hard X-ray burst observed with the SMM-HXRBS experiment. Evolution of the X-ray emission compared to the evolution of the radio event. (From Raoult *et al.*, 1984).

that at the injection site the two magnetic structures interact. At that time the energy that is released in the interaction region increases sharply. Another possible interpretation was given by Sprangle and Vlahos (1983) and is discussed in Section 2.4.6.

Rust *et al.* (1980), Benz *et al.* (1983b), Aschwanden *et al.* (1985) and Dennis *et al.* (1984) have also studied the correlation of hard X-rays with decimetric radiation, which originates at lower altitudes. Their results on decimetric type

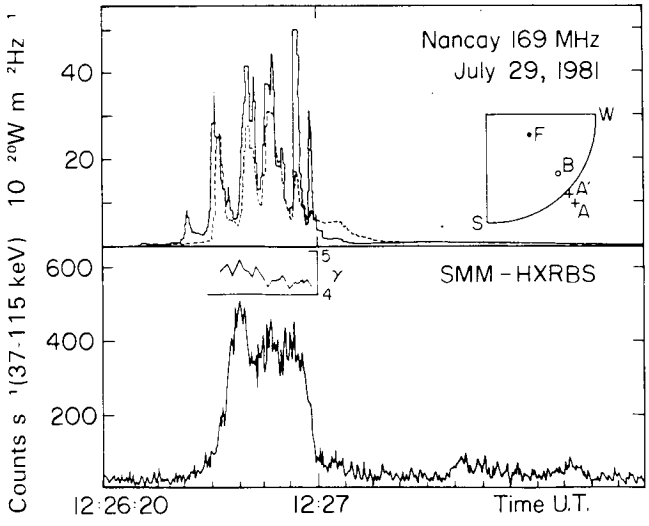

Figure 2.2.19 Top: Evolution of the radio flux from sources A, A′ (solid line) and B (broken line) see text. Bottom: Evolution of X-ray spectral index and hard X-ray emission. (From Raoult *et al.*, 1984).

III bursts reinforced many of the conclusions reported for metric bursts. Aschwanden *et al.* (1985) have found decimetric type III bursts to be associated with hard X-ray events in 45% of the cases. The association rate increases with the number of bursts per group, duration, bandwidth and maximum frequency of the group. Some single bursts (but not all) are correlated with hard X-ray spikes. In some cases the difference in time of maximum between type III and hard X-rays is a few tenths of a second, which may be significant. This may imply that ordinary cross-field drifts or diffusion from closed to open field lines are too slow. The acceleration of the electrons by intense electromagnetic waves, as proposed by Sprangle and Vlahos (1983) seems to be a likely interpretation (see Section 2.4.6 for details). These bursts occur at frequencies of 300 MHz to > 1 GHz, corresponding to densities $> 3 \times 10^9$ cm^{-3} (Benz *et al.*, 1983b).

Strong *et al.* (1984) investigated a double impulsive flare in radio, soft and hard X-ray emissions. The decimetric radio emission of both events contains U bursts. In several cases they have harmonic structure. From the total duration and extent in frequency of the U bursts the geometry of the loop guiding the electron beam can be calculated. The average length of these loops is 94,000 km and 157,000 km, and the average height 24,000 km and 45,000 km in the two flares respectively. The U bursts are sometimes correlated in time with hard X-ray spikes (Figure 2.2.20). If the elongated soft X-ray source is interpreted as a loop, its projected size is only 30,000 km. Post-flare soft X-ray loops have been found in the second flare with footpoints separated by 115,000 km. The presence of loops of different sizes is also evident in the microwave spectrum which shows evidence for 3 peaks

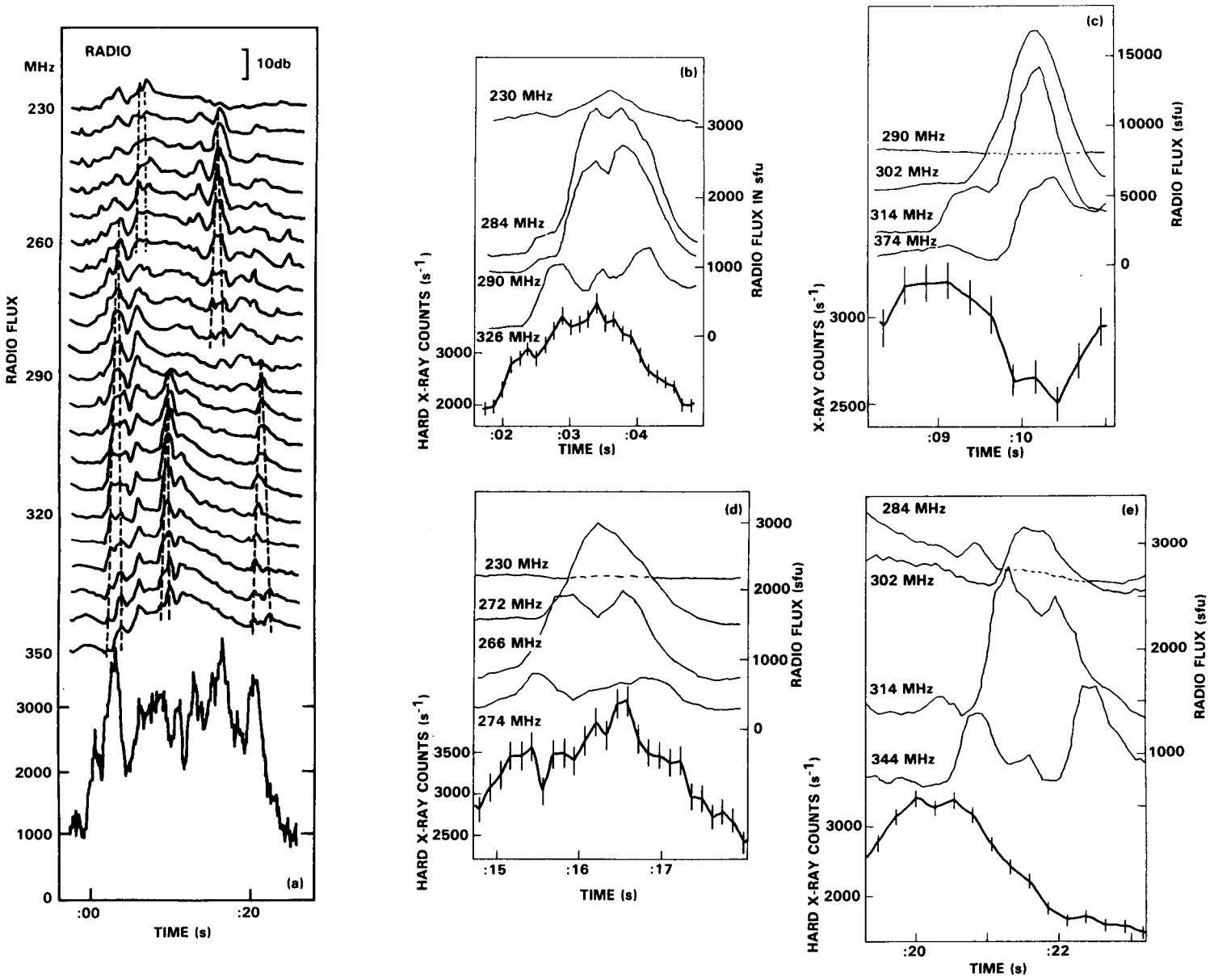

Figure 2.2.20 Correlation between U-bursts and hard X-ray spikes in the August 31, 1980, 1251 UT flare. Data from radio spectrometer at Bleien (Zürich) and HXRBS on SMM. Left: U-bursts are outlines in the upper part and compared with the X-ray count rate in the lower part. Right: Details of left figure showing correlation of X-ray spikes with rising part of U-bursts (from Strong *et al.*, 1984).

indicating sources with widely different magnetic field strengths. Apparently energetic particles have immediate access to small (soft X-ray) loops and large (U burst, post-flare) loops suggesting that the acceleration site is at the boundary or interface between the two loop systems.

The decimetric emission of flares can be divided into radiations which generally occur *during the impulsive phase* and the type IV emission generally observed *after the impulsive phase*. The impulsive phase bursts are found to vary considerably in shape (Wiehl *et al.*, 1985). A large fraction can be interpreted as due to type III-like beam instabilities. The bursts may have some unexpected forms, however, such as narrow bandwidth ($\Delta\nu/\nu \leq 0.2$), called blips by Benz *et al.* (1983a) or very high drift velocities (an example is shown in Figure 2.2.21). These deviations from the normal shape are probably caused by the disturbed properties of the ambient plasma.

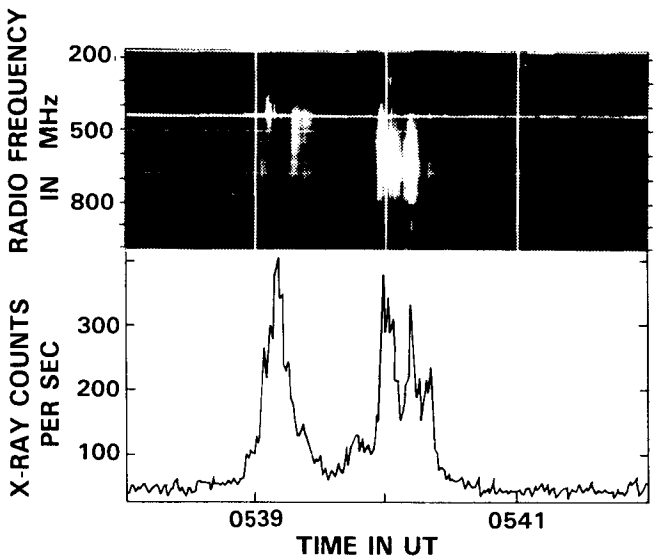

Figure 2.2.21 Top: Dynamic spectrogram of type III-like decimetric emission with very high drift rate, observed on May 19, 1980 with the analog spectrometer at Bleien (Zürich). Enhanced emission is bright, horizontal lines are terrestrial interference, and vertical lines are minute marks. Bottom: Hard X-ray count rate as observed at energies > 30 keV by HXRBS on SSM.

All decimetric bursts during the impulsive phase do not appear to be explained by particle beams. About 25% of all cases are in this category and they are strongly associated with hard X-rays (70%). These bursts have been divided into 4 classes by Wiehl *et al.* (1985). 1) Diffuse *patches* of emission probably originate from trapped particles either by synchrotron or loss-cone radiation. 2) *Grass-like* chains of small spikes resemble elements of metric type II bursts. They may be caused by shock waves. 3) Nonperiodic broadband *pulsations* with pre-flash hard X-ray emission. The decimetric emission in these cases precedes both hard X-ray and Hα emission, as shown by Benz *et al.* (1983b) from a study of 3 flares. However, a more general study of 45 such events (Aschwanden *et al.*, 1985) has shown that pulsations usually start after the hard X-rays and end before them. Most important, pulsations and hard X-rays do not seem to correlate closely. Durations of single elements are between 20 and 100 ms. The elements are of similar bandwidth (several 100 MHz) and have about the same low-frequency end. 4) *Spikes* of short (< 100 ms), narrowbanded (3-10 MHz) emission occur in large groups. They are associated with shorter and more impulsive hard X-ray bursts than the average. They tend to occur in the early impulsive phase (Benz, 1985). The single elements are scattered in a chaotic manner between ~ 400 and > 1000 MHz (corresponding to densities of 0.3 – 1 × 10^{10} cm^{-3}). Their circular polarization can be between 25 - 40%. They probably are similar to the microwave spikes observed at 2.6 GHz by Slottje (1978), probably also produced by the electron cyclotron masering.

2.2.6. Discussion of Models for X-ray and Microwave Emission

Information about the accelerated electrons are obtained through models which depend on parameters such as local ambient density, temperature and magnetic field which are poorly known. Three major problems face us in our interpretation of the observations:

- what is the relative role of thermal and nonthermal electrons in producing X-rays at different energies?
- does nonthermal production of hard X-rays arise from beams of electrons (thick-target model) or from a trapped population of electrons or from a combination of both.
- do the observations imply a single or a two step acceleration process?

We discuss below several attempts to model the energy release and answer some of the questions posed above.

2.2.6.1 Trap Plus Precipitation vs Two Step Acceleration Models

The two competing interpretations of the energy-dependent hard X-rays are trap plus precipitation models (Kane, 1974; Melrose and Brown, 1976; Bai and Ramaty, 1979; Vilmer *et al.*, 1982; MacKinnon *et al.*, 1983; Ryan, 1985) and second-step acceleration models (Bai and Ramaty, 1979; Bai, 1982; Bai *et al.*, 1983a, 1983b; Bai and Dennis, 1985). Interestingly, the first paper that analyzed hard X-ray delays (Bai and Ramaty, 1979) invoked both interpretations, the trap model for small delays below 150 keV, and second-step acceleration for large delays (15 s) above 150 keV. Bai and Ramaty (1979) and Vilmer *et al.* (1982) used a pure trap

model, and MacKinnon *et al.* (1983), Trottet and Vilmer (1983), and Ryan (1985) considered the effect of precipitation. MacKinnon *et al.* (1983) reported that, in the weak diffusion limit, precipitation does not change the essential nature of the trap model. A detailed discussion of trap models is given later in this Section.

We emphasize first that the second-step acceleration is different from the conventional "second-phase" acceleration proposed by Wild, Smerd and Weiss (1963), since the delay between the two steps is tens seconds and not tens of minutes.

Bai and Dennis (1985), who have studied many flares exhibiting hard X-ray delays, note the following points favoring the second-step acceleration interpretation. (1) In impulsive flares which exhibit hard X-ray delays, the delay time as a function of hard X-ray energy is quite different from what is expected from the collisional trap plus precipitation models. Instead of increasing gradually with energy, the delay time exhibits a sudden increase at high energies. (2) In very gradual flares such as the ones observed on April 26 and May 13, 1981, the ambient density deduced with the trap model is of the order of 10^9 cm^{-3} (see Figure 2.2.17). This is too low to explain the observed emission measure of soft X-rays (assuming of course, that the hard and soft X-ray emitting regions are coincident). Actually, the density deduced for the May 13 flare from the observed emission measure and volume is 3×10^{10} cm^{-3} (Tsuneta *et al.*, 1984a). The above argument does not exclude the possibility of trapping of energetic electrons in a huge loop, (this was proposed by Tsuneta *et al.*, 1984a), but it proves that trapping is not the primary cause of large hard X-ray delays (or spectral flattening with time) observed in these gradual flares. (3) The association between hard X-ray delay and proton acceleration (see Section 2.3), is naturally explained by the second-step acceleration model. In Fermi type acceleration, stochastic acceleration by a fluctuating magnetic field, or shock acceleration, there exist threshold energies (or injection energies) for both electrons and protons above which the acceleration can overcome the Coulomb energy loss (e.g., Ginzburg and Syrovatskii, 1964; Sturrock, 1974; Ramaty, 1979). Therefore, when these kinds of acceleration mechanism accelerate protons to gamma-ray producing energies, they will also accelerate electrons with energies greater than the injection energy to higher energies. On the other hand, in trap models it is hard to see the connection between proton acceleration and trap electrons. (4) The total bremsstrahlung fluence above 270 keV is roughly proportional to the 4-8 MeV fluence (see Chupp 1982 and Figure 2.3.4). On the other hand, when the 4-8 MeV fluence is compared with the hard X-ray fluence above 30 keV, the correlation is very poor (Bai and Dennis, 1985). Actually many flares with large fluences in > 30 keV hard X-rays did not produce observable nuclear gamma-rays. With the second-step acceleration, this is easily explained. In the second-step acceleration model, both high energy electrons and gamma-ray producing protons are accelerated by the second step, hence we expect a good correlation between hard X-rays > 270 keV and 4-8 MeV fluences. On the other hand, the fluence of low-energy hard X-rays (> 30 keV), which is due to electrons accelerated by the first-step mechanism, is not expected to correlate well with the gamma-ray fluence, which is due to the second-step mechanism. (5) In trap models the photon spectrum is somewhat steeper at the beginning of the burst than in a thick-target beam model, and it gradually flattens to be about the same as the thick-target model near the peak. On the other hand, if the second-step acceleration is operating, the photon spectrum at the peak of the burst is expected to be flatter because of additional acceleration at high energies. Consistent with the second-step model, the photon spectrum measured at the peak of the burst is flatter on the average for gamma-ray line flares than for non-gamma-ray line flares, which do not in general show hard X-ray delays. The site of the second-step acceleration is proposed to be the corona instead of the chromosphere (Bai and Ramaty, 1979; Bai *et al.*, 1983b); therefore, in this model at least, high energy electrons are assumed to be trapped in the corona. Hence, it is possible that in many flares hard X-ray delay is partly due to trapping and partly due to the second-step acceleration, as proposed by Bai and Ramaty (1979). It is usually difficult to determine their relative importance unless we know the ambient density of the flare loop (trap region). For the May 13, 1981 flare the ambient density is deduced to be 3×10^{10} cm^{-3} (Tsuneta *et al.*, 1984), and for this density the hard X-ray delay is much smaller than the observed one. For the gradual flare of April 26, 1981, the same is true (Bai, Kiplinger and Dennis, 1985).

Let us now summarize the recent progress made on models that invoke trap and precipitation. Vilmer *et al.* (1982) applied the trap model to explain observations of high-energy X-ray delays, and McKinnon *et al.* (1983) considered the effect of precipitation on the trap model. Trottet and Vilmer (1983) have also studied the case where the precipitation from the trap is in the strong diffusion limit (e.g., wave-particle interaction). The basic ingredients of the model are: (1) a trap of uniform density n_o, (2) a continuous injection of nonthermal electrons in the trap, with constant spectral index γ, during a finite time t_o, (3) a time dependent injection function having a maximum at $t_o/2$, (4) energy losses entirely due to electron-electron collisions, (5) precipitation from the trap gives rise to a thick target component, either in the weak diffusion limit (Coulomb collisions) or in the strong diffusion limit (wave-particle interaction). The computed X-ray time profiles depend then on t_o, n_o and the precipitation process considered. In the weak diffusion limit, although hard X-ray emission starts simultaneously at all energies, the higher energy channels reach their maxima later than the lower ones. For given t_o and γ such delays are a function of n_o. Figure 2.2.22a shows that $\Delta t(E) = t_{max}$

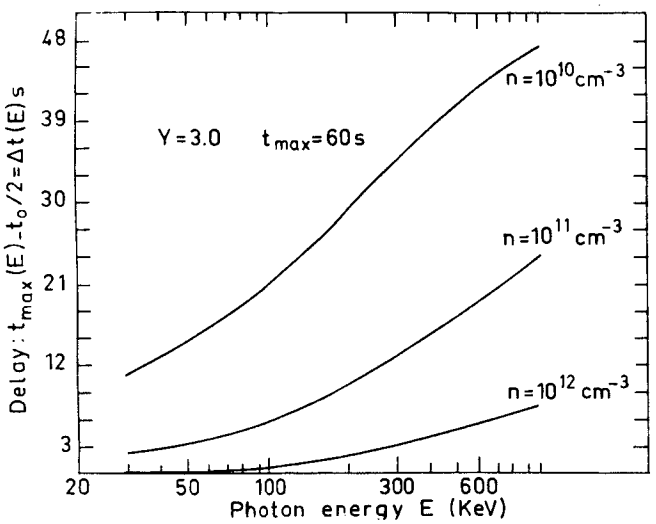

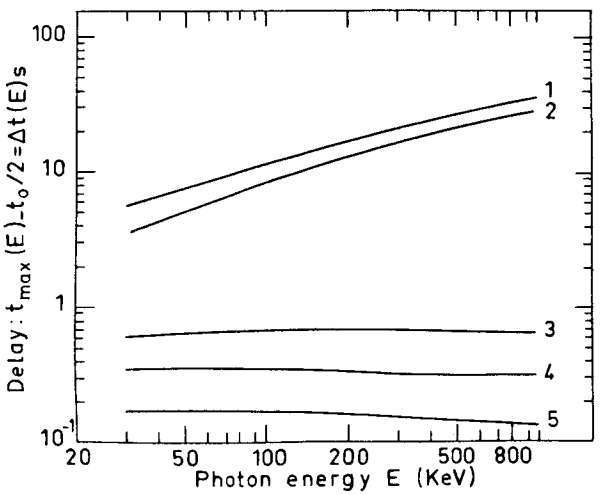

Figure 2.2.22 (a) Computed delays $\Delta t(E) = t_{max}(E) - t_o/2$ for $\gamma = 3.0$, $t_{max} = 60$ sec, for the weak diffusion case as a function of the photon energy E, for different values of the trap density. (b) Computed delays as a function of the photon energy E, using the same parameters as in (a), for different precipitating rates: perfect trap (1) weak diffusion (2) and strong diffusion (3), (4), (5) using $a_o^2/L \simeq 10^{-5}$, 2×10^{-5}, 5×10^{-5} respectively (from Trottet and Vilmer, 1983).

$(E)-t_o/2$ increases with increasing energy and decreasing density n_o. For a given energy E, $\Delta t(E)$ also increases with t_o. The ratio between the X-ray flux produced in the trap I_{trap} and the flux due to precipitated electrons I_{prec} depends neither on the energy nor on the density n_o. The total hard X-ray spectrum (trap + precipitation) hardens with time. When precipitation is in the strong diffusion limit, its rate depends on the particle energy and α_o^2/L (the ratio between the loss-cone angle and the characteristic length of the trap). The X-ray time profile depends on two characteristic times, the energy loss time t(E), which increases with E, and the precipitation time t_p which decreases with E. When t_p is larger than t_E (large scale loops or small α_o), $\Delta t(E)$ increases with energy, but does not exceed a few seconds. When t_p is of the order of or smaller than t_E, Figure 2.2.22a shows that $\Delta t(E)$ is very small, approximately constant with E and weakly dependent on n_o. In this last situation no observable delays are expected. On the contrary I_{trap}/I_{prec} is strongly dependent on the energy E(I_{trap}/I_{prec} decreases when E increases) and decreases when α_o^2/L increases. The hardness of the hard X-ray spectrum remains approximately constant with time. Moreover for the same injection function and trap density, the X-ray spectrum is somewhat harder than in the weak diffusion regime before the maximum (Trottet and Vilmer, 1983).

According to Trottet and Vilmer (1983), the main considerations that favor trap and precipitation models are as follows: (1) Hard X-ray imaging sometimes shows high and large X-ray sources, with power law spectra, suggesting a coronal thick target trap with continuous injection/acceleration of electrons (type C flares discussed in Section 2.2.1.1). (2) Some events exhibiting large delays (up to 1 min) have been successfully interpreted through trap and precipitation models (see Vilmer *et al.*, 1982). The diversity of observed delays is easily explained by the variability of the trap density, injection time and nature of the scattering process. Certainly more work has to be done to describe more realistic situations, namely one has to develop time dependent models where the inhomogeneity of the ambient medium and the angular distribution of the energetic particles are taken into account. A first approach to this problem is to look for general time dependent solutions of the continuity equation. Vilmer *et al.* (1985) and Craig *et al.* (1985) have developed the mathematical framework that can be used for such a study. (3) The time lag between hard X-ray and γ-ray maxima is correlated with the γ-ray rise time.

Trottet and Vilmer (1983) have also argued that if a two step acceleration is at work some difficulties arise. Indeed Chupp (1983) has shown that the ratio of the prompt γ-ray line fluence in the 4-7 MeV band to the 2.223 MeV line fluence is approximately constant from one flare to another. According to Ramaty (1985), this requires a constant spectral shape for the ions. Moreover the total electron bremsstrahlung fluence above 270keV is roughly proportional to the 4-8 MeV excess fluence (Chupp *et al.*, 1984b). This suggests that high energy electrons and ions are accelerated by the same process and that this process is common to all flares. Thus, if delays reflect a second step acceleration, they should be observed, without exceptions, for all flares producing γ-ray lines and X-rays above the few 100 keV. In fact some observations contradict such an interpretation. Let us illustrate this point by two examples reported by Rieger (1982).

First, reverse delays between X-ray and γ-rays are clearly observed for the October 14, 1981 flare (4-7 MeV and 10-25 MeV channels peak before the 80-140 keV and 300 keV channels). Second, the June 21, 1980 flare exhibits variable delays from one peak to another, the first peaks occurring even simultaneously in all channels. In summary Trottet and Vilmer argued that even if a two step acceleration process cannot be definitively ruled out, available observations of time delays may reflect the interaction between the accelerated particles and the ambient medium rather than the characteristics of the acceleration mechanism itself.

Ryan (1985) also considered independently the effects of particle trapping on the time profiles of hard X-rays and γ-rays. His results reinforce the work reported above. Ryan used three different models. The first is that of a closed trap with a finite density of matter within the trap providing the slowing down mechanism for the particles and the particle target for photon production. The two other models employ particle diffusion in a tenuous trap to allow particles to precipitate to denser regions of the solar atmosphere where they interact to produce the photons. The characteristics of all of these models are (1) to reduce the impulsiveness of the acceleration as it is seen in the high energy photons and (2) to produce delays in the maxima of the photon fluxes at various energies. These effects must be taken into account in searching for evidence of additional acceleration mechanisms. The constant density coronal trap which has been considered in the past for electrons below 200 keV can produce significant delays for electrons of energies > 0.5 MeV and larger effects still for γ-rays produced by ~ 20 MeV protons. Particle densities of 10^{10} cm^{-3} can produce delays in the γ-rays of several tens of seconds. If particles are injected impulsively at one point in the loop, they diffuse toward both ends of the trap precipitating to the loss regions of high density. With this process, there is an intrinsic delay in the precipitation rate and thus the photon flux due to the finite time required for the particles to diffuse to both ends of the loop. The rise and decay times of this process are also proportional to the size of the trap. It should also be noted that the particle propagation effects in the observed photon flux for the constant density trap is also a function of the size of the trap. The study by Rosner *et al.* (1978) shows that the matter density in coronal non-flaring loops is inversely correlated with the length of the loop. Thus we have the situation where three mutually exclusive particle trap scenarios produce a reduced impulsiveness in the photon flux with respect to the particle acceleration or injection and the convolution of these effects with the acceleration profile produces a delay in the flux maxima with respect to the acceleration profile. In addition, the magnitude of these effects grow with the linear dimensions of the loop. The implications of this are that they complicate the search for and identification of a multi-step acceleration process and they limit the search for rapid fluctuations in photon flux, which is a signature or measure of the rapidity of the acceleration process.

2.2.6.2 Dissipative Thermal Model

We have emphasized in this section that heating and acceleration of the plasma tail occurs nearly simultaneously in flares. This poses a fundamental problem: How does the flare-energized (hot + tail) plasma expand along the field lines? Since the plasma outside the energy release region is at coronal temperatures (several million degrees Kelvin), the energized plasma interfaces with a "cold" ambient plasma. The steep temperature and/or density gradients accompanying the rapid energization may give rise to D.C. and stochastic electric fields which contain most of the electrons, but allow the fastest electrons in the tail of the distribution to escape. Brown, Melrose and Spicer (1979) suggested (following similar work by Manheimer (1977) in the pellet fusion plasma) that a return current, driven by the electrostatic potential at the interface, will set in and most probably will grow unstable, limiting the heat flux. This suggestion was followed by two extreme approaches: (1) Ignore the escaping electrons and use a fluid model to simulate the expansion of the hot plasma (see e.g., Smith and Harmony 1982 and references therein). (2) Describe qualitatively the hot plasma and concentrate on the escaping electrons (Vlahos and Papadopoulos, 1979 and Emslie and Vlahos, 1980). In the latter work it was also assumed that inside the energy release volume the tail was continuously replenished by sub-Dreicer electric fields. In reality both approaches were of a limited scope. The real problem is somewhere in between and we have to simulate the plasma below a critical velocity (which is not known) as a fluid and as particles above it. In other words, the need for a multifluid or Vlasov type simulation is obvious. Such simulation is currently possible. It is worth mentioning that several qualitative suggestions, based on the dissipative thermal model, appeared in the last few years.

Brown *et al.* (1980) suggested that the energy release volume in a flaring loop may consist of many hot sources with lifetimes and sizes below the instrumental resolution. The overall hard X-ray burst emission is made up of a "convolution" of these "multiple kernels". They investigated the effective (time-integrated) spectrum of hard X-rays from one such kernel, and showed that the majority of observed spectra could be explained by invoking a spread in the parameters characterizing the kernels. The hardest spectra are not, however, amenable to such an intepretation.

Smith (1985) suggested the following scenario for solar hard X-ray bursts which may explain the evolution of type B flares (cf. 2.2.1.1). At the beginning of the impulsive phase, we often see brightening of footpoints which indicates that a significant fraction of the energy released is going into accelerated electrons. This could occur due to fast tearing modes in a loop leading to electron acceleration via the modified two-stream instability (see Section 2.4). After these electrons evaporate a sufficient amount of chromospheric plasma, which then travels back up the loop, the electron plasma beta,

β_e, rises sufficiently to cut off the modified two-stream instability and the footpoint behavior ceases. The emission is then dominated by the primarily thermal single source near the top of the loop. There may still be some small regions in the loop where β_e is sufficiently small to allow acceleration of electrons required by the microwave emission.

Holman, Kundu, and Papadopoulos (1982) have shown that streaming suprathermal electrons will be isotropized by self-generated electrostatic waves (the "anomalous doppler resonance" instability) if the electron gyrofrequency (Ω_e) exceeds the plasma frequency (ω_e) somewhere along the loop, and if the minimum velocity in the suprathermal electron distribution is well above the mean thermal electron velocity in the ambient plasma. The first condition ($\Omega_e > \omega_e$) may hold in most flare loops, and the second condition will hold as long as the accelerated electron distribution does not extend down to the thermal distribution, or if the accelerated electrons escape into a cooler plasma. Holman, Kundu and Papadopoulos also show that if the suprathermal electrons are also responsible for the observed hard X-ray emission, the scattering of the particles can also lead to breaks in the hard X-ray spectrum. These breaks result from wave damping preventing all of the suprathermal electrons from being scattered. An important conclusion is that the microwave source structure does not necessarily indicate the location of the particle acceleration region. Similar conclusions can be reached from considerations of the loop geometry and the directivity of gyrosynchrotron emission (see Petrosian 1982).

Zaitsev and Stepanov (1983) showed that intense localized heating inside the energy release region may violate locally the condition that the plasma pressure is lower than the magnetic pressure, which in the past had permitted some numerical calculations of one-dimensional fluid models (e.g., Smith and Lilliequist, 1979). As a result, the magnetic field expands locally and setup a local magnetic trap, and $B^2/8\pi \gtrsim nkT_e$ and the magnetic field compresses the plasma again. This cycle repeats and sets in an oscillatory motion. Zaitsev's and Stepanov's results may explain the periodic pulsations observed in hard X-ray and microwave bursts.

Batchelor *et al.* (1985) made a new analysis of the thermal flare model proposed by Brown, Melrose and Spicer (1979). They assumed that the model leads to the development of a quasi-Maxwellian electron distribution that explains both the impulsive hard X-rays and microwaves as opposed to our previous interpretation that allows a significant number of nonthermal electrons to escape from the thermal source. This implies that (a) the part of the microwave spectrum for which $f < f_{max}$ consists of optically thick emission, so the source area, A_o, can be calculated from the Rayleigh-Jeans law, and (b) the plasma temperature can be measured from the hard X-ray spectrum by determining the best fit to a single-temperature thermal bremsstrahlung function. Using (a) and (b), Batchelor *et al.* (1984) calculated A_o at the time of maximum hard X-ray flux. Assuming that the source was an arch, they estimated its half-length $L_o \simeq A_o^{1/2}$. The theoretical time scale of the burst would then be $\tau_o = L_o/c_s$, where $c_s = (kT_e/m_p)^{1/2}$ is the ion-sound speed, the speed of expansion of the source during the initial rise of impulsive emission. To test the prediction of the model, Batchelor *et al.* (1985) analyzed microwave observations made at the Bern Radio Observatory and hard X-ray observations obtained with the SMM-HXRBS experiment. The results are shown in Figure 2.2.23, which is a plot of log t_r vs log τ_o, where t_r is the measured rise time of the hard X-ray emission and τ_o is computed from independent spectral parameters only. For 17 disk flares, the best fit relationship is found to be $t_r \approx 0.51\ \tau_o^{1.5}$, which is within the statistical uncertainties of the predicted relationship, $t_r \approx \tau_o$. Three limb flares lie to the left of the disk flares on the diagram, consistent with the interpretation that they were partially occulted by the solar limb, which would result in reduced values of L_o and τ_o as observed. This result is in good agreement with the model, and is not explained by any other known flare models which have been considered. The main problem with Batchelor *et al.* model, however, is that the behavior of the energetic electrons was not properly considered.

2.2.7 Summary

We shall now return to the questions which we have posed in the introduction and which have guided our discussions during the workshops:

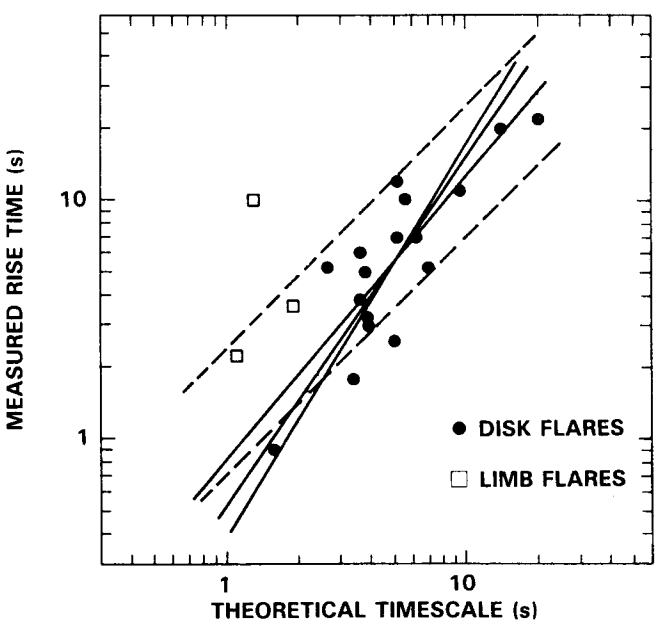

Figure 2.2.23 Correlation diagram of t_o and τ_o. Solid lines indicate best fits by linear least-squares fitting. Dashed lines are boundaries of the expected positions of disk points if the sources are arches from 2 to 4 times as long as they are thick (from Batchelor *et al.*, 1985).

(1) *What are the requirements for the coronal magnetic field structure in the vicinity of the energization source?*

In the previous section we have shown a great deal of evidence suggesting that flares and strong particle acceleration do not generally occur in isolated magnetic structures (like an isolated flaring loop). Such evidence has been collected independently from soft and hard X-ray imaging observations, microwave imaging observations, and meter wave one dimensional imaging and decimetric observations. Simultaneous microwave/meter, microwave/X-ray and meter/X-ray observations have given support to the idea that during the impulsive phase several discrete injection/acceleration regions are present, connecting both open and closed field lines, the former associated in many cases with very divergent magnetic field lines. It is, of course, difficult to generalize the "small" sample of results presented in this section but we feel confident that in several cases (involving strong acceleration) the acceleration region must comprise a rather large volume encompassing regions of different topologies, as suggested schematically in Figure 2.2.24a and 2.2.24b. Such schematic models have been proposed earlier; however, the new wealth of space and ground based data obtained during the past solar maximum, provide strong observational support to such models.

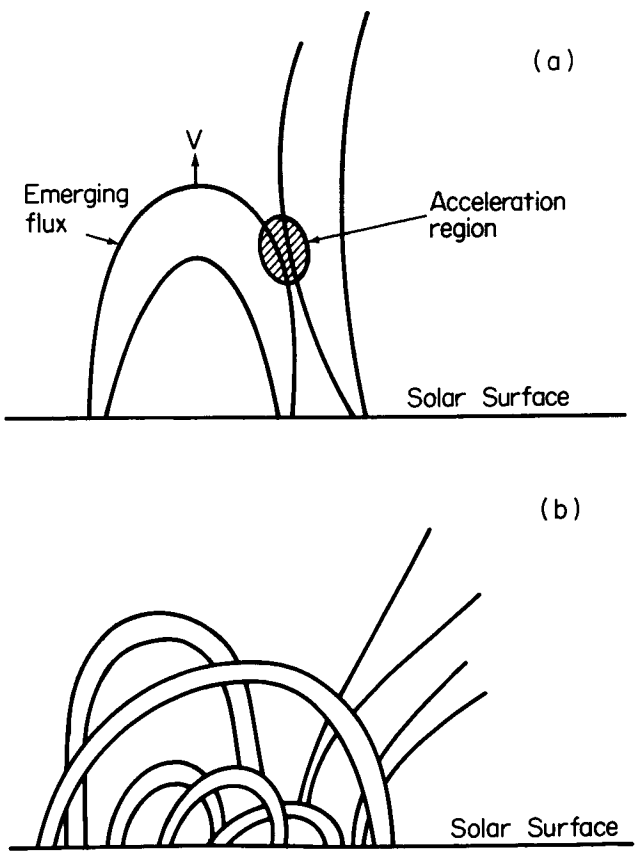

Figure 2.2.24 (a) The emerging flux model, (b) A catastrophic interaction of thousands of reconnecting layers.

(2) *What is the height (above the photosphere) of the energization source?*

A number of pieces of evidence in the past have placed the energization source in the low corona (microwave and decimetric burst observations). To this set we would like to add the observation on the starting frequency of type III burst and their correlation with hard X-ray bursts. We now believe that the acceleration source is in the low corona where the plasma density varies between 10^9 and 10^{10} cm^{-3}. The acceleration may start at lower densities and "drift" to higher densities with a variable speed or it is stationary at the low corona and the region where the beam becomes unstable to plasma waves "drifts" towards higher densities with time.

(3) *Does the energization start before and continue after the impulsive phase?*

We have presented evidence indicating that both heating and acceleration have signatures before and after the impulsive flare. This is contrary to the well accepted scenario that slow heating starts before the impulsive phase, followed by intense acceleration during the flare and it ends up with a hot plasma that gradually cools off.

(4) *Is there a transition between coronal heating and flares? What are the microflares?*

High sensitivity hard X-ray detectors have dispelled the myth that the corona operates in two modes "heating" and "flaring". We have presented evidence suggesting that microflares may be occuring all the time in the corona. In other words, the transition from "flaring" to "heating" may be more gradual than commonly perceived and depends strongly on the sensitivity of available instruments. The presence of nonthermal tails at all times, and microflares may be crucial requirements for the "coronal heating mechanisms".

(5) *Are there evidence for a purely thermal, purely nonthermal or a hybrid type of flare?*

This is an open question and may have an "energy dependent" answer. Usually evidence for "purely thermal plasma" is provided by soft and lower energy hard X-ray bursts. However, gamma-rays and type III, IV and V bursts are not considered to be produced from a "purely thermal plasma". At the other extreme, a "purely nonthermal flare" is also a myth. We have presented much evidence indicating that a "hot component" is always present in flares. Indeed, we have emphasized that accelerated electrons can quickly "thermalize" and turn in to a "hot plasma". In summary we feel that a hybrid model is the best resolution to this dilemma and as we shall see later theoretically it is the easiest to explain.

(6) *What are the time characteristics of the energization source?*

There is strong evidence that the time profiles of flares at different wavelengths sometimes show sub-second or

even milli-second pulses. In several cases the pulses repeat at regular or quasi-regular intervals. The brightness temperature for each of these pulses is sometimes so high that a coherent emission mechanism must be invoked. Delays between microwave and hard X-ray pulses have also been reported. We believe that these fast pulses are evidence of "micro-injection" similar to the ones discussed earlier and a "flare" is composed of many micro-releases of energy. The understanding of such fast pulsation is still relatively poor.

(7) *Is there any observational evidence for a two step acceleration mechanism?*

A few key observations have guided our past thinking on particle acceleration in flares. One of them was the event analyzed by Frost and Dennis (1971). In this event, the impulsive phase was followed by a type II burst, which implies the presence of a shock, coinciding with the enhancement of relativistic particles. Thus the conclusion was drawn that during the impulsive phase (or first phase from the point of view acceleration) mildly relativistic electrons where accelerated. This phase was followed several minutes later by a second phase which coincided with the formation of a shock that further accelerated ions and relativistic electrons. During the SMM workshops no evidence was presented for such delays (of the order of tens of minutes) between the acceleration of mildly relativistic and relativistic electrons and ions. The delays between pulses in different energy channels are of the order of seconds (10-50 secs). Thus, we must refer to the two phase acceleration rather as a "two step acceleration" (Bai and Ramaty, 1979) (two acceleration mechanisms operating in close proximity, with one being delayed from the other by 10-50 seconds). A novel suggestion was also made during the workshop, namely that we must search for one acceleration mechanism for particles of all energies and one possibly for heating. Such a mechanism must result in no delays for the acceleration of particles to higher energies. But then the question may be asked: How does one create delays out of a synchronous acceleration mechanism? The answer is by using a trapping and precipitation model. The debate between these two approaches was not resolved during the workshops and the arguments are presented in Section 2.2.6.

2.3 PHENOMENA ASSOCIATED WITH IONS AND RELATIVISTIC ELECTRONS IN SOLAR FLARES

Evidence for the acceleration of ions and relativistic electrons in solar flares is obtained primarily from gamma-ray line and continuum emissions and from neutron and charged-particle observations. Gamma-ray lines and neutrons result from nuclear interactions of accelerated protons and heavier ions with the ambient solar atmosphere, while gamma-ray continuum is due to electron bremsstrahlung and the superposition of broad and unresolved narrow gamma-ray lines.

In this section we present the gamma-ray and neutron observations and their implications and discuss the charged particle observations. We also examine the relationship between the acceleration of ions and other flare phenomena.

2.3.1 Gamma-Ray Observations

Gamma-ray lines and continuum have been observed from many flares. The first observations, carried out by detectors on OSO-7 (Chupp *et al.*, 1973), were followed by observations on HEAO-1 (Hudson *et al.*, 1980), HEAO-3 (Prince *et al.*, 1982), SMM (Chupp *et al.*, 1981) and HINOTORI (Yoshimori *et al.*, 1983). The gamma-ray spectrometer (GRS) on SMM, in particular, has provided a broad base of data (e.g., Chupp 1984) which forms the basis of much of the discussion in this Section. In addition, the hard X-ray burst spectrometer (HXRBS) on SMM has provided important data regarding the temporal and spectral behavior of the X-ray continuum below ~ 0.3 MeV. We consider the spectra of the observed gamma rays, the timing of the fluxes in the various photon energy bands and the correlation of the gamma-ray data with other flare manifestations.

2.3.1.1 Gamma-ray Spectra

An example of a gamma-ray spectrum, observed by GRS from the April 27, 1981 limb flare, is given in Figure 2.3.1. Here the distribution of the net detector counts (the difference between source and background counts) is shown as a function of photon energy deposited in the detector, for energies >0.27 MeV, the GRS detection threshold. As can be seen, this spectrum is a superposition of continuum emission, most likely due to electron bremsstrahlung, and narrow and broad lines resulting from ion interactions. The narrow lines are due to proton and alpha-particle interactions with the ambient medium, while the broad lines are from the interactions of accelerated heavy particles with ambient H and He. As indicated, the strongest narrow lines are at 6.13 MeV from ^{16}O, at 4.44 MeV from ^{12}C, at 2.31 MeV from ^{14}N, at 2.223 MeV from neutron capture on hydrogen, at 1.634 MeV from ^{20}Ne, at 1.37 MeV from ^{24}Mg, at 0.85 MeV from ^{56}Fe and at 0.51 MeV from positron annihilation. The 2.223 MeV line, normally very strong for disk flares, is greatly suppressed in limb flares (Wang and Ramaty, 1974). Theoretical nuclear gamma-ray line spectra were calculated earlier by Ramaty, Kozlovsky and Lingenfelter (1979).

Because the contribution of the nuclear lines to the total emission below $\sim$ 1 MeV is quite small, this component can be separated from the bremsstrahlung by fitting a power-law photon spectrum to the data below 1 MeV and then subtracting this power law from the data at higher energies. However, this technique can only approximate the nuclear

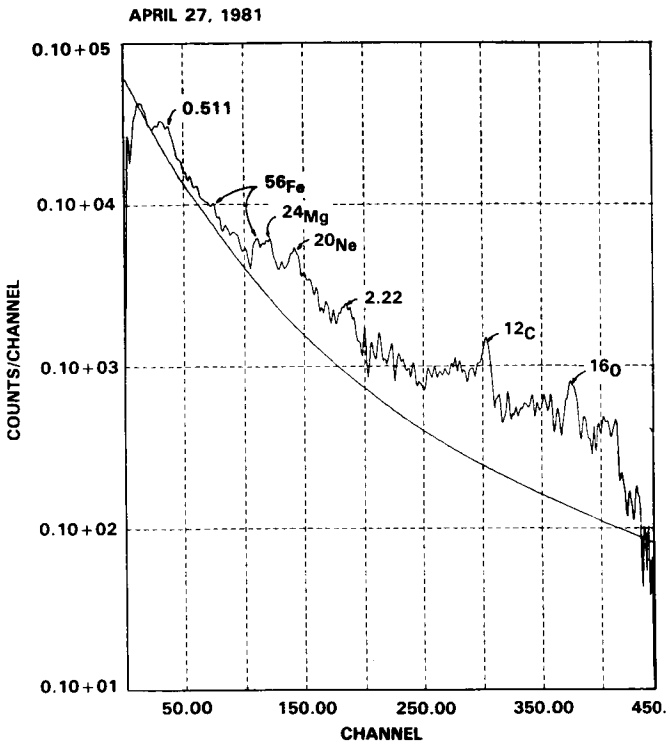

Figure 2.3.1 Observed GRS count spectrum of the April 27, 1981 flare. The solid curve is an estimate of the contribution of electron bremsstrahlung.

contribution, since forms other than power laws could also be fit to the data < 1 MeV. Nevertheless, the fact that the excess radiation can indeed be attributed to nuclear lines is supported by the structure of the spectrum, which shows peaks at anticipated line energies, and by the vanishing of the excess above ~ 7.5 MeV, a feature characteristic of a spectrum dominated by nuclear lines. Also, the good correlation (Chupp 1982) of the excess fluence (time-integrated flux) in the 4-8 MeV band with the 2.223 MeV line fluence for several flares provides additional support for the nuclear origin of the 4-8 MeV excess. The 2.223 MeV line from solar flares is a signature of neutrons produced in nuclear reactions of flare-accelerated ions. That the gamma-ray emission from solar flares in the 4-8 MeV region is predominantly nuclear was first pointed out by Ramaty, Kozlovsky and Suri (1977) and Ibragimov and Kocharov (1977).

2.3.1.2 Time Dependences and Correlations with Other Flare Phenomena

Observations of the time dependences of the gamma-ray fluxes from solar flares provide a great deal of information on the acceleration and interaction of the energetic particles. These time dependences are determined by the temporal structure of the acceleration process, by the lag, due to propagation and trapping, between the acceleration and the interaction of the particles, and by the delay between the interaction of the particles and the emission of photons. Significant delays are caused by the finite capture time of the neutrons in the photosphere for the 2.223 MeV line (Wang and Ramaty, 1974) and both by the finite lifetimes of the various positron emitting nuclei and the slowing-down times of the positrons for the 0.511 MeV line (e.g., Ramaty *et al.*, 1983a). However, for the June 21, 1980 flare, the time profile of the 0.511 MeV line was analyzed in detail (Murphy and Ramaty, 1985), and it was found to depend predominantly on the delayed decay of the positron emitters. This implies a very short (< 10 sec) slowing-down and annihilation time.

On the other hand, bremsstrahlung and most nuclear line emissions are produced essentially instantaneously at the time of the interaction of the particles and therefore serve as the best tracers of the time dependences of the acceleration and interaction processes. Timing studies based on these radiations define the total duration of particle interaction in flares, as well as the overall temporal structure of the emission. But of particular interest is the temporal relationship between the fluxes in the various energy channels, as these data provide information on the relationship between ion and electron acceleration, and possibly on the existence of multiple acceleration steps.

The GRS gamma-ray observations >0.3 MeV indicate a range of total flare durations from ~10 sec to over 1000 sec (e.g., Figure 2.3.2). The total emission in the majority of these events consists of at least a few emission pulses, each of which can be followed over a wide energy band. These separate emission pulses can be as short as ~ 10 sec and as long as ~ 100 sec and their duration within a given flare is roughly proportional to the total event duration. In a preliminary study (Gardner *et al.*, 1981) of the separate emission pulses in several GRS events, it was found that the time of flux maximum in the 4.1-6.4 MeV band occurred between 0±1 sec and 45 sec later than the corresponding maximum of the ~ 0.3 MeV flux, the delay being proportional to the emission pulse rise time. In addition to these, most gamma-ray line flares also show delays between the various gamma-ray and hard X-ray bands (Bai and Dennis, 1985). But it is important to note *that there are cases where no delays are detected.* An example is shown in Figure 2.3.3, where the maxima in the various energy bands from 0.04 MeV to 25 MeV in several emission pulses are simultaneous to within the GRS instrumental resolution of ±1 sec.

Another aspect of the timing studies is the relationship between the starting times of the fluxes in different energy channels. Forrest and Chupp (1983) have studied this relationship for the 40-65 keV flux and the 4.1-6.4 MeV flux in two impulsive flares. They found that the starting time, defined as the time when flux above background was first detected, was the same in each energy band within of ±2 sec for the smaller flare and ±0.8 sec for the larger flare, in spite of the fact that these two flares show evidence for

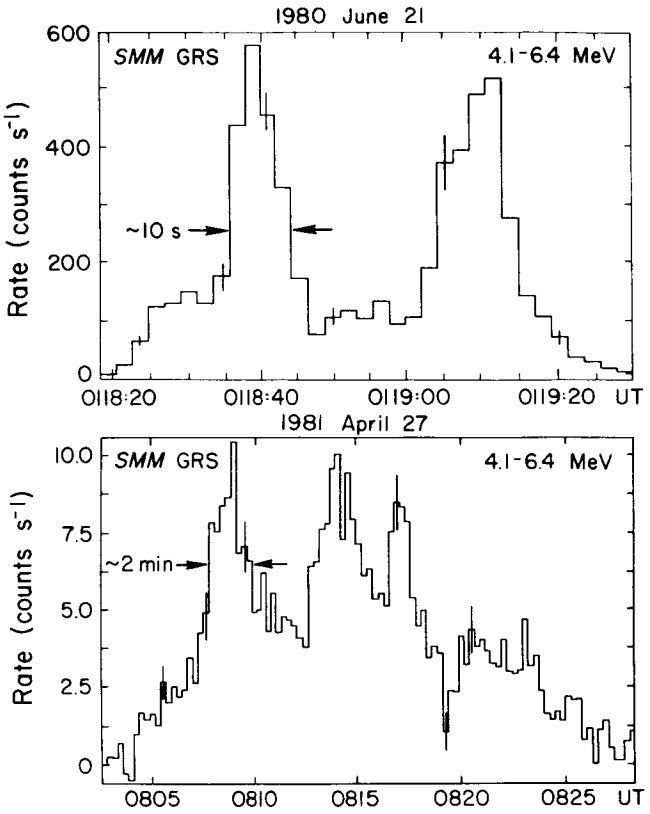

Figure 2.3.2 The observed time histories in an energy band dominated by gamma-ray lines from a fast gamma-ray flare (top panel) and a slow gamma-ray flare (bottom panel). From Forrest (1983).

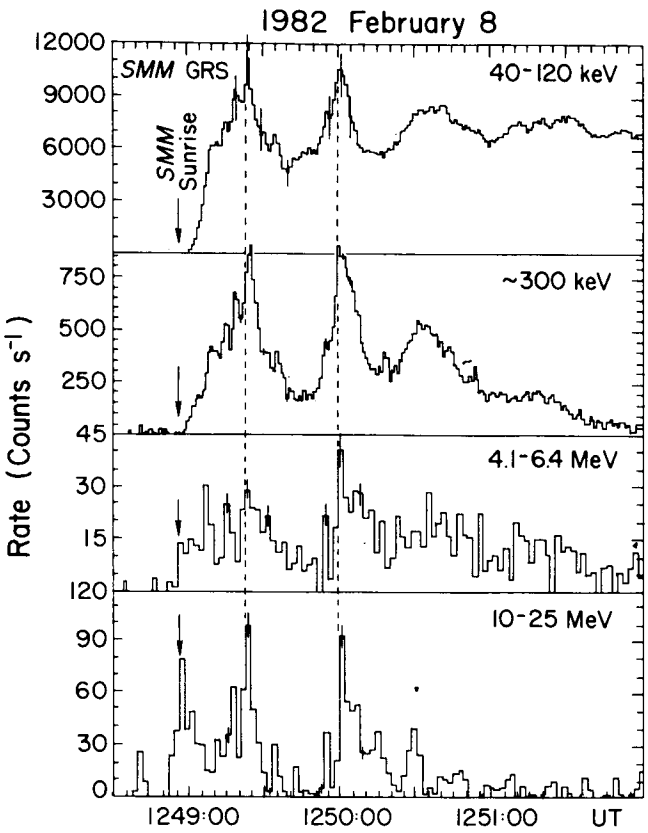

Figure 2.3.3 The observed time histories in 4 energy bands for a gamma-ray flare. From Chupp (1984).

a delay in the maxima of the fluxes of the same two energy bands.

In addition to the timing studies, information on the relationship between ion and relativistic electron acceleration can be obtained by comparing the bremsstrahlung with the nuclear gamma-ray emissions from many flares. In Figure 2.3.4, the ordinate gives the bremsstrahlung fluence >0.27 MeV, found from a power-law fit for each solar flare event (see 2.3.1.1), and the abscissa gives the corresponding nuclear fluence above the power law for the energy range 4-8 MeV. As can be seen, for 4-8 MeV nuclear fluences greater than the GRS sensitivity threshold, relativistic electron bremsstrahlung is always accompanied by nuclear gamma-ray emission.

Gamma-ray emission is seen from flares of many different types, suggesting that ion acceleration could be a rather basic process. The first 2½ years of GRS data already show that (1) a gamma-ray event may be associated with any Hα class, (2) 20% (10 out of 50) of flares of class $\gtrsim$ 2B have associated 4-8 MeV excess (Cliver *et al.*, 1982), (3) 75% of all GRS events have associated Hα class B (brilliant) emission, (4) 50% (13 out of 26) of GOES A X-ray events with peak intensity $\gtrsim$ X2 have significant 4-8 MeV excess, (5) GRS events are always associated with a solar microwave burst ($\gtrsim$ 1GHz) and (6) 53% (19 out of 36) of 9 GHz bursts with peak flux density $\gtrsim$ 1200 solar flux units had significant 4-8 MeV excess (Cliver *et al.*, 1983).

2.3.2 Neutron Observations

Neutrons produced in solar flares have been observed directly by the GRS experiment (Chupp *et al.*, 1982, 1983) and by neutron monitors on the ground (Debrunner *et al.*, 1983). Neutron production in flares has also been inferred from observation of the 2.223 MeV line (e.g., Prince *et al.*, 1983), and from the detection (Evenson *et al.*, 1983) of prompt interplanetary protons resulting from the decay of neutrons produced in flares. The interplanetary proton flux (from the June 3, 1982 flare) due to neutron decay is shown in Figure 2.3.5. As we shall see, these data provide very important complementary information to that obtained from the direct neutron and the 2.223 MeV line observations. The prompt appearance of solar neutrons at Earth, indicated both

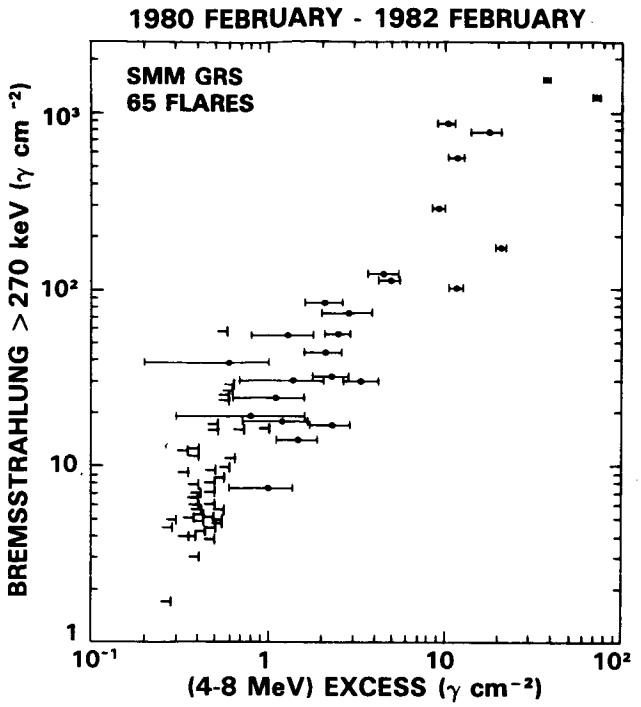

Figure 2.3.4 A correlation plot of the electron bremsstrahlung and nuclear line emission from 65 flares. From Forrest (1983).

by the ground based and SMM observations, require the prompt acceleration of high-energy protons in the flare. Protons should be accelerated to hundreds of MeV in less than 1 minute.

2.3.3 Implications of the Gamma-Ray and Neutron Observations

Gamma-ray and neutron observations of solar flares can provide information on the spectrum of the accelerated particles, on the total number and energy content in these particles, on the electron-to-proton ratio as a function of energy, on the anisotropy and interaction site of the accelerated particles, and, possibly, on the composition of the accelerated particles and the ambient medium (Ramaty *et al.*, 1983a; Ramaty, 1985). To obtain this information, the observations must be compared (e.g., Murphy and Ramaty, 1985) with theoretical calculations which evaluate the expected gamma-ray and neutron emissions using the basic nuclear processes (Ramaty, Kozlovsky and Lingenfelter, 1979), particle interaction models (Ramaty, Kozlovsky and Lingenfelter, 1975; Zweibel and Haber, 1983) and various energetic particle spectra. The spectra that produce the best fits can then be compared to the predictions of particle acceleration models (e.g., Pesses, 1983; Lee and Ryan, 1985; Forman, Ramaty and Zweibel, 1985 and Section 2.4). The acceleration

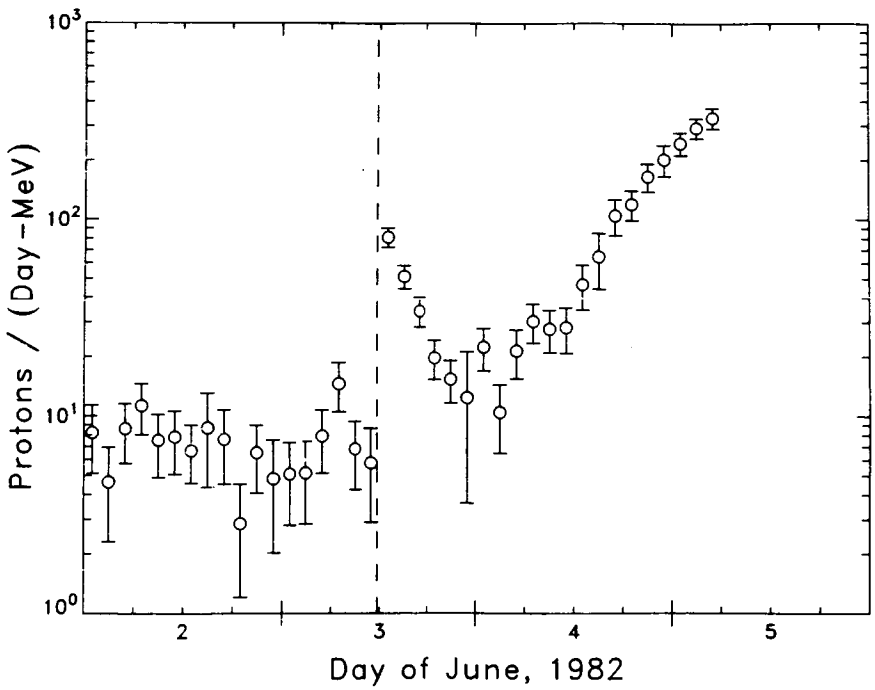

Figure 2.3.5 The flux of 25-45 MeV protons observed at ISEE-3. The gamma-ray arrival time is indicated by the dashed line. From Evenson *et al.* (1983).

mechanisms that have been considered so far are the stochastic Fermi mechanism and shock acceleration. The former predicts (Ramaty, 1979) an ion spectrum, which, in the nonrelativistic range, is a Bessel function of the second kind, provided that the diffusion mean-free-path, λ, and the escape time from the acceleration region, T, are energy independent. The parameter that characterizes this Bessel function spectrum is $\alpha T = V^2T/\lambda c$, where V is the velocity of the scattering elements. Shock acceleration can predict many spectral forms; the simplest of these, however, is a power law in momentum, resulting from diffusive acceleration by an infinite planar shock with no losses.

The most appropriate interaction model for gamma-ray and neutron production in flares is the thick-target model on which the particles stop in the interaction region; the arguments that favor this model have been summarized recently (Murphy and Ramaty, 1985). The thick-target results presented here are based on the assumption that the angular distribution of the energetic particles in the interaction region is isotropic. The calculation of the yield of nuclear-line emission is essentially independent of this assumption because this emission is nearly isotropic with respect to the direction of the fast particles, but the calculation of the bremsstrahlung and high-energy neutron yields are quite sensitive to the angular distribution of the particles. Calculations that take into account anisotropy of the particles have not yet been published.

2.3.3.1 Energy Spectra of the Accelerated Particles

Gamma-ray and neutron observations can be used to test the validity of the functional forms of the energetic-particle spectra predicted by acceleration theories, as well as to set constraints on the values of the parameters that characterize these spectra. The relevant observations are (1) the ratio of the 4-8 MeV nuclear gamma-ray fluence to the 2.223 MeV line fluence, which provides a measure of the ion spectrum in the 10 to 100 MeV/nucleon range, and (2) the energy spectrum of neutrons released into interplanetary space, which provides information on the ion spectrum in the 100 to 1000 MeV/nucleon region. Technique (1) can only be used for disk flares, because, for limb flares, the 2.223 MeV line is strongly attenuated by Compton scattering in the photosphere (Wang and Ramaty, 1974). Values of αT, the parameter that characterizes the Bessel-function spectrum, and s, the spectral index of the power law, obtained (Murphy and Ramaty, 1985) by applying technique (1) to 8 disk flares are listed in Table 2.3.1 (events 1 through 8).

Table 2.3.1 Energetic Particle Parameters (from Murphy and Ramaty 1985 except as noted)

	Bessel Function		Power Law		Interplanetary Observations	
Flare	αT	$N_p(>30MeV)$	**S**	$N_p(>30MeV)$	**Spectral Index**	$N_{p,esc}(>30MeV)$
1. Aug. 4, 1972	0.029 ± 0.004	1.0×10^{33}	3.3 ± 0.2	7.2×10^{32}	—	4.3×10^{34}
2. July 11, 1978	0.032	1.6×10^{33}	3.1	1.3×10^{33}	—	—
3. Nov. 9, 1979	0.018 ± 0.003	3.6×10^{32}	3.7 ± 0.2	2.6×10^{32}	—	—
4. June 7, 1980	0.021 ± 0.003	9.3×10^{31}	3.5 ± 0.2	6.6×10^{31}	$\alpha T\simeq0.015$	8×10^{29}
5. July 1, 1980	0.025 ± 0.006	2.8×10^{31}	3.4 ± 0.2	1.9×10^{31}	—	$<4\times10^{28}$
6. Nov. 6, 1980	0.025 ± 0.003	1.3×10^{32}	3.3 ± 0.2	1.0×10^{32}	—	3×10^{29}
7. April 10, 1981	0.019 ± 0.003	1.4×10^{32}	3.6 ± 0.2	1.0×10^{32}	—	—
8. June 3, 1982	0.034 ± 0.005	2.9×10^{33}	3.1 ± 0.1	2.2×10^{33}	$s\simeq1.7$	3.6×10^{32}
9. June 21, 1980	0.025	7.2×10^{32}	—	—	$\alpha T\simeq0.025$	1.5×10^{31}
*10. Dec. 9, 1981	—	$<2\times10^{31}$	—	—	—	1.0×10^{32}

*from Cliver *et al.* (1983)

The value of αT for the June 21, 1980 limb flare (event 9 in Table 2.3.1) was derived from neutron observations. In Figure 2.3.6, the time-dependent neutron flux observed from the June 21, 1980 flare (Forrest, 1983) is compared with calculated neutron fluxes resulting from both Bessel-function spectra and power laws, normalized to the observed 4-7 MeV fluence. As can be seen, a Bessel-function spectrum, with $\alpha T = 0.025$, can simultaneously fit both the shape and absolute normalization of the observed neutron flux; on the other hand, a power-law spectrum cannot provide such a simultaneous fit for any value of s. In Section 2.3.4.1 we compare the αT's derived from gamma-ray and neutron observations with the αT's obtained by fitting Bessel functions to the spectra observed in interplanetary space.

The only other flare for which published neutron time profiles are available is the June 3, 1982 flare (Chupp *et al.*, 1983; Debrunner *et al.*, 1983; Evenson *et al.*, 1983). An analysis similar to that for the June 21, 1980 flare showed (Murphy and Ramaty, 1985) that a neutron time profile resulting from a Bessel-function proton spectrum again provided an acceptable fit to the data. The resultant value of $\alpha T \simeq 0.04$ is in good agreement with that determined independently from the 4-7MeV-to-2.223MeV flux ratio (see Table 2.3.1). This is the only flare for which the two techniques have so far been used simultaneously.

2.3.3.2 Total Particle Numbers and Energy Contents

In addition to setting constraints on energy spectra, the gamma-ray line and neutron observations also determine the total number of particles and the energy content in them, at least for particle energies above the gamma-ray production thresholds (generally a few MeV/nucleon). Total numbers of accelerated protons above 30 MeV, derived for the 9 flares discussed above, are also shown in Table 2.3.1. Also shown in this table is an upper limit on the number of protons that interact at the Sun for the December 9, 1981 flare, derived from the measured upper limit on the 2.223 MeV line fluence (Cliver *et al.*, 1983) and assuming that $\alpha T = 0.025$. The comparison of these numbers with the numbers of particles observed in interplanetary space is discussed in Section 2.3.4.2. Because of the chosen normalization, 30 MeV/nucleon, the

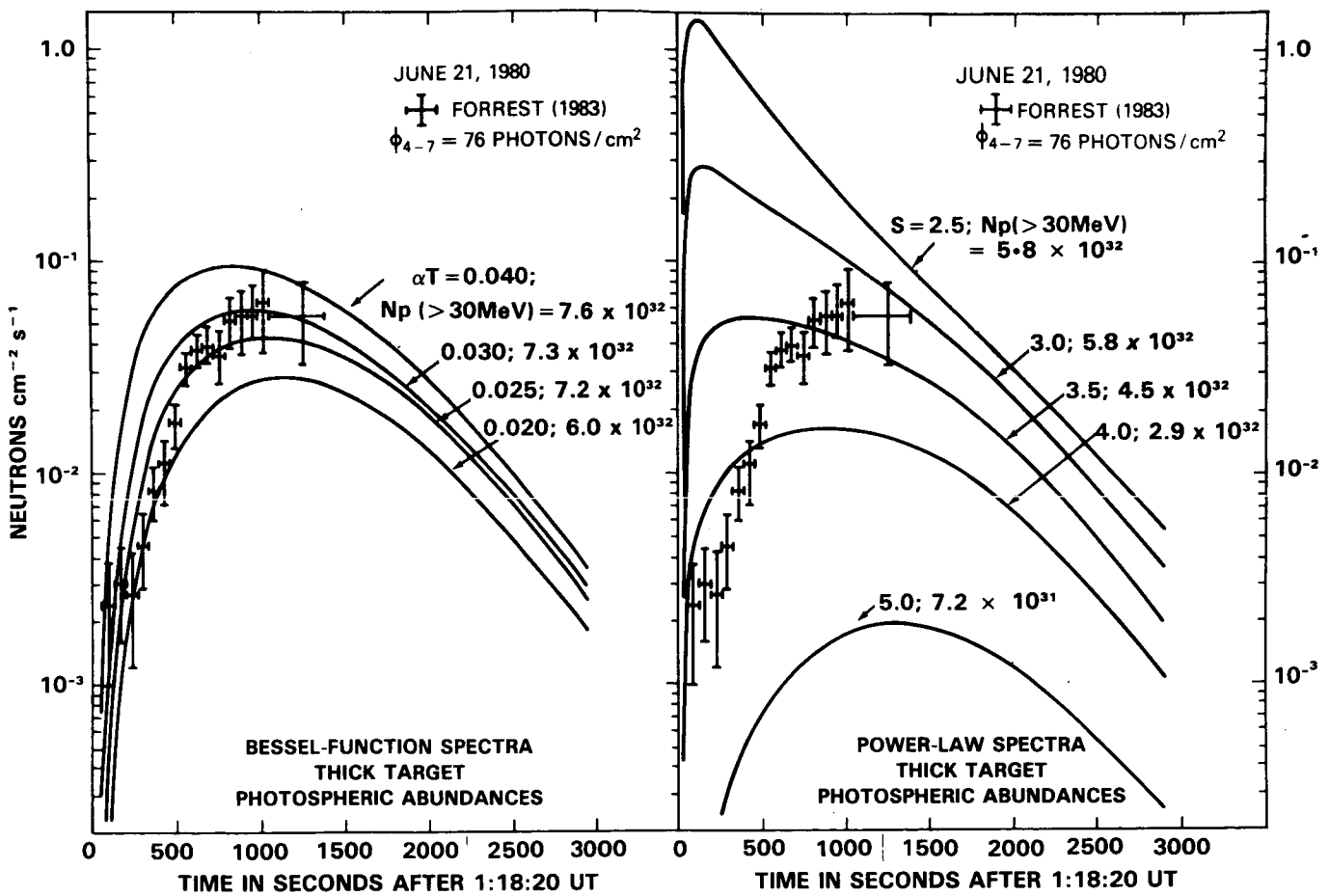

Figure 2.3.6 Calculated neutron time profiles for the June 21, 1980 flare and their comparison with observations. From Murphy and Ramaty (1985).

proton numbers do not depend much on the assumed functional form of the spectrum, as can be seen in Table 2.3.1. On the other hand, the total energy contents do depend critically on the shape of the spectrum at low energies. Values of the energy content in ions of energies greater than 1 MeV/nucleon were derived for several flares using Bessel-function spectra (Ramaty, 1985): these energy contents range from $\sim 5 \times 10^{28}$ ergs for the July 1, 1980 flare to $\sim 2 \times 10^{30}$ ergs for the August 4, 1972 flare.

2.3.3.3 The Electron-to-Proton Ratio

Having described the derivation of the spectrum and normalization of the protons which produce the gamma-ray lines and neutrons, we proceed now to describe a similar derivation for the relativistic electrons which produce the gamma-ray continuum by bremsstrahlung. The relationship between an isotropic power-law electron distribution in the thick-target model and the resultant photon fluence was given previously (Ramaty and Murphy, 1984), but, as already mentioned, no calculations have yet been published for anisotropic distributions.

As discussed above, the gamma-ray continuum at energies below ~ 1 MeV is primarily electron bremsstrahlung, at energies between 1 and 8 MeV it is a superposition of bremsstrahlung and broad and unresolved narrow nuclear lines, while at higher energies, in addition to bremsstrahlung from primary electrons there could be a contribution from photons from π^0 decay and from bremsstrahlung by electrons and positrons from charged π decay. The gamma-ray continuum above 10 MeV from the June 21, 1980 flare should be mainly electron bremsstrahlung, since the proton spectrum derived from the neutron observations is too steep to yield many π mesons. The electron spectrum incident on the thick-target interaction region for this flare, deduced from the observed (Chupp, 1982) gamma-ray spectrum between 0.27 and 1 MeV and the integral fluence above 10 MeV (Rieger *et al.*, 1983) can be approximated (Ramaty and Murphy, 1984) by a power law with spectral index ~ 3.5. This spectrum is shown in Figure 2.3.7, together with the proton spectrum obtained from the neutron and nuclear gamma-ray observations. In Section 2.3.4.3 we compare the e/p ratio implied by these results with that observed in interplanetary space.

The proton spectrum deduced for the June 3, 1982 flare. ($\alpha T \simeq 0.04$) implies a larger π-meson production relative to electron bremsstrahlung than for the June 21, 1980 flare. Consequently, the observed >10 MeV fluence from the June 3 flare could contain an important contribution from π-meson decay. For more detail, see Murphy and Ramaty (1985).

2.3.3.4 Anisotropy and the Interaction Site of the Particles

Gamma-ray and neutron observations offer the opportunity to study the anisotropy of the accelerated particles. An important result concerns the neutrons that escape from the Sun. It was pointed out (Ramaty *et al.*, 1983b) that the fact that such neutrons were seen from a limb flare (Chupp *et al.*, 1982) indicates that the primary protons could not have penetrated to very large depths in the photosphere. The observed neutrons have energies of several hundred MeV and therefore must be produced by protons of at least such energies. Such protons, should they travel in straight lines, would penetrate to great photospheric depths, on the order of a few tens of g/cm^2. Neutrons produced at such depths in limb flares could not escape from the photosphere in the direction of the Earth. The implication is that the primary protons must be stopped at much shallower depths, probably at the top of the photosphere. The stopping mechanism could be magnetic mirroring (Zweibel and Haber, 1983) or scattering off magnetic irregularities at the foot points of loops. These effects could also isotropize the particles. For the June 3, 1982 flare, Murphy and Ramaty (1985) find that the directional neutron flux at $50° \lesssim \theta < 90°$, obtained from interplanetary observations of protons from neutron decay, is

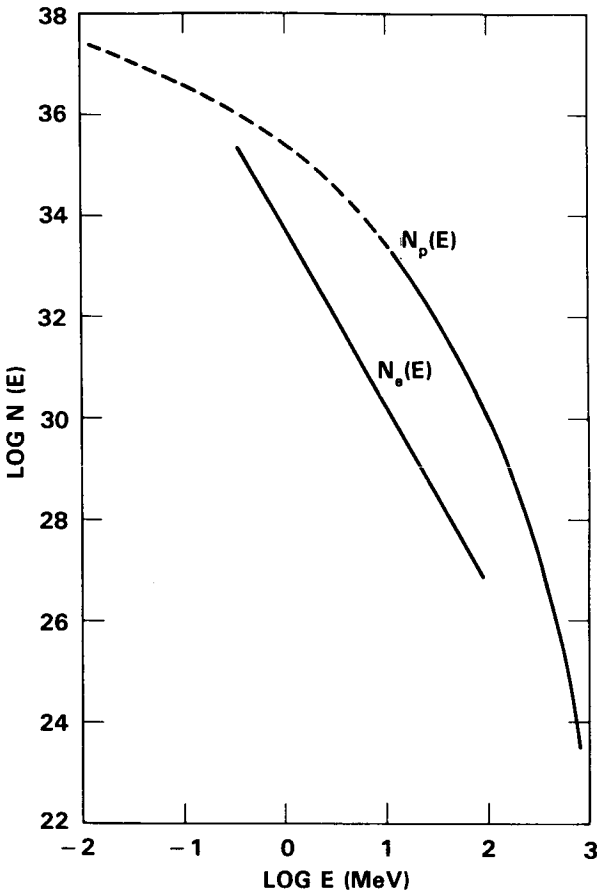

Figure 2.3.7 Calculated spectra and normalizations of the total numbers of protons and electrons accelerated in the June 21, 1980 flare. From Ramaty and Murphy (1984).

essentially the same as that at $90° < \theta < 180°$, obtained from the 2.223 MeV line observations. Here θ is the angle between the normal to the photosphere and the direction of observation. This result seems to imply that the flux of protons up to energies of ~ 100 MeV in the interaction region cannot be very anisotropic.

On the other hand, Vestrand *et al.* (1985) found that flares with gamma-ray continuum >0.27 MeV exhibit a center-to-limb variation, which would be consistent with the downward beaming of relativistic electrons. In addition, Rieger *et al.* (1983) have found that all GRS events with significant emission > 10 MeV are from flares near the solar limb. This observation implies the anisotropy of either the ultra-relativistic electrons, if the >10 MeV emission is bremsstrahlung, or the very high energy protons, if this emission results from π mesons.

The gamma-ray line observations can, in principle, also provide information on the beaming of the ions at the interaction site through the widths of the lines and through Doppler shifts. The observational information on this issue, however, is not clear, primarily because detailed observations with high-resolution detectors have not yet been carried out. The basic theoretical ideas have been described by Ramaty and Crannell (1976) and by Kozlovsky and Ramaty (1977).

The gamma-ray observations suggest that the ambient density in the interaction site of the energetic particles should exceed a few times 10^{11} cm^{-3} and therefore this site should be the chromosphere. This result is based primarily on the observed (Share *et al.*, 1983) time profiles of the 0.511 MeV line and their comparison (Ramaty and Murphy, 1984; Murphy and Ramaty, 1985) with theoretical time profiles

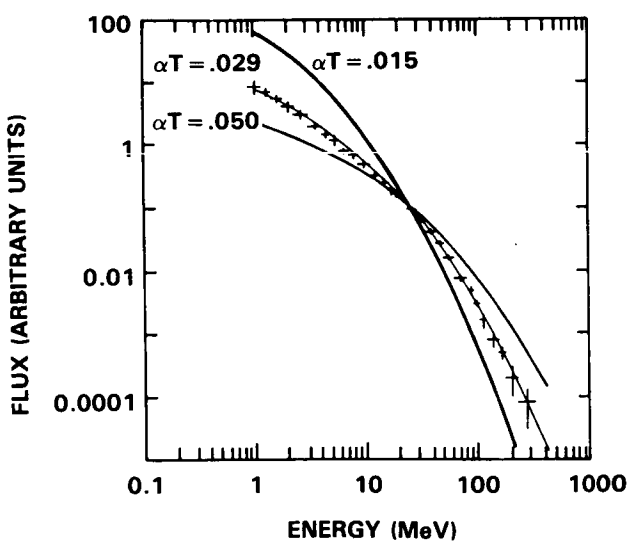

Figure 2.3.8 An example of fitting Bessel functions to the spectrum of the August 21, 1975 flare. From McGuire and von Rosenvinge (1985).

which take into account the lifetimes of the various positron-emitting nuclei and the slowing-down and annihilation times of the positrons.

2.3.3.5 Compositions

Gamma-ray line spectra, such as shown in Figure 2.3.1, offer the opportunity for studying relative elemental compositions. The contribution of proton and alpha-particle interactions in the thick-target model is significantly larger than that of the heavier nuclei. Therefore, the structure of the total nuclear spectrum is much more sensitive to the relative abundances of the ambient medium, i.e., the chromosphere, than to those of the energetic particles. Studies in progress (Murphy 1985) indicate that the chromospheric abundances, deduced from the gamma-ray observations, could differ from those of the photosphere in a manner similar to that observed in the energetic particles (see 2.3.4.4).

2.3.4 Interplanetary Charged-Particle Observations

2.3.4.1 Energy Spectra

Interplanetary protons and heavier ions resulting from acceleration in solar flares are observed up to energies of several hundreds MeV by instruments on spacecraft (e.g., McGuire and von Rosenvinge, 1985) and up to energies of about 10 GeV by ground based detectors (e.g., Debrunner *et al.*, 1984). Flare-accelerated relativistic electrons are also observed by detectors on spacecrafts up to energies of tens of MeV (Lin *et al.*, 1982; Evenson *et al.*, 1984). The particle energy spectra deduced from these measurements are generally subject to uncertainties introduced by coronal and interplanetary propagation. These uncertainties, however, can be minimized by considering only particle events that are well-connected magnetically to the detector and by constructing the particle energy spectra at times of maximum intensity at each energy (see McGuire and von Rosenvinge, 1985). This technique was used recently (McGuire and von Rosenvinge, 1985) to analyze the proton and alpha-particle energy spectra from a sample of particle events which show no evidence of interplanetary shock acceleration or multiple flare injection. It was found that many flares have proton spectra which are best fit by Bessel functions (see Section 2.3.3) over a broad energy range (from a few MeV to a few hundred MeV). An example is shown in Figure 2.3.8. The implied values for the whole sample, $\alpha T = 0.025 \pm 0.01$, are in good agreement with those derived for other flares from the gamma-ray and neutron observations (see Section 2.3.3.1). Moreover, for one flare, that of June 21, 1980, the Bessel-function spectrum with $\alpha T = 0.025$, derived from the neutron and gamma-ray observations, provides an acceptable fit to the interplanetary proton spectrum which was also observed (McDonald and Van Hollebeke, 1985) from

this flare. These results provide support for the validity of the stochastic Fermi mechanism for ion acceleration in flares. But it should be noted that acceleration by planar shocks with losses (Forman, Ramaty and Zweibel, 1985) or by spherical shocks (Lee and Ryan, 1985, see also Section 2.4) can produce spectra that, in the energy range of interest, are indistinguishable from the Bessel-function spectra and therefore can also fit the observations. Furthermore, the observed alpha-particle spectra are generally steeper than the proton spectra, and this result is inconsistent with the assumptions of constant diffusion mean-free-path and escape time that are made in the simple treatment of stochastic Fermi acceleration (see Section 2.3.3). Stochastic Fermi acceleration with rigidity-dependent diffusion was treated by Barbosa (1979, see also Forman, Ramaty and Zweibel, 1985), but no detailed comparisons of the resultant spectra with data have yet been made.

Another spectral form which fits the data of many flares is an exponential in rigidity, but no acceleration mechanism that predicts this form has yet been proposed. Occasionally, the proton spectra show (McGuire and von Rosenvinge, 1985) a complex structure that cannot be fit by any simple form. Such spectra could result from the combination of more than one acceleration process.

Particle acceleration at shock fronts is known to occur at many sites. As already mentioned (see Section 2.3.3) a prediction of acceleration by planar shocks with no losses is that the differential particle number per unit momentum should be a single power law. This implies (Ellison and Ramaty, 1985) that the differential particle flux per unit kinetic energy can be approximated by power laws in the nonrelativistic and ultrarelativistic limits, with the spectral index steepening by a factor of 2 above a kinetic energy equal to the particle rest-mass energy. The observed proton energy spectra for some flares can be fit (McGuire and von Rosenvinge, 1985) by single power laws up to kinetic energies of several hundred MeV, consistent with planar shock acceleration without losses. Moreover, the spectra predicted by such acceleration could also fit the proton spectra that are occasionally observed to extend up to 10 GeV. Recently, solar-flare proton spectra, obtained from the combination of spacecraft and ground-based data (Debrunner *et al.*, 1984), show the characteristic steepening at ~ 1 GeV.

The energy spectra of relativistic interplanetary electrons from solar flares were studied by Lin, Mewaldt and Van Hollebeke (1982) and recently by Evenson *et al.* (1984). The observed spectra, if fit by power laws in kinetic energy over narrow energy intervals, show great variability from flare to flare. This is illustrated in Figure 2.3.9, where the filled symbols indicate gamma-ray flares. As can be seen, the relativistic electron spectra of such flares are among the hardest observed. For the June 21, 1980 flare, in particular, the electron spectral index, ~ 3.2, obtained from the interplanetary observations, is in good agreement with the index

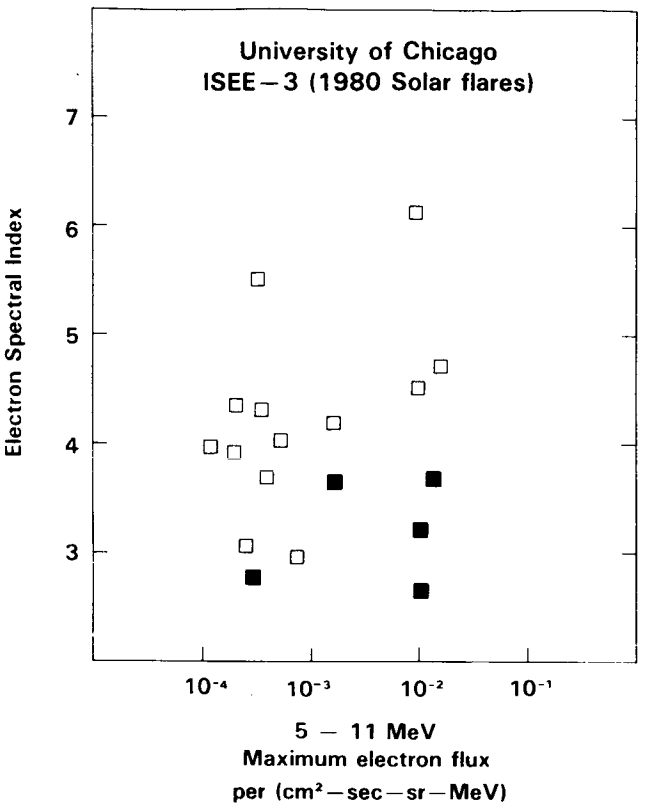

Figure 2.3.9 Spectral indices and fluxes from electron events observed in interplanetary space. The filled symbols indicate gamma-ray flares. From Evenson *et al.* (1984).

derived from the gamma-ray continuum (see Section 2.3.3.3). Power-law spectra at ultrarelativistic energies are consistent with both stochastic and shock acceleration with no losses.

2.3.4.2 Total Proton Numbers in Interplanetary Space

The number of protons that interact at the Sun and the number that escape into interplanetary space are listed for several flares in Table 2.3.1. The meager data base notwithstanding, these results appear to suggest at least 2 categories of events: (1) events in which the number of interacting ions greatly exceeds the number escaping (events 4, 5, 6 and 9), and (2) events in which the number of escaping ions exceeds the number interacting (events 1 and 10). It remains an unanswered question whether the variability of the ratio between the two particle numbers is caused by a variable escape probability from the Sun or by different acceleration processes. It is interesting to note that for the June 3, 1982 flare, the numbers of escaping and interacting ions differed only by less than an order of magnitude. The complex time dependences of the gamma-ray emissions from this flare

(Chupp *et al.*, 1983; Share *et al.*, 1983) might require particle acceleration in at least two phases (Murphy and Ramaty, 1985).

2.3.4.3 The Electron-to-Proton Ratio

The ratio of interplanetary electron fluxes and proton fluxes at the same energy are shown in Figure 2.3.10. As can be seen, the largest values of this highly variable ratio correspond to gamma-ray flares. The time dependence of the fluxes of these electron-rich events are diffusive (see Figure 2.3.11), indicating that strong interplanetary shocks were not associated with these events.

For the June 21, 1980 flare, which is an electron-rich as well as a gamma-ray event, the interplanetary electron-to-proton ratio can be compared with the corresponding ratio derived from the gamma-ray and neutron data. The interplanetary ratio at $\sim$ 30 MeV is about 0.05 (Evenson *et al.*, 1984), while the gamma-ray and neutron data (see Figure 2.3.7) imply that this ratio at 30 MeV is smaller by approximately a factor of 100. This difference could result from either the preferential escape of the relativistic electrons, or an anisotropy of the electrons in the gamma-ray production region. In the latter case, the isotropic bremsstrahlung calculation that was used to obtain the results of Figure 2.3.7 would underestimate the electron number.

2.3.4.4 Compositions

The most recent results on the elemental composition of solar energetic particles were presented by Cook, Stone and Vogt (1984). It was found that, for flares for which the abundances are not a strong function of energy/nucleon, the observed compositions appear to vary about an average which could reflect the composition of the medium from which the particles are accelerated. This composition is different from that of the photosphere, but seems to be in agreement with the composition of the corona and the solar wind. As discussed in Section 2.3.3.5 the gamma-ray observations suggest that the composition of the chromosphere also differs from that of the photosphere. Thus, several independent methods of abundance determinations seem to imply that important compositional modifications occur during transport of matter from the photosphere to the rest of the solar atmosphere.

In addition to elemental composition, interplanetary particle observations also provide information on isotopic compositions (e.g., Mewaldt, Spalding and Stone, 1984) and charge (Gloeckler, 1985) states. We shall not discuss these here in detail, except to mention that the charge-state observations strongly suggest that the solar-flare particles seen in interplanetary space are probably accelerated in the corona. This conclusion is based on the observed charge-state dis-

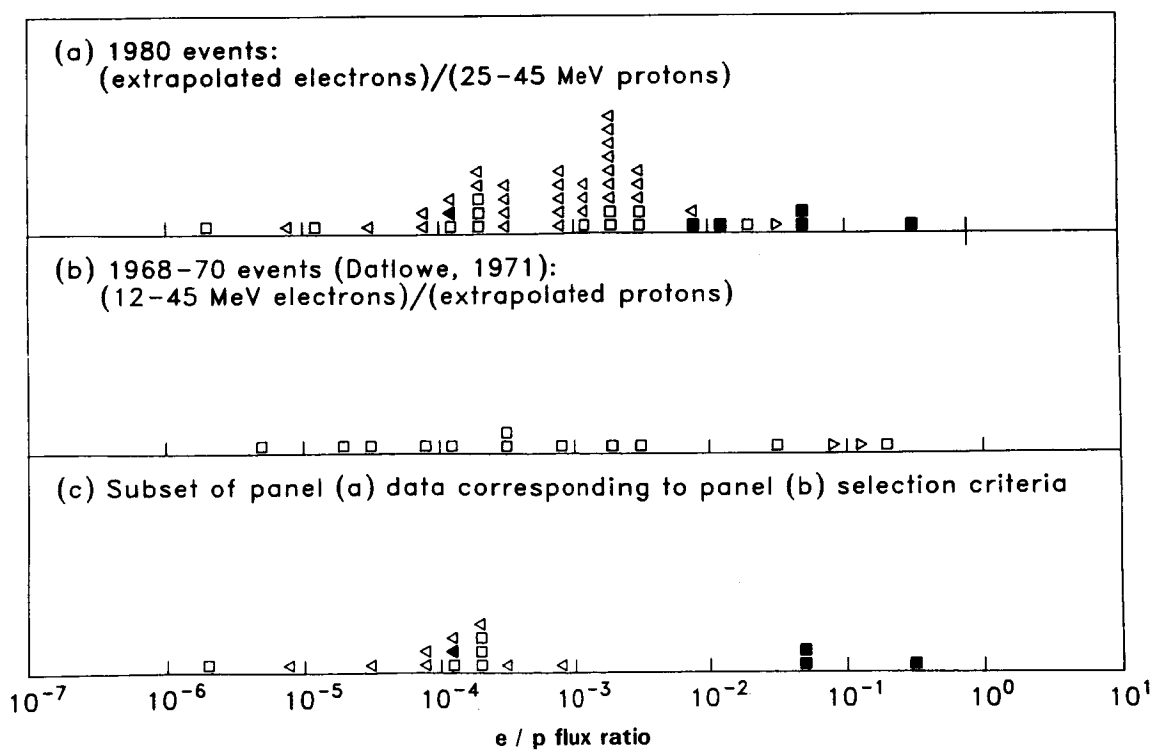

Figure 2.3.10 Electron-to-proton ratios. Square symbols indicate measurements, triangles indicate upper or lower limits and filled symbols indicate gamma-ray flares. From Evenson *et al.* (1984).

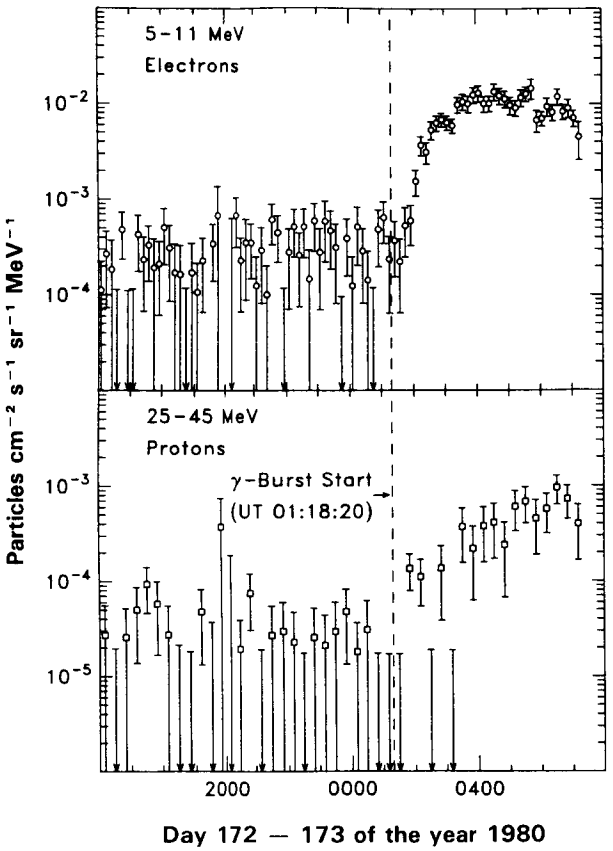

Figure 2.3.11 Interplanetary particle time profiles from the June 21, 1980 gamma-ray and electron-rich flare. From Evenson *et al.* (1984).

tributions, which seem to agree with a plasma of coronal temperatures, and on the presence of singly-charged He, which implies that the amount of matter traversed during escape is very small. A similar conclusion follows also from the apparent absence of spallation products (^{2}H, ^{3}H, Li, Be, B) from the observed particles. We note, however, that at typical coronal temperatures singly-charged He is not the dominant charge state of He.

2.3.5 The Nature of the Ion and Relativistic Electron Acceleration Mechanisms

A variety of observational evidence (discussed in Section 2.2) has shown that energy release in flares is strongly related to the acceleration of nonrelativistic electrons. This acceleration has been commonly referred to as first-phase acceleration to distinguish it from such phenomena as Type II radio emission which were refered to as second-phase acceleration (Wild, Smerd and Weiss, 1963; De Jager, 1969; Ramaty *et al.*, 1980). Prior to the SMM and other recent gamma-ray observations, it was believed that ion and relativistic electron acceleration occurs only in this second phase. However, the very impulsive nature of the gamma-ray emission and its close temporal association with the standard signatures of first-phase acceleration (e.g., hard X-ray emissions), demonstrate that ion acceleration can also take place in the first phase. This result, together with the fast onset and rapid rise of the gamma-ray fluxes, sets strong constraints on the nature of the acceleration mechanism. For example, it must be possible to accelerate ions and electrons to tens of MeV within a few seconds and ions to hundreds of MeV in less than a minute. Which of the various proposed flare acceleration mechanisms can satisfy these constraints remains an unanswered question.

We already discussed in Section 2.2.6 that first-phase acceleration might proceed in two steps, as proposed by Bai and Ramaty (1979), Bai (1982) and Bai *et al.* (1983b). The assumption of the two-step model that the ion and relativistic electron accelerations are closely coupled is supported by the data, in particular by the good correlation between the ~ 0.3 MeV bremsstrahlung and the 4-8 MeV nuclear emission (Figure 2.3.4). But there are conflicting points of view regarding the relationship between ion acceleration and nonrelativistic electron acceleration, which tests the basic postulate of the two-step model. The finding that there seems to be a set of characteristics that are common to only gamma-ray line flares (Bai *et al.*, 1983a; Bai and Dennis, 1985) argues for a second acceleration step. These characteristics are: (1) For gamma-ray line flares, the time profiles of higher energy (> 100 keV) X rays are delayed relative to those of lower energy X rays (~50 keV), or, equivalently, the hard X-ray spectrum flattens with time during the burst. In some instances, the time profiles of the 4-8 MeV nuclear gamma rays are also delayed relative to the X-rays (Bai, 1982). (2) The energy spectra of the hard X-ray flux at the peak of emission is, on average, significantly flatter for gamma-ray line flares than for flares without detectable gamma-ray lines. (3) Gamma-ray line flares seem to be better correlated with Type II and Type IV radio bursts than are flares with no detectable gamma-ray lines.

On the other hand, it is not clear that gamma-ray flares always have these distinguishing characteristics and, furthermore, explanations other than second-step acceleration might exist for at least some of them. As mentioned in Section 2.3.1.2 the peaks of the fluxes in various energy channels can be simultaneous within the detector time resolution, as can be seen in Figure 2.3.3. In addition, the comparison of the starting times of the photon fluxes in the various channels could be more relevant in determining the reality of second-step acceleration than the comparison of the peak times because delays between the peak times could be due to energy-dependent Coulomb losses in a trap model (which was discussed extensively in Section 2.2.6). As noted earlier for two impulsive flares, the starting times of the 4.1-6.4 MeV and the 40-65 keV fluxes were essentially the same, even though these two fluxes show evidence for a delay in their times of maximum (Forrest and Chupp, 1983).

Given that there is substantial ion and relativistic electron acceleration in the first phase, it is natural to ask whether any further particle acceleration occurs in the second phase by shock acceleration in the corona, as originally proposed by Wild, Smerd and Weiss (1963). Support for such a concept comes from the poor correlation between the ion population that interacts at the Sun and that observed in interplanetary space which could be a manifestation of the two acceleration phases. Additional evidence comes from the observations of solar flare heavy ions in interplanetary space, wherein it appears that the source of the ions is a large volume in the corona (Mason *et al.*, 1984). On the other hand, it is possible that this lack of correlation is simply due to the unequal and variable upward and downward escape conditions which are determined by unknown magnetic configurations. Furthermore, the good agreement between the proton spectra deduced from the gamma-ray observations and those observed in interplanetary space suggests that, for at least some flares, these two ion populations are commonly accelerated.

2.3.6 Summary

The opening of a new channel of information on the acceleration of particles in solar flares by routine gamma-ray and neutron observations is one of the major achievements of SMM. We summarized the most important available gamma-ray and neutron data and presented their interpretations in a manner as independent of specific models as possible. We then explored the relationships of these results with other flare phenomena.

As gamma-ray and neutron emissions are signatures of ion and relativistic electron acceleration, we have explored the relationship of these emissions to the other unambiguous manifestation of particle acceleration: the direct detection of accelerated particles in interplanetary space. We have also explored the relationships of the gamma-ray emission with other flare phenomena, in particular hard X-ray emission, in an attempt to resolve the question of multiple-step accelerations.

We return to the questions posed in the introduction:

1. *What are the time characteristics of the energization source?*

Gamma-ray emission from flares is prompt. Within detector sensitivity, the starting times of the nuclear gamma-ray emission and nonrelativistic bremsstrahlung X-ray emission are the same; but the peaks of the fluxes in the various energy channels can be delayed one relative to the other (Section 2.3.1.2). These results demonstrate that acceleration of ions and relativistic electrons are closely associated with the primary energy release in flares.

2. *Does every flare accelerate protons?*

The good correlation of the relativistic electron bremsstrahlung fluence > 0.27 MeV and the ion-associated nuclear excess fluence in the energy range 4-8 MeV suggest that, for 4-8 MeV fluences greater than the GRS sensitivity threshold, relativistic electron acceleration is always accompanied by ion acceleration. There also seems to be an overall association of gamma-ray emission with many diverse flare phenomena, suggesting that ion acceleration could be quite common.

3. *What is the location of the interaction site of the energetic particles?*

The gamma-ray line observations suggest that the interaction site of the ions and relativistic electrons is located at densities $> 10^{11}$ cm^{-3} (i.e., in the chromosphere) and the neutron observations imply that mirroring or scattering should stop the highest-energy ions from penetrating the photosphere (Section 2.3.3.4). The comparison of neutron release into interplanetary space and towards the photosphere is consistent with isotropic neutron production, at least up to 100 MeV (Section 2.3.4). But gamma-ray continuum observations suggest that relativistic electrons are anisotropic (Section 2.3.4).

4. *What are the energy spectra for ions and relativistic electrons?*
   Does the spectrum vary from flare to flare?

The energy spectra of the ions that interact at the Sun cannot be fit by single power laws in kinetic energy. Better fits are obtained with more curving spectra such as those resulting from stochastic Fermi acceleration or shock acceleration with losses (Section 2.2.3.1). The spectral index αT varies from flare to flare but over a fairly narrow range: $0.015 \lesssim \alpha T \lesssim 0.040$.

5. *What is the relationship between particles at the Sun and interplanetary space?*

The spectra of flare protons observed in interplanetary space are in many cases similar to those of particles interacting at the Sun (Section 2.3.4.1). The range of spectral indices, $0.015 \lesssim \alpha T \lesssim 0.035$, is in reasonable agreement with the range deduced from the gamma-ray measurements, suggesting that, for most flares, a common mechanism could accelerate both particle populations. On the other hand, the numbers of ions inferred from the gamma-ray and interplanetary observations do not agree on a flare by flare basis. This could be due to unequal and variable upward and downward escape probabilities or to two acceleration phases (Section 2.3.5). The hardest relativistic electron spectra and the highest electron-to-proton ratios are observed from gamma-ray flares.

6. *Is there any evidence for more that one acceleration mechanism?*

The prompt nature of the gamma-ray emission from flares demonstrates that ion and relativistic electron acceleration can occur in the first phase of particle acceleration. A second phase of particle acceleration, due to the passage of a shock wave through the corona, probably also accelerates ions and relativistic electrons, but the gamma-ray signatures

of these particles have not yet been identified. The possibility that first-phase acceleration could consist of multiple steps has also been considered, but the evidence for such steps remains equivocal.

2.4 THEORETICAL STUDIES OF PARTICLE ACCELERATION

In the last two Sections we specified the main requirements for the acceleration source. We now turn our attention to the recent development of ideas on bulk energization. It is well accepted today that the transformation of magnetic energy into plasma energy is the main process that provides the observed transient energization in solar flares. We present in this Section several mechanisms that can, under certain conditions, accelerate electrons and ions to high energies.

2.4.1 Particle Acceleration in Reconnecting Magnetic Fields

2.4.1.1 Resistive Tearing Instability

There have been a number of recent attempts (Van Hoven, 1979; Smith, 1980; Heyvaerts, 1981) to *estimate* the electric fields produced by the resistive tearing instability, but the results disagree. Most of this work concentrates on the *dynamic* energy-release mechanism (Furth *et al.*, 1963; Coppi *et al.*, 1976), with the aim of simulating the temporal development of the flare impulse. The principal reason for the lack of agreement on the acceleration performance of tearing reconnection is that the induced electric fields critically depend on the *small-scale* magnetic structure and on the *energy-transport* history as the instability nears the point of saturation, and such nonlinear behavior is poorly known. The situation (in the simplest case) is as follows: the resistive tearing instability (or reconnection) grows in a sheared magnetic field B(r) in which the field lines locally have the changing orientation of the steps of a spiral staircase. In the vicinity of that step which is perpendicular to the nearest wall (boundary), the magnetic field is decoupled from the plasma so that it is no longer frozen and can spontaneously tear and reconnect (Van Hoven, 1979). The reversal of the direction of the orthogonal components of the nearby field lines and their later merging, are shown in Figure 2.4.1. As resistive tearing commences, the electric field changes from its pre-existing low equilibrium value of $\underset{\sim}{E}_o \simeq \eta J_o \underset{\sim}{e}_z$, (where $\eta(T)$ is the resistivity and J_0 is the current) in two essential ways.

The $\underset{\sim}{B}$ field-aligned z component ηJ_z grows at the reconnection point (Van Hoven, 1979), causing an increasing acceleration of electrons and protons along $\underset{\sim}{e}_z$. E_z can (according to some estimates) reach the Dreicer (1959) value E_D, at which the electric force becomes greater than the collisional drag, and the electrons will be freely accelerated.

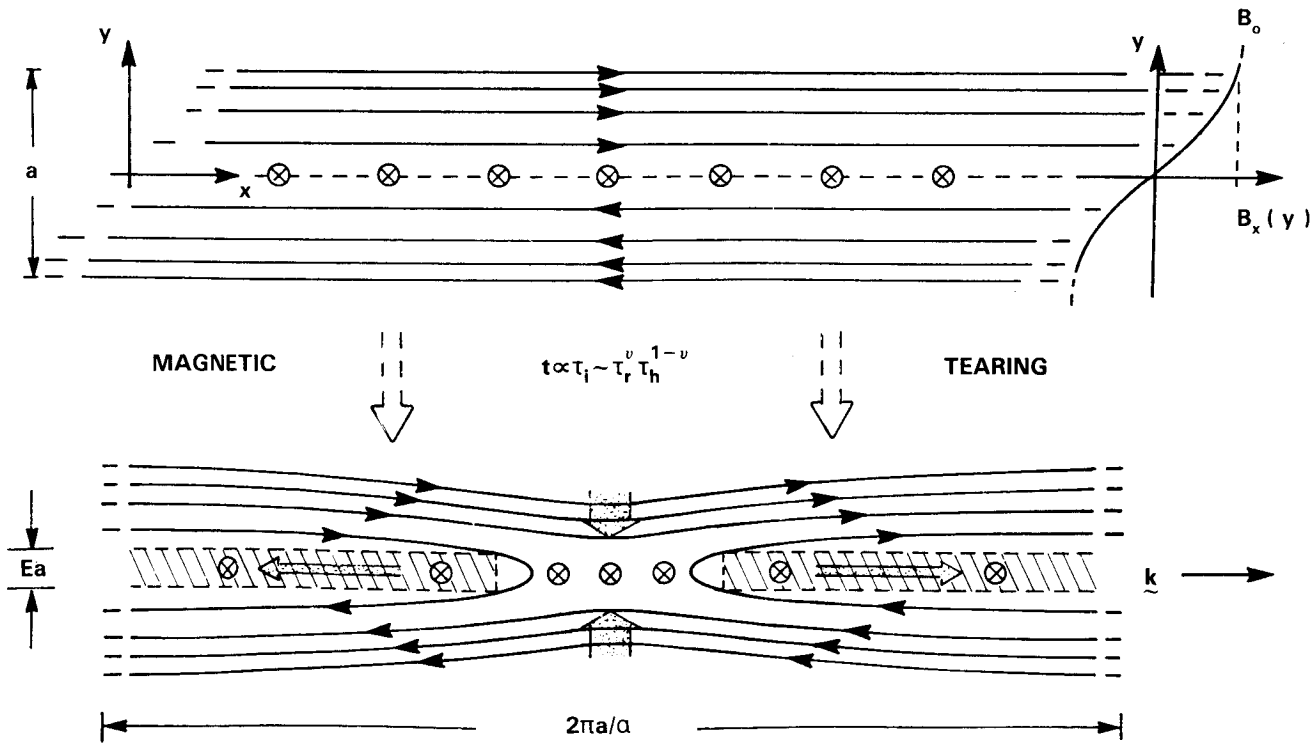

Figure 2.4.1 The development of magnetic tearing. The tail-of-the-arrow symbols show the direction of $\underset{\sim}{J}(x, 0)$ which is antiparallel to $\underset{\sim}{B}(x, 0)$. The stippled arrows show flow velocities.

At the same time, the preexisting stationary plasma begins to move across the magnetic-field direction, as shown by the stippled arrows in Figure 2.4.1. The growing flow velocity v outside the resistive layer produces a rising $\underset{\sim}{E} = -\underset{\sim}{v} \times \underset{\sim}{B}$ electric field *across* $\underset{\sim}{B}$, which generates an increasing mass-independent drift velocity $(\underset{\sim}{E} \times \underset{\sim}{B})/B^2$ of the plasma inside the resistive layer. *Thus, there are two distinct mechanisms, available in a reconnecting field, for accelerating particles.* The crucial (and yet incompletely answered) question is how large do these accelerating *E* fields become as the magnetic tearing proceeds through its energy supply. The answer depends sensitively on the time development of the field structure at the reconnection point, which (in turn) depends on the local resistivity and on the external boundary conditions. In addition, the most interesting limit for large electric fields is the "non-constant-ψ" (long-wavelength, roughly) case (Drake *et al.*, 1978; Steinolfson and Van Hoven, 1983) for which the magnetic gradients are sharper, and the growth is faster and more prolonged. Most nonlinear computations presently available use boundary conditions chosen for mathematical convenience (not for solar applications), constant resistivity (set at an artificially high level to limit the expenditure of computer time) and short wavelengths (same reason). An entirely different scale of calculations, involving a full treatment of the energy transport, is needed to properly follow the variation of the local resistivity $\eta(T)$ as Joule heating, radiation losses and thermal conduction come into play (Van Hoven *et al.*, 1984; Steinolfson and Van Hoven, 1984a). Relevant nonlinear computations of the resistive tearing instability have been performed by Van Hoven and Cross (1973), Schnack and Killeen (1978), Drake *et al.* (1978), Ugai (1982, 1983), and Steinolfson and Van Hoven (1984b).

The group at the University of California (Irvine) has investigated two aspects of reconnection growth and saturation. Nonlinear computations have been made which specifically evaluate electric fields, and linear calculations have been performed on a reasonably complete energy-transport model. The new nonlinear results (Steinolfson and Van Hoven, 1984b) apply to the canonical single-tearing layer, with periodic boundaries parallel and remote boundaries perpendicular to it, and constant resistivity. However, exteme care is given to the spatial resolution on which the electric fields depend, and on attaining the non-constant-ψ limit at relatively high levels of magnetic Reynolds number. The results have proved to be somewhat disappointing, as far as their potential for a flare model are concerned. Initially non-constant-ψ excitations do indeed grow faster (by an order of magnitude) and farther (by two orders in energy) than constant-ψ modes. However, the growth rate falls (by one-half to one order of magnitude) soon after the nonlinear threshold is crossed (island width $\approx$ resistive-layer thickness), thereby slowing the energy output. In addition, the outward Fermi-acceleration flow develops a stagnation point, and then reverses. Finally, a new magnetic island grows as the reconnection point bifurcates (see detailed discussion by Priest *et al.* in Chapter 1). This more complex and wider island structure holds down the parallel electric field to a value (weakly increasing with S up to 10^6) of order 10^{-3} of the Dreicer field (Dreicer, 1959). This study is continuing, with emphasis on the effects of boundary conditions at the ends of the tearing layer, which now cause a back pressure leading to the flow stagnation, and of energy transport which can accelerate the reconnection. Energy-transport effects are the prime focus of Van Hoven's and Steinolfson's second effort in this context. They have treated Joule heating, thermal conduction, and (especially) optically-thin radiation which proves to have the dominant influence in a reconnection layer. At coronal temperatures, the radiative loss function gives rise to thermal instabilities (Field 1965), so that a temperature perturbation spontaneously grows. Van Hoven *et al.* (1984) have discussed the linear mode structures and growth rates, and have demonstrated the existence of a tearing-like and a faster radiative mode at coronal temperatures. A crucial aspect is that the addition of radiation drives the temperature down at the reconnection point, in contrast to the expected behavior in which the local Ohmic-heating peak would raise the temperature (T_e). The radiative decrease of T_e has the effect of increasing the Coulomb resistivity $\eta \propto T_e^{-3/2}$, with the potential of accelerating the magnetic-tearing rate. Steinolfson and Van Hoven (1984a) have also examined the reconnection behavior of the faster radiative mode. It has a growth time which does not vary with temperature (resistivity) and is 30 times shorter (for coronal conditions) than that of the tearing mode. They have now shown that this mode, at a comparable level, exhibits 30% of the reconnected flux of the slower tearing mode. The radiative instability thus has the potential for providing fast magnetic-energy release. In addition, the parallel electric field ηJ_z of the radiative mode is 200 times larger (at low levels) than that in the equivalent tearing mode. Nonlinear computations are needed to demonstrate the validity of these low-level indications.

2.4.1.2 Particle Dynamics Around the Neutral Point

The effects of turbulence in analytical and computational models have been excluded from most previous studies. It was assumed that the background magnetic field is initially smooth and that perturbations are symmetric and/or infinitesimal. There are indications (Matthaeus *et al.*, 1984) that finite-amplitude fluctuations can lead to turbulence in X-point dynamics, thereby increasing reconnection rates. Consequently, turbulent reconnection might maintain strong X-point electric fields at high conductivity. The question of whether a sub-population of particles might be accelerated to high energies by the reconnection-zone electric field has been studied extensively (e.g., Speiser, 1967; Vasyliunas, 1980). A typical approach has been to calculate the trajec-

tories of "test particles" in model MHD magnetic and electric fields. The electric field has usually been included parametrically. Sato *et al.* (1982) followed test particle orbits in the dynamic electric field of a symmetric, forced and nonturbulent MHD simulation. It was found that test particles do not spend much time near the X-type neutral points, but can easily be trapped near O-type neutral points. This is a crucial point in the assessment of the importance of reconnection as a particle accelerator. In non-steady incompressible simulations, strong accelerating electric fields do not appear near the O-points. A long residence time near the O-point is thus unlikely to produce significant particle acceleration. The short residence times of particles near the X-point region has been viewed as a limitation on the efficiency of the X-point acceleration mechanism. Matthaeus *et al.* (1984) followed orbits in the fields generated by an incompressible, MHD spectral-method simulation (see e.g., Matthaeus and Montgomery, 1981 and Matthaeus, 1982). The magnetic field configuration is a periodic sheet pinch which undergoes reconnection. Test particles are trapped in the reconnection region for a period of the order of an Alfven transit time in the large electric fields that characterize the turbulent reconnection process at the moderate magnetic Reynolds number ($S = \tau_R/\tau_A = 1000$, where τ_R is the resistive time and τ_a is Alfven transit time) used in their simulation. They found that a small number of particles gained substantial energy at the end of their simulation.

2.4.1.3 The Coalescence Instability

Tajima (1982) used a fully self-consistent electromagnetic relativistic particle code (Langdon *et al.*, 1976; Lin *et al.*, 1974) to study the coalescence of two current filaments. In the solar atmosphere these filaments may represent two different loops. They showed that during the linear stage the energy release is small (comparable to the Sweet-Parker rate) but this stage is followed by the nonlinear phase of the coalescence instability (Wu *et al.*, 1984; Leboeuf *et al.*, 1982) which increases the reconnection rate by two or three orders of magnitude. An important result from their simulation is that the plasma compressibility leads to an explosive phase of loop coalescence and its overshoot results in amplitude oscillations in temperature (by adiabatic compression and decompression). These oscillations resemble in structure the double sub-peak amplitude profile of the 1980 June 7 and 21 observations of microwave emission Nakajima *et al.* (1984b) observed on 1982 November 26 with the 17 GHz Nobeyama interferometer. Brunel *et al.* (1982) found that the ion distributions formed during the coalescence were characterized by intense heating and the presence of a long nonthermal tail. A word of caution about these results is in order here. Although the results seem very encouraging, the plasma parameters used in these simulations are far from those experienced in the solar environment. Thus, we can only use these results to stimulate new thinking and techniques for simulation, specifically oriented to solar physics in the near future.

2.4.1.4 Laboratory "Simulations" of Solar Flares

Another important tool for the exploration of the physical processes that take place during a flare is the use of laboratory experiments that "simulate" the solar environment and study the dynamics of the energy release process. Numerous such experiments have been performed in the past (e.g., Stenzel and Gekelman, 1985; Bratenhal and Baum, 1985). Recently, a group of scientists in U.S.S.R. have reported several major results obtained from laboratory experiments. (1) They detected the formation of current sheets, followed by increased plasma density and magnetic energy in the vicinity of the current sheet region (Somov *et al.*, 1983; Altyntsev *et al.*, 1984). (2) They have observed a sudden excitation of turbulence which was accompanied by fast energy release and particle acceleration, (Altyntsev *et al.*, 1977; Altyntsev *et al.*, 1981a). (3) Finally, during the nonlinear stage the field structure is very complex and includes several magnetic islands (Altyntsev *et al.*, 1983). The main result from the studies is that during a flare several fine, spatial and temporal, characteristics of the energy release can be studied in small laboratory experiment.

2.4.2 Electron Acceleration Along the Magnetic Field With Sub-Dreicer Electric Fields

In the simulations reported above the main question is: What is the strength of the electric field during the nonlinear phase of each of the instabilities? Let us now move one step forward and ask the question: What will happen to the plasma in the presence of a pre-existing electric field? Holman (1985) studied qualitatively the acceleration of runaway electrons out of the thermal plasma, the simultaneous Joule heating of the plasma, and their implications for solar flares. He shows, in agreement with Spicer (1983), that the simple electric field acceleration of electrons is incapable of producing a large enough electron flux to explain the bulk of the observed hard X-ray emission from flares as nonthermal bremsstrahlung. For the bulk of the hard X-ray emission to be nonthermal, at least 10^4 oppositely directed current channels are required, *or an acceleration mechanism that does not result in a net current in the acceleration region is required*. He also finds, however, that if the bulk of the X-ray emission is thermal, a single current sheet can yield the required heating and acceleration time scales, and the required electron energies for the microwave emission. This is accomplished with an electric field that is much less than the Dreicer field ($E/E_D \sim 0.02$-0.1). To obtain the required heating time scale and electron energies, the resistivity in the current sheet must be much greater than the classical

resistivity of a plasma with $n = 10^9$ cm^{-3}, $T_e = 10^7$K. A plasma density of $\simeq 10^{11}$ cm^{-3} is required in the flaring region or, if the density in the current sheet is less than 10^{11} cm^{-3}, the resistivity in the sheet must be anomalous. The identity of the microinstability that will enhance the resistivity is an open question.

Moghaddam-Taaheri and Vlahos (1985) developed a quasi-linear code to study the time development of runaway tails in the presence of a D.C. electric field as well as Coulomb collisions. It is well known that particles with velocities larger than the critical velocity $v_{cr} = (E_D/E_\parallel)^{1/2} v_e$ can overcome the drag force due to collisions and therefore can run away. As the bulk is depleted, the rate of particle flux in the tail decreases and causes the formation of a positive slope on the distribution of the runaway tail. This process sets up a spectrum of plasma waves with phase velocities on top of the runaway tail. The anomalous Doppler shift of these waves makes it possible for them to interact with fast electrons in front of the tail, when they acquire the appropriate parallel velocity to satisfy the resonance condition $k_\parallel v_\parallel = \omega_k + \Omega_e$. At this point, electrostatic turbulence can be driven by both Cherenkov and anomalous Doppler effects. Using different values of $E_\parallel$ Moghaddam-Taaheri and Vlahos showed that for $E_\parallel/E_D \simeq 0.2$ (The Dreicer field for a plasma with density $n_o = 10^{11}$ cm^{-3} and $T_e = 1$ keV is $E_D = 6 \times 10^{-2}$ V/m) or higher, electrons first stream along B and then are isotropized and thermalized. For $E_\parallel < 0.2\ E_D$ the anomalous Doppler-resonance scattering is weak and the tail is continuously accelerated to higher and higher velocities. They suggested that weak electric fields ($E_\parallel < 0.2\ E_D$) along a large fraction of the loop would be a better candidate for electron acceleration than the strong localized electric fields.

2.4.3 Lower Hybrid Waves

Tanaka and Papadopoulos (1983) have studied numerically the nonlinear development of cross-field current-driven lower hybrid waves (modified two-stream instability). They showed that for $\beta_e = (nkT_e/(B^2/8\pi)) < 0.3$ and ion drift velocity $\simeq$ 2-3 V_i symmetric electron tails are formed, with average velocity $\simeq$ 4-5 V_e. Smith (1985) has applied these results to the solar flare. He proposed that fast tearing modes occur in a current carrying loop (Spicer 1982). This leads to dissipation of the poloidal magnetic field and to bulk motion of the ions across the primarily toroidal field up to 0.3 v_A, (Drake, private communication), where the Alfven speed v_A is the speed in the poloidal field B_p. There are no calculations for the energetics of fast tearing, but calculations for slow tearing (Arion, 1984) indicate that 46% of the energy released goes into ion kinetic energy for the collisional tearing mode. It must be admitted that simulations (e.g., Terasawa, 1981) do not show such a large fraction of the energy going into ion kinetic energy; however, no simulations have approached the magnetic Reynolds number regime of 10^{10} - 10^{12} relevant for the Sun. For reasonable parameters (e.g., $B_p = 200$G, $n = 1.5 \times 10^{10}$ cm^{-3}, $v_A = 3.5 \times 10^8$ cm s^{-1}, $T_i = 3 \times 10^7$K, $v_i = (kT_i/m_i)^{1/2} = 5 \times 10^7$ cm s^{-1}), the bulk velocity 0.3 $v_A \sim$ 2-3 v_i, which is sufficient to excite the modified two stream instability. The modified two-stream instability is sensitive to the plasma beta (β) and saturates for levels of $\beta \geq 0.3$. Thus once β increases due to additional heating and/or a density increase due to evaporated material traveling back up the loop, the instability turns off and efficient electron acceleration would no longer occur.

2.4.4 Fermi Acceleration and MHD Turbulence

Fermi or stochastic acceleration of particles in turbulent fields is defined as the process that causes particles to change their energy in a random manner with many increases and decreases that lead finally to stochastic acceleration. Stochastic acceleration can also result from resonant pitch-angle scattering from Alfven waves with wavelengths of the order of the particle gyroradius. A simple way of understanding this mechanism is to imagine the random walk of a particle colliding with randomly moving infinitely-heavy scatterers (see Ramaty, 1979 or Heyvaerts, 1981 for a detailed discussion). The solution of the diffusion equation for the particle distribution (Tverskoi, 1967) can be expressed in terms of modified Bessel functions for $E << mc^2$ (a case applicable to non-relativistic protons) and as an exponential for $E >> mc^2$ (a case relevant to electrons). There are no analytical solutions for energies in between. The model is defined only if the velocity of the particle is equal to or larger than the velocity of the randomly moving scatterers (e.g., Alfven velocity). In other words, this mechanism needs a pre-acceleration or heating mechanism to inject particles above the momentum $p_o = M_i V_A$. A similar conclusion can be reached from the analysis of MHD waves resonantly interacting with the particles. For example, a quasi-linear equation can be written that will connect the spectrum of the unstable waves with the diffusion coefficient and the minimum resonance velocity can be estimated from the resonant condition between the waves and particles. A particle can resonate with an Alfven wave only when $\omega = k_\parallel V_A = k_\parallel V_\parallel + n\Omega^*$ or $|V_\parallel - V_A| = V_A |n\Omega^*/\omega|$ (where Ω^* is the relativistic gyrofrequency). Since the highest turbulent frequency of the spectrum is less than the ion gyrofrequency Ω_i, $|V_\parallel - V_A| > V_A |\Omega^*/\Omega_i|$ which implies that particle momentum must be larger than $M_i V_A$ to resonate. For a magnetic field strength $B \cong 500$G and $n \sim 10^{10}$ cm^{-3} the Alfven speed is $\sim$ 3000 km/s and the threshold velocity for ions is 0.1 MeV. Melrose (1983) has shown that magneto-acoustic turbulence with frequency $\omega \simeq 30$ s^{-1} can accelerate ions from a threshold velocity of 0.1 MeV to 30 MeV in 2 secs if $(\delta B/B)^2 \simeq 0.1$.

2.4.5 Shock Acceleration

Shock acceleration is currently one of the most intensely studied subjects in the space and astrophysical literature (Drury, 1983). During the workshop several new studies of shock acceleration were presented. We review here the main results.

2.4.5.1 Ion Acceleration

Lee and Ryan (1985) have calculated the temporally and spatially dependent distribution function of particles accelerated by a spherically symmetric coronal blast wave. The motivation here is to introduce an important geometrical effect into the calculation of an evolving acceleration to see if familiar features of accelerated particles can be reproduced. In order to carry out these calculations a few assumptions were made which limit the applicability and interpretation of the results. First, the particles are transported in a diffusive manner, thereby yielding less information about the earliest shock effects. Secondly, the density of the medium decreases as r^{-2} and the collisions are neglected making the calculations most relevant in dealing with high altitude and interplanetary acceleration as opposed to acceleration in the lower corona. Finally, a diffusion coefficient is chosen in a reasonable form but is independent of energy. This has an effect on the spectrum of the prompt arrival of particles at the earth. The three dimensional geometry yields both the acceleration effects from the shock, the diffusive escape of particles from the finite-size acceleration region and the deceleration effects from the divergent flow behind the shock. The results of the calculations can be summarized as follows. The spectrum of particles accelerated by the shock is soft initially but hardens as time progresses, approaching a power law in the limit. The distribution of particles at a particular energy peaks in time as a function of that energy. The lower energy particles peak in number sooner and subsequently decay away. Higher energy particles take longer to accelerate as one would expect. The time to reach maximum is roughly proportional to the particle energy, although significant numbers of particles at high energies exist initially. The particle distribution peaks at the shock front and decays away in a roughly power law fashion ahead of and behind the shock.

Decker and Vlahos (1984) have studied the role of wave-particle interactions in the shock-drift acceleration mechanism. Between shock crossings the ions are permitted to interact with a pre-defined spectrum of MHD waves [e.g., Alfven (parallel and oblique)] assumed to exist upstream and downstream of the shock. The amplitude and spatial extent of wave activity in the upstream region is varied as a function of angle θ_{Bn} between the shock normal and upstream magnetic field to simulate a decrease in wave activity as θ_{Bn} approaches 90°. For each simulation run, they followed several thousand test ions which were sampled from a specified pre-acceleration distribution and ensemble-averaged results compared for the wave and non-wave situations. The results show that even a moderate level of wave activity can substantially change the results obtained in the absence of waves. This occurs because at a "single encounter" (during which the ion remains within a gyroradius of the shock), the waves perturb the ion's orbit, increase or decrease the number of shock crossings, and therefore increase or decrease the shock-drift energy gain relative to the no wave situation. In particular the presence of waves generally increases both the fraction and average energy of transmitted ions and produces a smaller, but much more energetic population of ions reflected by the shock.

Tsurutani and Lin (1984) have obtained some preliminary results on shock acceleration from a comprehensive study of 37 interplanetary shocks which were observed by the ISEE-3 spacecraft near 1 AU. In this study the normals to the shock surface and the shock speed were determined from plasma and magnetic field parameters, and the energetic particle response was catagorized. The main finding was that particle acceleration to $\gtrsim$ 2 keV for electrons and $\gtrsim$ 47 keV for ions depended on the speed of the shock along the upstream magnetic field and on the ratio of the downstream to upstream magnetic field intensities. These results indicate that magnetostatic reflections of the particles off the shock itself play a very important role in the acceleration process. Figure 2.4.2 shows the 37 shock events plotted versus the shock speed in the upstream medium, and the angle θ_{Bn} between the shock normal and the upstream magnetic field (small θ_{Bn} implies quasi-parallel shock, θ_{Bn} near 90° implies quasi-perpendicular shock). The intensity of the particle acceleration due to each shock is indicated by the symbols: an open circle indicates little or no acceleration or a flux increase of $< 20\%$ above ambient pre-shock levels; a filled circle indicates an increase of $\geq 20\%$ but $< 200\%$; and a plus indicates increases of more than 200%. Typical uncertainties in θ_{Bn} are $\sim 12°$. We see that the open circles group toward the bottom left of the figure while pluses tend to the upper right, with filled circles in between. The lines are drawn for constant shock velocity along the upstream magnetic field, $v_{sB} = v_s/\cos\theta_{Bn}$. The line $v_{sB} = 250$ km/sec then separates those events with little or no particle acceleration from those with signficant particle acceleration. Figure 2.4.3 shows the same events with v_{sB} plotted against the ratio $|B_2|/|B_1|$ of downstream to upstream magnetic field strength. If the shock acts as a moving magnetic mirror,then this mirror will be least effective for small ratios of $|B_2|/|B_1|$ and vice versa. Figure 2.4.3 shows that this is the case: the open circles all have $|B_2|/|B_1| < 1.7$ and $v_{sB} < 250$ km/sec. Events with larger v_{sB} and small $|B_2|/|B_1|$ (< 1.7) only result in moderate events (filled circles), while events with both $|B_2|/|B_1| > 1.7$ and $v_{sB} > 250$ km/sec give rise to large events.

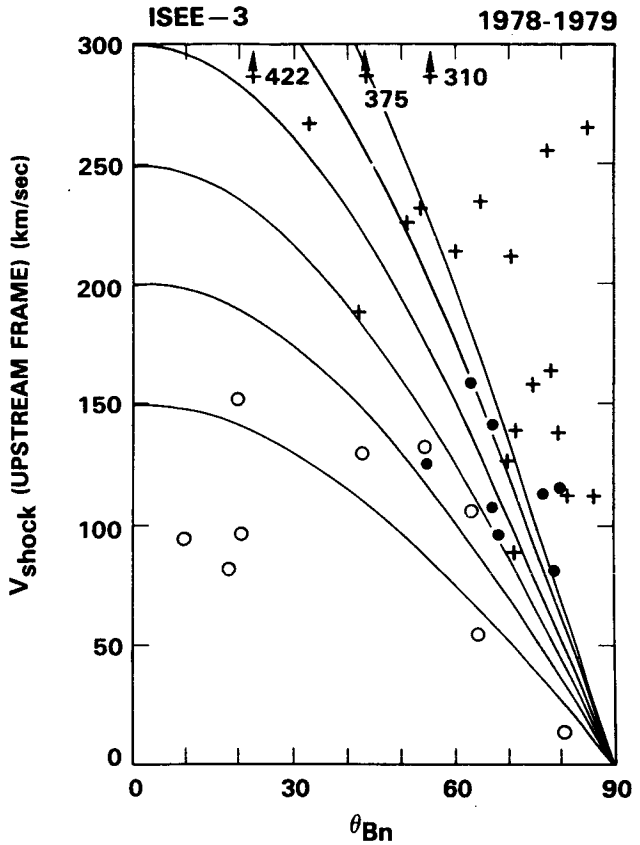

Figure 2.4.2 The shock speed (v_s) in the upstream medium is plotted versus the angle θ_{Bn} between the shock normal and the upstream magnetic field for 37 events observed with ISEE-3 (from Tsurutani and Lin, 1984).

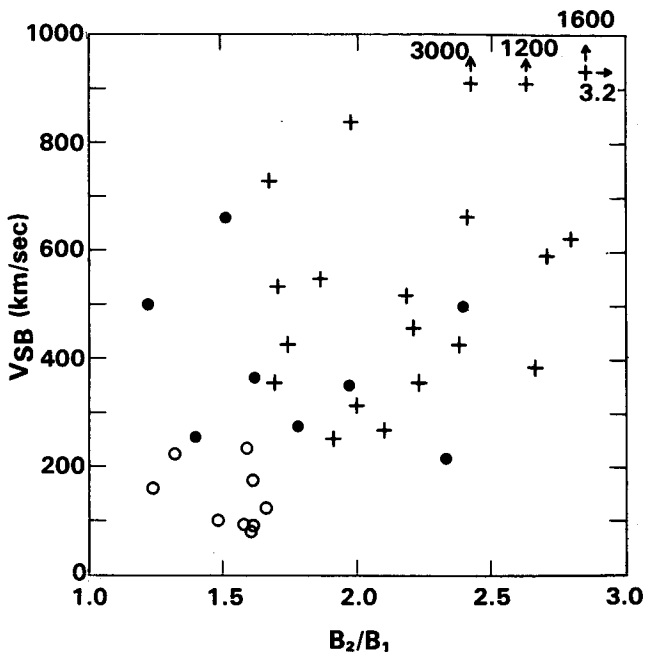

Figure 2.4.3 A scatter plot of the particle flux increases as function of the shock velocity (V_s) relative to the upstream medium (slow solar wind) and the shock normal angle θ_{Bn}. The particle flux increases (over the upstream ambient) are indicated by the type of event point used. Open circles represent events with little or no effects (less than 20% increases), solid circles are moderate events with 20-200% increases, and crosses are large events with > 200% increases. The contours are lines of constant velocity along the upstream magnetic field, $V_{SB} = V_s/\cos \theta_{Bn}$ (from Tsurutani and Lin, 1985).

2.4.5.2 Electron Acceleration

Type II bursts, associated with flare-generated shock waves, require Langmuir waves for the production of radio emission at ω_e and at $2\omega_e$. These plasma waves are most easily generated by streaming suprathermal electrons, as for Type III bursts. Since shock-drift acceleration produces streaming suprathermal electrons upstream of the shock front, Holman and Pesses (1983) have studied the effectiveness of shock-drift acceleration for generating Type II bursts, and the observational consequences. They find that the required level of Langmuir turbulence can be generated with a relatively small number of accelerated electrons ($n_b/n \gtrsim 10^{-6}$) if the angle between the shock normal and the upstream magnetic field (ψ) is greater than 80° (for a 1000 km s^{-1} shock). Except for herringbone structure, which requires electron velocities ~ c/3, the electrons need only be accelerated to velocities that are a few times greater than the mean electron thermal velocity upstream of the shock. Band splitting is explained by the fact that when ψ is within a few degrees of 90°, no electrons are accelerated. The split bands are predicted to arise from different spatial locations (separated by ~ 1') upstream of the shock front. Observations of Type II bursts associated with coronal transients have shown that the emission sometimes arises from locations below and to the sides of the projected front of the white light transient. Since a shock front is expected both ahead of and at the sides of the transient, this indicates that special conditions are required for the generation of the Type II burst. Such a condition appears to be satisfied by shock drift acceleration, since the radio burst is only generated when ψ is large (when the shock is quasi-perpendicular).

Wu (1984) and Leroy and Mangeney (1984) have proposed independently that upstream electrons will be reflected and energized to high energies by the quasi-perpendicular shock. The theory is based on the adiabatic mirror reflection, in the appropriate reference frame, of incident electrons by the increase in magnetic field strength which takes place in the shock-transition region. The average energy per reflected electron scales for sufficiently large θ_{Bn} as ≃

$[(4/\cos^2\theta_{Bn})\frac{1}{2}\, m_e v_o^2]$, where v_o is the shock velocity. Since only particles with large perpendicular velocity will be reflected, this mechanism creates a ring electron distribution upstream of the shock. This distribution is unstable to plasma and maser instabilities and can be the source of Type II bursts. All the geometric effects discussed by Holman and Pesses (1983) are also present in this mechanism. It can be shown that for $\theta_{Bn} \simeq 80\text{-}85°$ the flare accelerated electrons can be further energized to 5-10 times their initial energy. Tsurutani and Lin (1984) applied the same ideas to ions (see discussion above).

Electrons drift in the shock transition due to one of the following processes: (a) magnetic field gradient, (b) temperature gradient, or (c) ExB drift. Ions, on the other hand, do not drift if they are unmagnetized (e.g., when the ion gyroradius is larger than the shock transition thickness). When the electron drift velocity exceeds a certain threshold, cross-field current-driven instabilities are excited and are the source of energy dissipation in collisionless shocks. We discussed above that lower hybrid drift (or the modified two-stream) instability can become an efficient acceleration process. Vlahos *et al.* (1982) applied this mechanism to the acceleration of electrons during loop coronal transients events. Lower hybrid waves excited at the shock front propagate radially toward the center of the loop with phase velocity along the magnetic field which exceeds the thermal velocity. The lower hybrid waves stochastically accelerate the tail of the electron distribution inside the loop. Vlahos *et al.* discussed how the accelerated electrons are trapped in the moving loop and give a rough estimate of their radiation signature. They found that plasma radiation can explain the power observed in stationary and moving Type IV bursts.

2.4.6 Acceleration of Electrons by Intense Radio Waves

A number of observations have shown the nearly simultaneous release of secondary electrons streaming from the surface of the sun (Type III bursts) and the precipitating electrons associated with hard X-ray bursts (see Kane, Pick and Raoult, 1980; Kane, 1981b; Kane, Benz and Treumann, 1982; Dennis *et al.*, 1984). One possible explanation for the accelerated electrons that are responsible for the Type III bursts is that they result from the primary precipitating electrons which drift out of a flaring loop and get into open field lines. However, this mechanism suffers from a number of difficulties; among them is the fact that the drift rate is exceedingly slow (Vlahos, 1979), contrary to observations. Achterberg and Kuijpers (1984) proposed cross-field diffusion from MHD turbulence, but the time scale for such diffusion is still much longer than the observed temporal correlation between X-rays and Type III bursts.

A recent parallel development has been the discovery of intense (10^{10} – 10^{11} Watts), narrow-band, highly polarized microwave bursts observed by Slottje (1978, 1979) and Zhao and Jin (1982). These observations have been interpreted as the signatures of unstable electron distributions, formed inside a flaring loop, by the flare released precipitating electrons (Holman, Kundu and Eichler, 1980; Melrose and Dulk, 1982; Sharma, Vlahos and Papadopoulos, 1982; Vlahos, Sharma and Papadopoulos, 1983). These observations together with the lack of a viable explanation for the secondary accelerated electrons have motivated Sprangle and Vlahos (1983) to examine in detail the interaction of a circularly polarized electromagnetic (e.m.) wave propagating along a spatially varying, static, magnetic field as a possible acceleration mechanism responsible for the observed secondary electrons. In this process, the relativistic electron-cyclotron frequency and the wave phase change in such a way that the resonance between the particles and the wave is maintained in a uniform magnetic field (Kolomenskii and Lebedev, 1963; Roberts and Buchsbaum, 1964). For such a process, the intense, polarized, narrow-band e.m. waves observed by Slottje (1978, 1979) provide a link between the energetic electrons inside the flaring loop and those observed in the outer corona or interplanetary space (Type III bursts). An overall schematic of the acceleration process proposed by Sprangle and Vlahos (1983) is shown in Figure 2.4.4. Here the precipitating primary electrons are accelerated inside a flaring loop and stream toward the chromosphere. These precipitating electrons can then excite an intense, polarized, narrow-band e.m. wave. This e.m. wave is assumed to escape the flaring loop region and propagate along a open flux tube where it can accelerate the secondary electrons (see Figure 2.4.4). A question can be raised here about the possibility of reabsorption of the e.m. wave before it can escape from the flaring loop. This is especially important when the excited e.m. wave is near the fundamental electron-cyclotron frequency or upper-hybrid frequency. The main assumption here is that the excited wave approaches the second harmonic resonance with the particles inside the flaring loop where the total electron distribution is not Maxwellian. It is therefore amplified instead of damped (Sharma, Vlahos and Papadopoulos, 1982; Vlahos, Sharma and Papadopoulos, 1983). Sprangle and Vlahos (1983) concluded that the e.m. wave can accelerate approximately 10^{-4} of the ambient electrons in the acceleration region to approximately 100 keV.

Kane, Benz and Treumann (1982) suggested that the close relation between type III and X-ray bursts is evidence for the fact that the acceleration region shares open and closed field lines. Vlahos believes that this mechanism will be competing with the one presented above, since the trapped electrons will become quickly the source for e.m. radiation and will accelerate electrons together with the primary acceleration source. In other words primary and secondary accelerated electrons will be injected into open field lines during the flash phase of the flare.

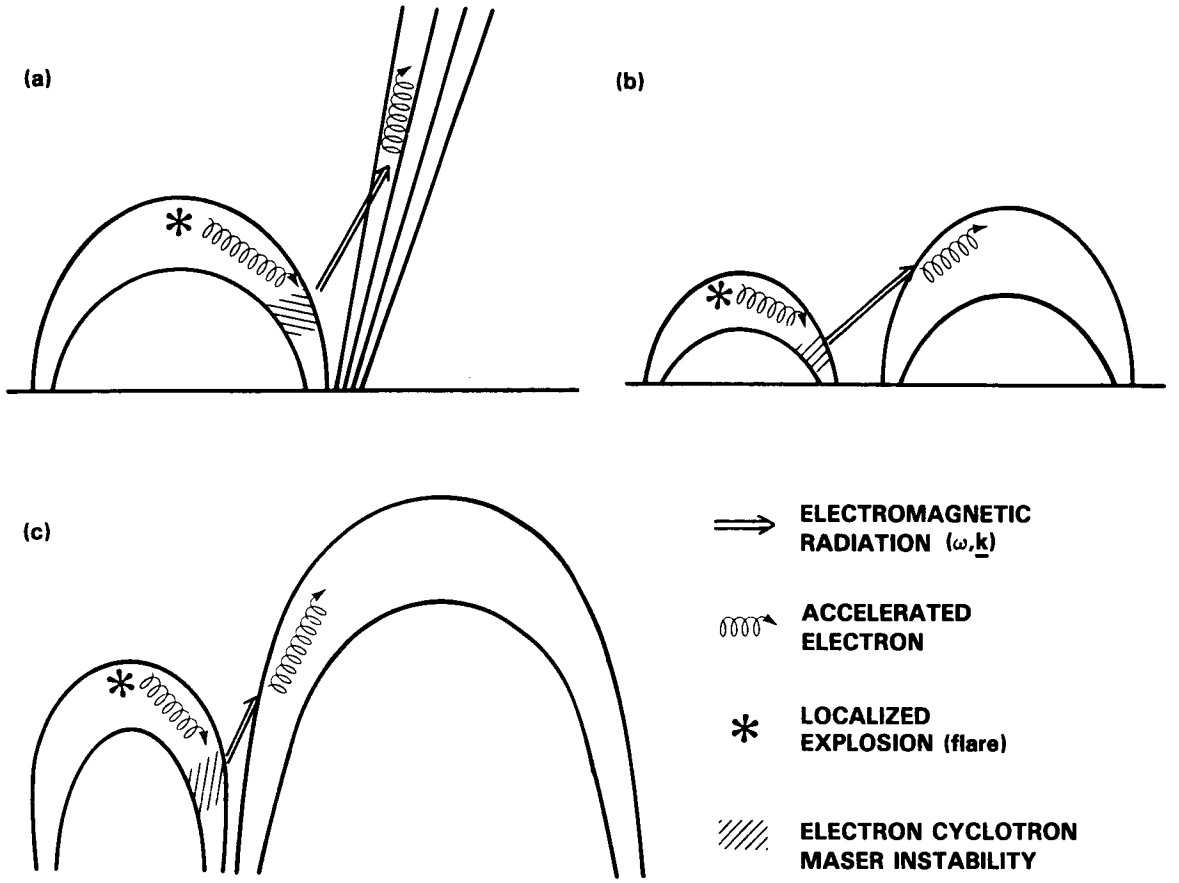

Figure 2.4.4 The development of the intense radio emission driven acceleration is shown for three different models. Flare released energetic electrons are precipitating towards an increasing magnetic field, reflected and form a loss-cone velocity distribution. Loss-cone driven electron cyclotron radiation can escape from the loop and accelerate electrons to high energies inside (a) open field lines, which will explain the hard X-ray/Type III correlation (b) nearby loop, which will explain the triggering of quadruple like structure observed by the VLA (c) large closed loop, which will explain the hard X-ray/Type U correlation (Strong *et al.* (1984), see Section 2.2.5 and Figure 2.2.21) or the hard X-ray/Type V correlation discussed in Section 2.2.

2.4.7 Preferential Acceleration of Heavy Ions

One of the more intriguing results of energetic solar particle flux measurements at ~ 1 AU is the discovery of anomalous enhancements in the abundance of some ionic species during occasional "unusual" events, often called ^{3}He-rich flares (Ramaty *et al.*, 1980, and references therein). Three different types of enhancements can be distinguished in these events: (1) the enhancement of the isotope ^{3}He by as much as three and a half orders of magnitude, at energies ~ 1-10 MeV nucleon^{-1}; (2) enhancement of heavy (A > 4) ions by a factor of 5-10; (3) deviations of other charge states from solar abundances. These are often correlated with ^{3}He-rich flares. A review of the observations and theoretical interpretations is given by Kocharov and Kocharov (1984). Fisk (1978) proposed the most successful model so far since it seems to explain not only the enhancement (1), but also (2) and (3). It is based on selective preheating of the ^{3}He and certain heavy ions such as Fe by resonant interaction with ion cyclotron waves. Such waves can be driven unstable by electron currents or ion beams. In a pure hydrogen plasma, the ion cyclotron waves have a frequency above the proton cyclotron frequency Ω_H (i.e., $\omega = (\Omega_H^2 + k^2c_s^2)^{1/2} \approx 1.2 - 1.4\,\Omega_H$ where c_s is the sound speed) (Kadomtsev, 1965). However, in the presence of a noticeable amount of doubly ionized ^{4}He^{++} and for some combinations of drift velocities and plasma parameters, waves near the ^{4}He^{++} cyclotron frequency can be excited. Since $\omega \approx 1.2\,\Omega_{^3He^{++}} \approx \Omega_{^3He^{++}}$, ^{3}He^{++} can be resonantly accelerated. In addition, ions with A/Q ≈ 3.3 and A/Q ≈ 4.5 can be accelerated by the harmonics (i.e. $\omega = n\Omega_i - k_z v_z$) although less effi-

ciently. The subject of ion energization by ion cyclotron waves in multispecies plasmas has been recently examined by Papadopoulos, Gaffey and Palmadesso (1980) and Singh, Schunk, and Sojka (1981). It was noted that, for wave amplitudes exceeding a threshold, which depends on A/Q, ion acceleration does not require resonance but can be very strong even for significant frequency mismatch. The physical process responsible for this is resonance overlapping. The general theory was given by Chirikov (1979), while its application to lower hybrid heating of fusion plasmas can be found in several publications (Fukuyama *et al.*, 1978; Karney and Bers, 1977; Hsu, 1982). It has been called non-resonant stochastic acceleration to be distinguished from the process requiring cyclotron resonance [i.e., $\omega = n\Omega_i - (k_z v_z)$], and was first shown by Papadopoulos *et al.* to exhibit a large selectivity in the ionic A/Q ratio. Varvoglis and Papadopoulos (1983) revised the model advanced by Fisk (1978) by including the proper nonlinear physics of particle energization by electrostatic ion cyclotron (EIC) waves. Their model retains two basic concepts of Fisk: the energization by EIC waves and the need for a second stage of acceleration. However, there is no need for exciting $^4He^{++}$ cyclotron waves, since the dominant process is non-resonant and can be accomplished by hydrogen cyclotron waves. The A/Q selectivity in the flux available for energization in the second stage process enters through the nonlinear saturation level $e\phi/T_H$, which in conventional theories (Dum and Dupree, 1970; Palmadesso *et al.*, 1974) depends on the current that drives the instability.

2.4.8 Summary

In contrast to the dynamic and dramatic development of the observations theoretical studies concerning particle acceleration in a solar environment during a flare are progressing at a steady rate. Part of the problem, of course, is our poor understanding of the energy-release process in flares, specifically our poor understanding of the reconnection theory in solar flares. Nevertheless, the workshop has stimulated several new ideas and provided many concrete questions for theoretical studies. Here, we pose several questions regarding theoretical studies of particle acceleration in solar flares.

(1) *Is there a single mechanism that will accelerate particles to all energies and also heat the plasma?*

We do not know of any such mechanism today. The mechanisms discussed by us either have a threshold for acceleration (like the stochastic Fermi acceleration and shock acceleration) or heat and accelerate the tail to mildly relativistic energies (Joule heating and sub-Dreicer E-field acceleration or Joule heating and lower hybrid waves). We then come to the conclusion that the *existing* theoretical understanding of particle acceleration favor the two step acceleration (with one important twist, the two mechanisms must operate simultaneously at the same place or in close proximity to each other).

(2) *How fast will the existing mechanisms accelerate electrons up to several MeV and ions to 1 GeV?*

Electric fields, lower hybrid waves and Joule heating can start, and then heat and accelerate the electrons to 10-100 keV in fractions of a second. *If a shock or a turbulent spectrum of waves is already present*, it is possible to accelerate the electrons further to relativistic energies in 2-50 secs. Melrose (1983) has already pointed out that magnetosonic turbulence can accelerate ions from 0.1 MeV to 30 MeV in 2 s but the question of pre-accelerating ions to 0.1 MeV and the driving force for the magnetosonic waves has remained open.

(3) *If shocks are formed in a few seconds, can they be responsible for the prompt acceleration of ions and electrons? How are these shocks related to large-scale shocks which are responsible for the Type II bursts?*

The shock acceleration as discussed here will not be appropriate for the prompt acceleration of particles, since almost all the above theories have assumed a plane quasi-parallel or quasi-perpendicular shock. In the vicinity of the energy release region the shock curvature and structure must be taken into account. The shocks developed inside the energy release volume during a flare are formed in the middle of an enhanced level of turbulence and laminar shock drift or purely diffusive acceleration calculations in a parallel shock are not valid. In summary, our current understanding of particle acceleration in shocks cannot give us an answer to the above question.

An important question regarding the formation of shocks inside the energy release region is the lack of evidence for Type II-like signatures in the decimetric radio frequencies. Such continuation for the Type III bursts is clearly present. This of course brings us to the next question of the relation of flares (and shocks developed inside the energy release volume) to large scale shocks, responsible for the Type II bursts and particle acceleration in space. This question remains unresolved.

(4) *Can the electron-cyclotron maser spread the acceleration region?*

We suggested that beams of electrons streaming towards converging magnetic field lines will be reflected and form loss-cone type velocity distributions in the low corona. A fraction ($\lesssim$ 1-5%) of the kinetic energy of the energetic electrons will drive electromagnetic waves that can easily spread the acceleration region to larger volume outside the flaring region.

(5) *Which of the acceleration mechanisms discussed above can explain the observed energy spectra (see discussion on Section 2.3)?*

Most of our discussions on the acceleration mechanisms have been focussed on the energetics and not on the details of the energy spectrum of the accelerated particles. The only mechanisms that have successfully explained the observed spectra is the stochastic Fermi acceleration and quasi-parallel diffusive shock acceleration. This of course does not exclude other mechanisms for flare acceleration but places important constraints on them. A detailed study of the energy spectrum of the accelerated particles must be the goal for any successful acceleration mechanism in solar flares.

Fermi acceleration and acceleration by quasi-parallel shocks although successful in explaining the energy spectrum, have not yet fully addressed other questions e.g., shock and turbulence formation time, formation of appropriate wave spectra from MHD waves, relation of MHD waves to energy release process, etc.

2.5 ACHIEVEMENTS — OUTSTANDING QUESTIONS

As it is always the case in science, new and more precise measurements bring us higher in the helix of knowledge by replacing or revising older concepts with new ones. At the same time, however, new and more sophisticated questions are posed which demand even more sophisticated theoretical studies. Comparing the results reported in this chapter with the Skylab work which was reported in two articles by Kane *et al.* (1980) and Ramaty *et al.* (1980), one clearly sees this evolution on many concepts of particle acceleration in solar flares. The main achievements are highlighted below:

1. The X-ray imaging has, for the first time, provided evidence for discrete isolated footpoints during the impulsive phase. The footpoints gradually evolve and form a single source of hot plasma in the decay phase of some flares. Other flares never develop footpoints and the thermal plasma dominates their evolution. Finally, the majority of the existing X-ray imaging data are very complex and "refuse" to be placed in simple classes (e.g., A, B, C etc.). The rather simplistic division of flares to "thermal" and "nonthermal" seems to be a convenient abstraction for simple theoretical models. In reality thermal and nonthermal plasma is dialectically connected; "nonthermal plasma" is quickly thermalized and from a locally heated plasma energetic particles emerge. The X-ray imaging has provided evidence for the interconnection of thermal and nonthermal plasma.

2. The radio images have also put a mark on our understanding of evolution of the magnetic topologies that can lead to a flare. Interacting loops and bipolar structures commonly observed suggest that loop-like structures are the elementary components of the flare process.

The isolated loop structure has been assumed to be one of the possibilities for energy release in flares. There is now evidence that more complex magnetic topologies (e.g., interacting loops, emerging flux or even a catastrophic interaction of many loops) are at work during a flare. The loop, however, remains as the elementary structure that participates in these interactions.

3. The radio maps at meter wavelengths and detailed studies of the meter/X-ray correlation also point to the direction that the region of acceleration must encompass open and closed field lines, and that it is located at the low corona.

4. Analyzing the time evolution of the flare energy release process with high time resolution instruments has provided an unprecedented wealth of information that will take years to interpret physically. Pulsations arise in several wavelengths, some of them quasi-periodic, some of them chaotic. Fast pulses with durations that sometimes reach the instrumental resolution and delays between pulses in different wavelengths are among the new results. Some of the observed pulses are clearly the result of pulsations in the acceleration source, but in other cases the pulses are the result of the radiation mechanism.

5. For many years we believed that prior to a flare the Sun operates in a steady state norm that keeps the coronal plasma around 2×10^6K. During a flare the energization mechanism will "process" this 2×10^6K Maxwellian distribution to a new "heated" and "accelerated" plasma state. We have provided evidence that show that (1) the acceleration starts before the flash phase and continues after the impulsive phase of the flare, (2) "microflares" continuously occur in the corona and develop nonthermal tails. Thus, the acceleration may start from a distorted Maxwellian that is developed long before the impulsive phase. Furthermore, we presented evidence that suggest that the number of flares increases as the total energy per flare decreases, which indicates that there is no threshold for reconnection and "flaring" and "heating" smoothly join each other.

6. Intense, coherent, polarized microwave pulses sometimes occur during a flare. They may be the result of the conversion of kinetic energy of the precipitating electrons to electromagnetic radiation through the convergence of magnetic field lines.

7. Observations from gamma-ray detectors on SMM have dramatically changed our thinking of the way particles are accelerated in the Sun. The conventional two phase acceleration (a prompt first phase acceleration of mildly relativistic electrons followed by a slower second phase acceleration that energizes the ions and accelerates further the electrons to relativistic electrons) had to be abandoned, because in many flares fast synchronous (or nearly synchronous) pulses occur simultaneously in several energy channels. Hence, the concept of prompt acceleration of both electrons and ions to all energies in a few seconds is a new important discovery, which will change our thinking on par-

ticle acceleration. However, particles observed in interplanetary space may be accelerated by the second-phase acceleration.

8. We have evidence that the acceleration of relativistic electrons and ions must be a common phenomenon during flares.

We have outlined several questions that need further study in Sections 2.2.7, 2.3.7 and 2.4.8. We believe that many detailed observational studies are still needed and we outline some of them here:

- Stereoscopic observations of hard X-rays which have been discussed briefly in this chapter, may provide information about the precipitating electrons and the validity of the thick target model.
- X-ray imaging at higher energies and hard X-ray polarization measurements will be valuable for knowing the critical energy that divides the thermal from the nonthermal component of flares.
- Detailed studies of the time structures of hard X-ray bursts may give us clues to the time development of the energy release mechanism.
- Detailed studies of hard X-ray and radio microflares and the pre- and post-impulsive phase activity are of fundamental importance.
- Spectral evolution during hard X-ray pulsations is an important source of information.
- Radio maps in different wavelengths with high time resolution accompanied by detailed models of the radiating source will play an important role in our understanding of the evolution of magnetic field topologies in the course of a flare.
- Detailed studies of the delays of the starting and peak time in different energy channels will restrict our choices on particle acceleration mechanisms. Spectral evolution is also a powerful tool to study the presence of more than one acceleration mechanism.

A number of outstanding theoretical problems remain open for future studies:

- Several new concepts have recently emerged concerning the energy release process during reconnection but usually these concepts address questions related to the energetics and not to particle acceleration. We believe that detailed studies on heating, energetic tail formation and energy spectra of electrons and ions energized during reconnection are of fundamental importance.
- The details of the Magnetohydrodynamic waves that are excited during a flare are not well known. We believe that this is a major problem that deserves immediate attention. Of particular importance are questions related to the onset time, power spectrum of the excited waves, etc.
- Acceleration of ions, stability of propagating ion beams and the importance of energetic ions during a flare must be examined in detail.
- The mechanisms for electron and ion heating are not well understood and must be examined in detail.
- Prompt formation of shocks and shock acceleration of electrons and ions is a problem that must be reexamined in the light of the results presented in this chapter.
- The interaction of "hot" and "cold" plasma during a flare, the formation and propagation of the so called "conduction fronts" is a fundamental astrophysical problem. Detailed numerical, analytical and observational studies (using X-ray imaging) must continue.
- Magnetic models for the acceleration and radiation source, using model velocity distributions must be developed for both electrons and ions in all energies. These models serve to restrict or eliminate acceleration mechanisms by comparing the resulting radiation signatures from the model with the data.
- The response of coronal plasma to Sub-Dreicer and much stronger than the Dreicer electric fields is an area that we have not explored in detail. The formation of such potential drops in coronal conditions is also an open question.
- The time evolution of the acceleration mechanism is a higher order problem but the detailed observations, outlined above, demand such studies and must be placed in the agenda for careful study.

The achievements and outstanding questions posed in this chapter are of fundamental importance for the entire astrophysical community, since the impulsive energy release and particle acceleration observed during a flare is a phenomenon that must be occuring in many space and laboratory plasmas. We believe that our work will serve to generate new ideas and interpretations of the results presented during the workshop. We are aware that some of the questions posed by us are complex and will require detailed observational and theoretical studies for many years to come. We hope that our effort will be a guide for these studies.

2.6 ACKNOWLEDGEMENTS

The material presented in this chapter has been discussed by the members of team B in three separate one-week meetings of the Solar Maximum Mission Workshops at Greenbelt, Maryland in 1983-84. During the workshops, Marcos Machado led the discussion on "phenomena associated with mildly-relativistic electrons", Reuven Ramaty led the discussion on the "phenomena associated with ions and relativistic electrons" and Loukas Vlahos led the discussion on "theoretical studies of particle acceleration". The authors of this chapter would like to thank their colleagues, J. Brown, B. Dennis, M. Forman, G. Dulk, P. Cargill, A. Raoult, P. Sprangle, N. Vilmer, V. Tomozov and H. Wiehl, for many helpful discussions and suggestions.

2.7 REFERENCES

Achterberg, A. and Kuijpers, J. 1984, Astron. Astroph., *130*, 111.

Alissandrakis, C.E. and Kundu, M.R. 1985, in preparation.

Alissandrakis, C.E. and Preka-Papadema, P. 1984, Astron. Astroph., *139*, 507.

Altyntsev, A.T., Krasov, V.I. and Tomozov, V.M. 1977, Solar Phys., *55*, 69.

Altyntsev, A.T., Bardakov, V.M. and Krasov, V.I. 1981, ZhETF, *81*, 901.

Altyntsev, A.T., Krasov, V.I., Lebedev, N.V., Paperny, V.L. and Simonov, V.G. 1983, Preprint SibIZMIR No. 23-83, Irkutsk.

Altyntsev, A.T., Krasov, V.I. and Tomozov, V.M. 1984, Solar Flares and Plasma Experiments. Astronomiya, v. *25*, Moscow, p. 99-191.

Arion, D. 1984, Ap. J., *277*, 841.

Aschwanden, M.J., Wiehl, H.J. Benz, A.O. and Kane, S.R. 1985, Solar Phys., in press.

Athay, R.G. 1984, Solar Phys., *93*, 123.

Bai, T. 1982, in Gamma Ray Transients and Related Astrophysical Phenomena, R. E. Lingenfelter, *et al.* (ed.), (New York: AIP), p. 409.

Bai, T. and Ramaty, R. 1979, Ap. J., *227*, 1072.

Bai, T. and Dennis, B.R. 1985, Ap. J., in press.

Bai, T., Kiplinger, A.L. and Dennis, B.R. 1985, Ap. J., submitted.

Bai, T., Dennis, B.R., Kiplinger, A.L., Orwig, L.E. and Frost, K.J. 1983a, Solar Phys., *86*, 409.

Bai, T., Hudson, H.S., Pelling, R.M., Lin, R.P., Schwartz and von Rosenvinge, T.T. 1983b, Astrophys. J., *267*, 433.

Barbosa, D.D. 1979, Ap. J., *233*, 383.

Batchelor, D.A., Crannell, C.J., Dennis, B.R., Wiehl, H.J. and Magun, A. 1985, Ap. J., in press.

Benz, A.O. 1985, Solar Phys., in press.

Benz, A.O., Zlobec, P. and Jaeggi, M. 1982, Astr. Ap., *109*, 305.

Benz, A.O., Bernold, T.E.X. and Dennis, B.R. 1983a, Ap. J., *271*, 355.

Benz, A.O., Barrow, C.H., Dennis, B.R., Pick, M., Raoult, A. and Simnett, G. 1983b, Solar Phys., *83*, 267.

Benz, A.O., Achwanden, M.J. and Wiehl, J.J. 1984, Decimetric Radio Emission During Solar Flares, Kunming Workshop Proceedings, in press.

Bratenahl, A. and Baum, P.J. 1985, in Unstable Current Systems and Plasma Instabilities in Astrophysics, ed. M. R. Kundu and G. D. Holman, D. Reidel, p. 147.

Brown, J.C. 1971, Solar Phys., *18*, 485.

Brown, J.C. 1972, Solar Phys., *26*, 441.

Brown, J.C. 1973, Solar Phys., *28*, 151.

Brown, J.C. and McClymont, A.N. 1976, Solar Phys., *41*, 135.

Brown, J.C., Melrose, D.B. and Spicer, D.S. 1979, Ap. J., *228*, 592.

Brown, J.C. and Smith, D.F. 1980, Rep. Prog. Phys., *43*, 125.

Brown, J.C., Craig, I.J.D. and Karpen, J.T. 1980, Solar Phys., *67*, 143.

Brown, J.C., Mackinnon, A.L., Zodi, A.M. and Kaufmann, P. 1983a, Astron. Astrophys., *123*, 10.

Brown, J.C. Carlaw, V.A., Cromwell, D. and Kane, S.R. 1983b, Solar Phys., *88*, 281.

Brunel, F., Tajima, T. and Dawson, J.M. 1982, Phys. Rev. Lett., *49*, 323.

Butz, M., Hirth, W., Furth, E. and Harth, W. 1976, Sond. Kelinheubacher Berichte, *19*, 345.

Chirikov, B.V. 1979, Phys. Rev., *52*, 264.

Chupp, E.L. 1982, in Gamma Ray Transients and Related Astrophysical Phenomena, R. E. Lingerfelter, *et al.* (ed.), (New York: AIP), p. 363.

Chupp, E.L. 1983, Solar Phys., *86*, 383.

Chupp, E.L. 1984, Ann. Rev. Astron. Astrophys., *22*, 359.

Chupp, E.L., *et al.*, 1981a, Ap. J. (Letters), *244*, L171.

Chupp, E.L., Forrest, D.J., Higbie, P.R., Suri, A.N., Tsai, C. and Dunphy, P.P. 1973, Nature, *241*, 333.

Chupp, E.L., Forrest, D.J., Ryan, J.M., Heslin, J., Reppin, C., Pinkau, K., Kanbach, G., Rieger, E. and Share, G.H. 1982, Ap. J. (Letters), *263*, L95.

Chupp, E.L., Forrest, D.J., Kanbach, G., Share, G.H. 1983, 19th Int. Cosmic Ray Conf., (late papers Bangalore), p. 334.

Cliver, E., Share, G., Chupp, E., Matz, S., Howard, R., Koomen, M., McGuire, R., and Von Rosenvinge, T. 1982, Bull. AAS, *14*, 4, 874.

Cliver, E.W. *et al.*, 1983a.

Cliver, E.W., Forrest, D.J., McGuire, R.E. and Von Rosenvinge, T.T. 1983, in: 18th International Cosmic Ray Conference Papers (Late Papers), Bangalore, p. 342.

Cook, W.R., Stone, E.C. and Vogt, R.E. 1984, Ap. J., *279*, 827.

Coppi, B., Galvao, R., Pellat, R., Rosenbluth, M.N. and Rutherford, P.H. 1976, Sov. J. Plasma Phys., *2*, 533.

Costa, J.E.R. and Kaufmann, P. 1983, Astron. Astrophys. *119*, 131.

Crannell, C.J. Frost, K.J., Matzler, C., Ohki, K. and Saba, J.L. 1978, Ap. J., *223*, 620.

Craig, I.J.D., MacKinnon, A.L. and Vilmer, N. 1985, Mon. Not. Roy. Ast. Soc., submitted.

Datlowe, D.W., Elcan, M.J. and Hudson, H.S. 1974, Solar Phys., *39*, 127.

Debrunner, H., Fluckiger, E., Chupp, E.L. and Forrest, D.J. 1983, in: 18th International Cosmic Ray Conference Papers 4, Bangalore, p. 75.

Debrunner, H., Fluckiger, E., Lockwood, J.A. and McGuire, R.E. 1984, Journal Geoph. Res., *89*, 769.

Decker, R.B. and Vlahos, L. 1985, Journal Geop. Res., *90*, 47.

DeJager, C. 1969, in: COSPAR Symposium on Solar Flares and Space Research, eds. C. DeJager and Z. Svestka, p. 1.

DeJager, C. and De Jonge, G. 1978, Solar Phys., *58*, 127.

Dennis, B.R., *et al.*, 1983, NASA TM 84998.

Dennis, B.R., Benz, A.O., Ranieri, M. and Simnett, G. 1984, Solar Phys., *90*, 383.

Drake, J.F., Pritchett, P.L. and Lee, Y.C. 1978, UCLA Phys Rept. PPG-341, unpublished.

Droge, F. 1977, Astron. Astroph., *57*, 285.

Dreicer, H. 1959, Phys. Rev., *115*, 238.

Drury, L.O.C. 1983, Rep. Progr. Phys., *46*, 973.

Duijveman, A. 1983, Solar Phys., *84*, 189.

Duijveman, A. and Hoyng, P. 1983, Solar Phys., *86*, 289.

Duijveman, A., Hoyng, P. and Machado, M.E. 1982, Solar Phys., *81*, 137.

Dum, C.T. and Dupree, T.D. 1970, Phys. Fluids, *13*, 2064.

Dumas, G., Caroubalos, C. and Bougeret, J.L. 1982, Solar Phys., *81*, 2.

Elliott, H. 1969,in Solar Flares and Space Research, (ed. C. de

Jager and Z. Svestka), North Holland, Amsterdam, p. 356,
Ellison, D.C. and Ramaty, R. 1985, Advanced Space Res. (COSPAR), *4*, 7, 137.
Emslie, A.G. 1978, Ap. J., *224*, 241.
Emslie, A.G. 1980, Ap. J., *235*, 1055.
Emslie, A.G. 1981a, Astrophys. Letters, *22*, 171.
Emslie, A.G. 1981b, Ap. J., *245*, 711.
Emslie, A.G. 1983, Ap. J., *271*, 367.
Emslie, A.G. and Vlahos, L. 1980, Ap. J., *242*, 359.
Evenson, P., Meyer, P. and Pyle, K.R. 1983, Ap. J., *274*, 875.
Evenson, P., Meyer, P., Yanagita, S. and Forrest, D.J. 1984, Ap. J., *283*, 439.
Field, G.B. 1965, Astrophys. J., *142*, 531.
Fisk, L. A. 1978, Ap. J., *224*, 1048.
Forman, M.A., Ramaty, R. and Zweibel, E.G. 1985, in: The Physics of the Sun, eds. P. A. Sturrock *et al.*, Reidel, Dordrecht, in press.
Forrest, D.J. 1983, in: Positron-Electron Pairs in Astrophysics, eds. M.L. Burns, A.K. Harding and R. Ramaty, A.I.P., N.Y., p. 3.
Forrest, D.J. and Chupp, E.L. 1983, Nature, *305*, 291.
Frost, K.J. and Dennis, B.R. 1971, Ap. J., *165*, 655.
Fukuyama, A., Momota, H. Itatani, R. and Takizuka, T. 1977, Phys. Rev. Lett., *38*, 101.
Furth, H.P., Killeen, J. and Rosenbluth, M.N. 1963, Phys. Fluids, *6*, 459.
Gaizauskas, V. and Tapping, K.F. 1980, Ap. J., *241*, 804.
Gardner, B.M., Forrest, D.J., Chupp, E.L., *et al.*, 1981, Bull. AAS, 13, 903.
Ginzburg, V.L. and Syrovatskii, S.I. 1964, The Origin of Cosmic Rays, (New York: MacMillan).
Gloeckler, G. 1985, Advances Space Res. (COSPAR), *4*, 2, 127.
Heyvaerts, J. 1981, "Particle Acceleration in Solar Flares," in Solar Flare Magnetohydrodynamics, ed. E. R. Priest, Gordon and Breach, New York City, pp. 429-555.
Heyvaerts, J. and Priest, E.R. 1984, Astr. Astroph., *137*, 63.
Heyvaerts, J., Priest, E.R. and Rust, D.M. 1977, Ap. J., *216*, 123.
Holman, G.D. 1984, Ap. J., *293*, in press.
Holman, G.D. and Pesses, M.E. 1983, Ap. J., *267*, 837.
Holman, G.D., Eichler, D. and Kundu,M.R. 1980, in Proceedings of IAU Symposium 86, "Radio Physics of the Sun", Kundu, M.R. and Gergely, T.E., eds. (Dordrecht: Reidel), p. 457.
Holman, G.D., Kundu, M.R. and Papadopoulos, K. 1982, Ap. J., *257*, 354.
Hoyng, P., Brown, J.C. and van Beek, H.F. 1976, Solar Phys., *48*, 197.
Hoyng, P., Duijveman, A., Machado, M.E. *et al.*, 1981, Ap. J. (Letters), *246*, L155.
Hoyng, P., Marsh, K.A., Zirin, H. and Dennis, B.R. 1983, Ap. J., *268*, 865.
Hsu, J.Y. 1982, Phys. Fluids, *25*, 179.
Hudson, H.S., Canfield, R.C. and Kane, S.R. 1978, Solar Phys., *60*, 137.
Hudson, H.S., Bai, T., Gruber, D.G., Matteson, J.L., Nolan, P.L. and Peterson, L.E. 1980, Ap. J. (Letters), *236*, L91.
Ibragimov, I.A. and Kocharov, G.E. 1977, Sov. Astron. Lett., 3(5), 221.
Kadomtsev, B.B. 1965, Plasma Turbulence (London: Academic), p. 73.
Kai, K. and Kosugi, T. 1985, Publications of Astr. Soc. Japan, *37*, 155.
Kane, S.R. 1972, Solar Phys., *27*, 174.
Kane, S.R. 1973, in High Energy Phenomena on the Sun, ed. R. Ramaty and R. G. Stone), (Washington: NASA), p. 55.
Kane, S.R. 1974, in Coronal Disturbances, G. Newkirk, Jr. (ed), IAU Symp. *57*, Reidel, p. 105.
Kane, S.R. 1981a, Astrophys. Space Sci., *75*, 163.
Kane, S.R. 1981b, Ap. J., *247*, 1113.
Kane, S.R. 1983, Solar Phys., *86*, 355.
Kane, S.R. and Anderson, K.A. 1970, Ap. J., *162*, 1003.
Kane, S.R. and Pick, M. 1976, Solar Physics., *47*, 293.
Kane, S.R. and Raoult, A. 1981, Ap. J. (Letters), *248*, L77.
Kane, S.R., Pick, M. and Raoult, A. 1980, Astrophys. J., *241*, L113.
Kane, S,R., Benz, A.O. and Treumann, R.A. 1982, Ap. J., 263.
Kane, S.R., Kreplin, R.W., Martres, M.J., Pick, M. and Soru-Escaut, I. 1974, Solar Physics, *38*, 483.
Kane, S.R., Anderson, K.A., Evans, W.D., Klebesadel, R.W. and Laros, J. 1979, Ap. J. (Letters), *233*, L151.
Kane, S., Anderson, K., Evans, W., Klebesadel, R. and Laros, J. 1980, Ap. J., *239*, 85-88.
Kane, S.R., Fenimore, E.E., Klebesadel, R.W. and Laros, J.G. 1982, Astrophys. J., *254*, L53.
Karney, C.F.F. and Bers, A. 1977, Phys. Rev. Letters, *39*, 550.
Kaufmann, P., Iacomo, Jr. P., Koppe, E.H. Santos, P.M. Schaal, R. E. and Blakey, J.R. 1975, Solar Phys., *45*, 189.
Kaufmann, P., Piazza, L.R., Schaal, R.E. and Iacomo Jr., P. 1978, Ann. Geophys., *34*, 105.
Kaufmann, P., Strauss, F.M., Raffaelli, J.C. and Opher, R. 1980a, In: Donnelly, R.F., ed. — *Solar Terrestrial Predictions Proceedings*, V. 3, Solar Activity Predictions.
Kaufmann, P. Strauss, F.M., Opher, R. and Laporte, C. 1980b, Astron. Astrophys., *87*, 58.
Kaufmann, P. Strauss, F.M., Schaal, R.E. and Laporte, C. 1982a, Solar Phys., *78*, 389.
Kaufmann, P., Costa, J.E.R. and Strauss, F.M. 1982b, Solar Phys., *81*, 159.
Kaufmann, P., Strauss, F.M., Costa, J.E.R., Dennis, B.R., Kiplinger, A., Frost, K.J. and Orwig, L.E. 1983, Solar Phys., *84*, 311.
Kaufmann, P., Correia, E., Costa, J.E.R., Dennis, B.R. Hurford, G.J. and Brown, J.C. 1984, Solar Phys., *91*, 359.
Kaufmann, P., Correia, E., Costa, J.E.R., Sawant, H.S. and Zodi vaz, A.M. 1985, Solar Phys., *95*, 155.
Kawabata, K., Ogawa, H. and Suzuki, I. 1983, Solar Phys., *86*, 247.
Klein, L., Anderson, K., Pick, K.M., Trottet, G., Vilmer, N. and Kane, S.R. 1983, Solar Phys., *84*, 295.
Kocharov, L.G. and Kocharov, G.E. 1984, Space Sci. Rev., *38*, 89.
Kolomenskii, A.A. and Lebedev, A.N. 1963, Soviet Phys. Dokl., *7*, 745.
Kosugi, T., Kai, K. and Suzuki, T. 1983, Solar Phys., *87*, 373.
Kozlovsky, B. and Ramaty, R. 1977, Astrophys. Lett., *19*, 19.
Kuijpers, J., van der Post, P. and Slottje, C. 1981, Astron. Astrophys., *103*, 331.
Kundu, M.R. 1981, Proc. SMY Workshop, Crimea, p. 26.
Kundu, M.R. and Shevgaonkar, R.K. 1985, Ap. J., *291*, 860.
Kundu, M.R., Rust, D.M. and Bobrowsky, M. 1983, Ap. J., *265*, 1084.

Kundu, M.R., Schmahl, E.J., Velusamy, T. and Vlahos, L. 1982, Astron. Astrophys., *108*, 188.
Kundu, M.R., Machado, M., Erskine, F.T., Rovira, M.G. and Schmahl. E.J. 1984, Astron. Astrophys., *132*, 241.
Langdon, A.B. and Lasinski, B.F. 1976, Methods in Computational Physics, Academic Press, N.Y., Vol. *16*, p. 327.
Lantos, P., Pick, M. and Kundu, M. 1984, Ap. J., *283*, L71.
Leach, J. and Petrosian, V. 1981, Ap. J., *251*, 781.
Leboeuf, J.N., Tajima, T. and Dawson, J.M. 1982, Phys. Fluids, *25*, 784.
Lee, M.A. and Ryan, J.M. 1985, Ap. J., submitted.
Leroy, M. and Mangeney, A. 1984, Ann. Geoph. Gauthier Villars, in press.
Lin, A.T., Dawson, J.M. and Okuda, H. 1974, Phys. Fluids, *17*, 1995.
Lin, R.P. and Hudson, H.S. 1976, Solar Phys., *50*, 153.
Lin, R.P. *et al.*, 1981, Ap. J. (Letters), *251*, L109.
Lin, R.P., Mewaldt, R.A. and Van Hollebeke, M.A.I. 1982, Ap. J., *253*, 949.
Lin, R.P., Schwartz, R.A., Kane, S.R., Pelling, R.M., and Harley, K.C. 1984, Ap. J., (in press).
Machado, M.E. 1983a, Adv. Space Res., 2, No. *11*, 115.
Machado, M.E. 1983b, Solar Phys., *89*, 133.
Machado, M.E. and Lerner, G. 1984, Adv. Space Res., in press.
Machado, M.E., Duijveman, A. and Dennis, B.R. 1982, Solar Phys., *79*, 85.
Machado, M.E., Rovira, M.G and Sneibrun, C. 1985, Solar Phys., in press.
Machado, M.E. Somov, B.V. Rovira, M.G.and de Jager, C. 1983, Solar Phys., *85*, 157.
MacKinnon, A.L. and Brown, J.C. 1983, Astron. Astrop., *132*, 229.
MacKinnon, A.L., Brown, J.C. and Hayward, J. 1984, Solar Phys. in press.
MacKinnon, A.L., Brown, J.C., Trottet, G. and Vilmer, N. 1983, Astron. Astrophys., *119*, 297.
Makishima, K. 1982, Proc. HINOTORI symposium on solar flares, ed. Y. Tanaka, *et al.*, p. 120, published by the Institute of Space and Astronautical Science, Tokyo.
Manheimer, W. 1977, Phys. Fluids, *20*, 165.
Marsh, K.A. and Hurford, G. 1980, Ap. J. (Letters), *240*, L111.
Mason, G.M., Gloeckler, G. and Hovestadt, D. 1984, Ap.J., *280*, 902.
Matzler, C., Bai, T., Crannell, C.J. and Frost, K.J. 1978, Ap. J., *223*, 1058.
Matthaeus, W.H. 1982, Geoph. Res. Lett., *9*, 660.
Matthaeus, W.H., Ambrosiano, J.J. and Goldstein, M.L. 1984, Phys. Rev. Lett, L53, 1449.
Matthaeus, W.H. and Montgomery, D.C. 1981, J. Plasma Phys., *25*, 11.
McDonald, F.B. and Van Hollebeke, M.A.I. 1985, Ap. J. (Lett.).
McGuire, R.E. and von Rosenvinge, T.T. 1985, Advances Space Res. (COSPAR), *4*, 2, 117.
Melrose, D.B. 1983, Solar Phys., *89*, 149.
Melrose, D.B. and Brown, J.C. 1976, Mon. Not. Roy. Astron. Soc., *176*, 15.
Melrose, D.B. and Dulk, G.A. 1982, Ap. J., *259*, 844.
Mercier, C. 1975, Solar Phys., *45*, 169.
Mewaldt, R.A., Spalding, J.D. and Stone, E.C. 1984, Ap. J., *280*, 892.
Moghaddam-Taaheri, E. and Vlahos, L. 1985, Ap. J., submitted.
Moriyama, F. *et al.*, 1983, Annals of Tokyo Astron. Observatory, Vol. XIX, No. *2*, 276.
Murphy, R.J. Ph.D. Dissertation, University of Maryland (in preparation 1985).
Murphy, R.J. and Ramaty, R. 1985, Advances Space Res. (COSPAR), *4*, 7, 127.
Nakajima, H., Dennis, B.R., Hoyng, P., Nelson, G., Kosugi, T. and Kai, K. 1984a, Ap.J., submitted.
Nakajima, H., Dennis, B.R., Tajima, T., Brunel, F. and Sakai, J. 1984b, Ap. J. (Letters), submitted.
Nakajima, H., Kosugi, T. and Enome, S. 1983, Nature, *305*, 292.
Oda, M. 1983, Adv. Space Res., *2*, p. 207.
Ohki, K., Takakura, T., Tsuneta, S. and Nitta, N. 1983, Solar Phys., *86*, 301.
Orwig, L.E., Frost, K.J. and Dennis, B.R. 1980, Solar Phys., *65*, 25.
Palmadesso, P.J., Coeffey, T.P., Ossakow, S.L. and Papadopoulos, K. 1974, Geophys. Res. Letters, *1*, 105.
Parker, E.N. 1983a, Ap. J., *264*, 635.
Parker, E.N. 1983b, Ap. J., *264*, 642.
Papadopoulos, K. Gaffey, J.D., Jr., and Palmadesso, P.J. 1980, Geophys. Res. Letters, *7*, 1014.
Pesses, M.E. 1983, Advance Space. Res., *2*, ll, 255.
Petrosian, V. 1982, Ap. J. (Letters), *255*, L85.
Prince, T.A., Ling, J.C., Mahoney, W.A., Riegler, G.R. and Jacobson, A.S. 1982, Ap. J. (Letters), *255*, L81.
Prince, T.A., Forrest, D.J., Chupp, E.L., Kanbach, G. and Share, G.H. 1983, in: 18th International Cosmic Ray Conference Papers 4, Bangalore, p. 79.
Ramaty, R. 1979, Particle Acceleration Mechanisms in Astrophyics, American Institute of Physics, New York, p. 135.
Ramaty, R. 1985, in Holzer, T.E., Mahalas, D., Sturrock, P.A., Ulrich, R.K. (eds), Physics of the Sun p. 1.
Ramaty, R. and Crannell, C.J. 1976, Ap. J., *203*, 766.
Ramaty, R., Kozlovsky, B. and Lingenfelter, R.E. 1975, Space Sci. Rev., *18*, 341.
Ramaty, R., Kozlovsky, B. and Lingenfelter, R.E. 1979, Ap. J. (Suppl.), *40*, 487.
Ramaty, R., Kozlovsky, B. and Suri, A.N. 1977, Ap. J., *214*, 617.
Ramaty, R. and Murphy, R.J. 1984, in: High Energy Transients in Astrophysics, ed. S. Woosley, A.I.P., N.Y., p. 628.
Ramaty, R., Murphy, R.J., Kozlovsky, B. and Lingenfelter, R.E. 1983a, Solar Phys., 86.
Ramaty, R., Murphy, R.J., Kozlovsky, B. and Lingenfelter, R.E. 1983b, Ap. J. (Letters), *273*, L41.
Ramaty, R. *et al.*, 1980, Solar Flares, ed. P.A. Sturrock (Boulder: Colorado Associated University Press).
Raoult, A. and Pick, M. 1980, Astron. Astrop., *87*, 63.
Raoult, A., Pick, M. Dennis, B. and Kanes, S.R. 1984, Ap. J., submitted.
Rieger, E., Reppin, C., Kanbach, G., Forrest, D.J., Chupp, E.L. and Share, G.H. 1983, in: 18th International Cosmic Ray Conference Papers (Late Papers), Bangalore, p. 238.
Rieger, E. 1982, in Hinotori Symp. on Solar Flares (Tokyo: Inst. Space Astronautical Sci.), p. 246.
Roberts, C.S. and Buchsbaum, S.J. 1964, Phys. Rev. A., *135*, 381.
Rowland, H.L. and Vlahos, L. 1984, Astron. Astrop., *142*, 219.
Rosner, R., Tucker, W.H. and Vaiana, G.S. 1978, Ap. J., *220*, 643.

Rust, D.M., Benz, A.O., Hurford, G.T., Nelson, G., Pick, M. and Ruzdjak, V. 1981, Ap. J. (Lett), *244*, L179.
Ryan, J. 1985, Solar Phys. (submitted).
Sato, T., Matsumoto, H. and Nagai, K. 1982, J. Geoph. Res., *87*, 6089.
Schnack, D.D. and Killeen, J. 1979, Nucl. Fusion, *19*, 877.
Schwartz, R.A. 1984, Ph.D. Thesis, University of California, Berkeley, CA.
Share, G.H., Chupp, E.L., Forrest, D.J. and Rieger, E. 1983, in: Positron-Electron Pairs in Astrophys, eds. M.L. Burns, A.K. Harding and R. Ramaty, A.I.P., N.Y., p. 15.
Sharma, R.R. and Vlahos, L. 1984, Ap. J., *280*, 405.
Sharma, R.R., Vlahos, L. and Papadopoulos, K. 1982, Astron. Astrophys., *112*, 377.
Singh, N., Schunk, R.W. and Sojka, J.J. 1981, Geophys. Res. Letters, *8*, 1249.
Slottje, C. 1978, Nature, *275*, 520.
Slottje, C. 1979, in IAU Symposium 86, Radio Physics of the Sun, ed. M.R. Kundu and T.E. Gergely (Dordrecht: Reidel) p. 173.
Smith, D.F. 1980, Solar Phys., *66*, 135.
Smith, D.F. 1985, Ap. J., *288*, 801.
Smith, D.F. and Lilliequist, C.G. 1979, Ap. J., *232*, 582.
Smith, D.F. and Harmony, D.W. 1982, Ap. J., *252*, 800 (SH2).
Somov, B.V., Stepanov, V.E., Stepanyan, N.N and Tomozov, V.M. 1983, Phys. Solariterr., No. *20*, Potsdam, p. 5.
Speiser, T.W. 1967, J. Geoph. Res., *76*, 8211.
Spicer, D.S. 1982, Space Sci. Rev., *31*, 351.
Spicer, D.S. 1983, Advances in Space Research, *2*, 135.
Sprangle, P. and Vlahos, L. 1983, Ap. J., *273*, L95.
Steinolfson, R.S. and Van Hoven, G. 1983, Phys. Fluids, *26*, 117.
Steinolfson, R.S. and van Hoven, G. 1984a, Astrophys. J., *276*, 391.
Steinolfson, R.S. and Van Hoven, G. 1984b, Phys. Fluids, *27*, 1207.
Stewart, R.T. 1978, Solar Physics, *58*, 121.
Strong, K.T., Benz, A.O., Dennis, B.R., Leibacher, J.W., Mewe, R., Poland, A.I., Schrijver, J., Simnett, G., Smith, J.B. Jr. and Sylwester, J. 1984, Ap. J., in press.
Sturrock, P.A. 1974, in IAU Symp. 57, Coronal Disturbances, G. Newkirk (ed.), 437.
Sturrock, P.A., Kaufmann, P., Moore, R.L. and Smith, D. 1985, Solar Phys., *94*, 341.
Tajima, T. 1982, in Fusion Energy — 1981, (International Energy Agency, ICTP, Trieste, 1982), p. 403.
Takakura, T. 1985, Proc. Kunming Workshop in Solar Physics and Interplanetary Traveling Phenomena.
Takakura, T., Ohki, K., Tsuneta, S. and Nitta, N. 1983a, Solar Phys., *86*, 313.
Takakura, T., Kaufmann, P. Costa, J.E.R., Degaonkar, S.S., Ohki, K. and Nitta, N. 1983b, Nature, *302*, 317.
Tandberg-Hanssen, E., Kaufmann, P., Reichmann, E.J., Teuber, D.L., Moore, R.L., Orwig, L.E. and Zirin, H. 1984, Solar Phys., *90*, 41.
Tanaka, K. 1983, IAU Col. 71, Activity in Red Dwarf Stars, eds. P. B. Byrne and M. Rodono, p. 307.
Tanaka, K., Watanabe, T., Nishi, K. and Akita, K. 1982, Ap. J., *254*, L59.
Tanaka, M. and Papadopoulos, K. 1983, Phys. Fluids, *26*, 1697.
Tapping, K.F. 1983, Solar Phys., *83*, 179.
Terasawa, T. 1981, J. Geophys. Res., *86*, 9007.
Trottet, G. and Vilmer, N. 1983, Proceedings of the 18th ICRC Conference, SP 3-15.
Tsuneta, S., Takakura, T., Nitta, N., Ohki, K., Makishima, K., Murakami, T., Oda, M., and Ogawara, Y. 1983, Solar Phys., *86*, 313.
Tsuneta, S., Takakura, T., Nitta, N., Ohki, K., Tanaka, K., Makishima, K., Murakami, T., Oda, M., and Ogawara, Y. 1984a, Ap. J., *280*, 887.
Tsuneta, S., Nitta, N., Ohki, K., Takakura, T., Tanaka, K., Makishima, K., Murakami, T., Oda, M., and Ogawara, Y. 1984b, Ap. J., *284*, 827.
Tsuneta, S. 1983a, Ph.D. Thesis.
Tsuneta, S. 1983b, in Proc. Japan-France Seminar on Active Phenomena in the Outer Atmospheres of Stars and the Sun, eds., J.-C. Pecker and Y. Uchida, p. 243, (Paris: C.N.R.S.).
Tsuneta, S. 1984, Annals of the Tokyo Astron. Obs., *20*, 1.
Tsuneta, S. 1985, Ap. J., *290*, 353.
Tsurutani, B.J. and Lin, R.P. 1985, J. Geoph. Res., *90*, 1.
Tverskoi, B.A. 1967, Soviet Phys. JEPT, *25*, 317.
Ugai, M. 1982, Phys. Fluids, *25*, 1027.
Ugai, M. 1983, Phys. Fluids, *26*, 1569.
Uralov, A.M. and Nefed'ev, V.P. 1976, Astron. Zh., *83*, 1041.
Van Beek, H.F., Hoyng, P., Lafleur, B. and Simnett, G.M. 1980, Solar Phys., *65*, 39.
Van Hoven, G. 1976, Solar Phys., *49*, 95.
Van Hoven, G. 1979, Astrophys.J., *232*, 572.
Van Hoven, G. and Cross, M.A. 1973, Phys. Rev., *A7*, 1347.
Van Hoven, G., Tachi, T. and Steinolfson, R.S. 1984, Astrophys. J., *280*, 391.
Varvoglis, H.and Papadopoulos, K. 1983, Ap. J. (Lett.), *270*, L95.
Vasyliunas, V.M. 1980, J. Geoph. Res., *85*, 4616.
Velusamy, T. and Kundu, M.R. 1982, Ap. J., *258*, 388.
Vestrand, W.T., *et al.*, 1985, paper presented at the 25th Meeting of the Committee on Space Research, Graz.
Vilmer, N., Kane, S.R. and Trottet, G. 1982, Astron. Astrophys., *108*, 306.
Vilmer, N., Trottet, G. and MacKinnon, A.L. 1985, Astron. and Astrophys., submitted.
Vlahos, L. 1979, in IAU Symposium 86, Radio Physics of the Sun, ed. M.R. Kundu and T.E. Gergely (Dordrecht: Reidel), p. 173.
Vlahos, L. and Papadopoulos, K. 1979, Ap. J., *233*, 717.
Vlahos, L. and Rowland, H.L. 1984, Astr. Ap., *139*, 263.
Vlahos, L. and Sharma, R.R. 1984, Ap. J., *290*, 347.
Vlahos, L. and Gergely, E.T. and Papadopoulos, K. 1982, Ap. J., *258*, 812.
Vlahos, L., Sharma, R.R. and Papadopoulos, K. 1983, Ap. J., 275.
Wang, H.T. and Ramaty, R. 1974, Solar Physics, *36*, 129.
Wiehl, H.J., Benz, A.O. and Aschwanden, M.J. 1985, Solar Phys., *95*, 167.
Wiehl, J.J. and Matzler, C. 1980, Astron. Astrophys., *82*, 93.
Wiehl, H.J., Schochlin, W.A. and Magun, A. 1980, Astron. Astrophys., *92*, 260.
Wild, J.P., Smerd, S.F. and Weiss, A. A. 1963, Ann. Rev. Astron. Astrophys., *1*, 291.
Wolfson, J.D., Doyle, J.D., Leibacher, J.W. and Phillips, K.J.H. 1983, Ap. J., *269*, 1319.
Wu, C.S. 1984, J. Geoph. Res., *89*, 8857.
Wu, C.S. and Lee, L.C. 1979, Ap. J., *230*, 621.
Wu, C.C., Leboeuf, J.N., Tajima, T. and Dawson, J.N. 1984, Phys. Fluids, submitted.

Yoshimori, M., Okudaira, K., Hirasima, Y. and Kondo, I. 1983, Solar Phys., *86*, 375.
Zaitsev, V.V. and Stepanov, A.V. 1983, Sov. Astr. (Lett.), *8*, 132.
Zaitsev, V.V., Stepanov, A.V., and Sterline, A.M. 1985, Pisma V. Azh., V. 11, in press.
Zhao, R. and Jin, S. 1982, Scientia Sinica, *25*, 422.
Zodi, A.M., Kaufmann, P. and Zirin, H. 1984, Solar Phys., *92*, 283.
Zweibel, E.G. and Haber, D. 1983, Ap. J., *264*, 648.